Mislocalization of diverse RNA species to synapses in Alzheimer's disease and aging

Samuel Nathan Smukowski

A dissertation

submitted in partial fulfillment of the

requirements for the degree of

Doctor of Philosophy

University of Washington

2024

Reading Committee:

Paul Valdmanis, Chair

Melissa Barker-Haliski

Jessica Young

Program Authorized to Offer Degree:

Genome Sciences

University of Washington

Abstract

Mislocalization of diverse RNA species to synapses in Alzheimer's disease and aging

Samuel Nathan Smukowski

Chair of the Supervisory Committee:

Paul Valdmanis

Division of Medical Genetics, Department of Genome Sciences

The distribution of RNAs in neurons is non-random, and there are complex cellular mechanisms regulating the transport and localization of RNAs along neural projections to synaptic locations. This enables synapses to respond rapidly to synaptic signaling by synthesizing proteins from a pool of sequestered dormant mRNAs to alter synaptic strength, morphology, and connections. This phenomenon is called "localized translation" and is an essential mechanism facilitating plasticity in the brain and cognition. Alzheimer's disease (AD) is a neurodegenerative disease characterized by buildup of extracellular amyloid plaques and intracellular hyperphosphorylated tau neurofibrillary tangles in the brain followed by synapse and neuron loss and subsequent cognitive impairment. Previous studies of AD have revealed disruptions among cytoskeletal trafficking and RNA binding proteins which are essential for proper synaptic localization of RNAs. Differences in expression of non-coding RNAs including microRNAs and circRNAs, which serve regulatory functions in the expression of mRNAs, have also been observed. Therefore, it is likely mislocalization of RNAs to synapses is taking place in AD which would negatively impact the mechanism of localized translation and contribute to synaptic dysfunction in disease. Given how dynamic and finely regulated RNA localization is for

neuronal function, it is also possible changes in localization are taking place across lifespan. In this thesis, I investigate differences in RNA localization, including mRNAs, microRNAs, and circRNAs, in AD by RNA sequencing synaptosomes from patient and control tissue. Synaptosomes are fractionated particles encapsulating synaptic material. We find substantial differences in mRNA localization, and we also find differences in circRNA isoforms present at synapses. There are also correlations between differential expression of microRNAs and target mRNAs mislocalized in AD. Finally, we discover changes in synaptic RNAs across lifespan in mouse models that suggest AD may represent an acceleration of age-related changes. This research adds a new dimension to our understanding of AD pathology and suggests new targets for therapeutic interventions.

Acknowledgements

There are many people to thank who have substantially contributed towards my success at completing this dissertation. Acknowledgements go well beyond people in the present and include those who have had lasting impacts on my entire academic journey.

First and foremost, I must thank my advisor Dr. Paul Valdmanis. He has guided me every step of the way as I developed my research competency and embarked on a novel quest to investigate RNA localization in Alzheimer's disease. Dr. Valdmanis proposed a simple idea when I began my dissertation in his lab, and this launched me on a journey of discovery that I adapted into a comprehensive study in which I can take great pride. Not to mention Dr. Valdmanis was instrumental in helping me prepare an application for an NSF graduate fellowship which I eventually earned.

Second, I would like to thank all the lab members of the Valdmanis Lab, past and present. Meredith Course and Kathryn Gudsnuk were members of the Valdmanis Lab when I rotated and began my dissertation, and they made sure to help me off to a good start. Members that joined since I started that have helped considerably among projects in the lab include Eli Kaufman, Jenna Somberg, Tina Busald, Julianna Brutman, and Evangelos Nizamis. I wish everyone continued success in their careers.

Next, I would like to thank the members of my thesis committee that have given me helpful guidance as I developed my research project. My committee members include Dr. Melissa Barker-Haliski, Dr. Jessica Young, Dr. Mike MacCoss, and Dr. Andre Lieber. It was also fantastic to collaborate on other projects as well throughout my time here. I would also like to thank them for submitting letters of recommendation on my behalf as I submitted applications for awards over the past years. I also rotated in Dr. MacCoss's lab, and I would like to thank him for a stellar rotation.

I would also like to thank Dr. Jeffrey Savas and members of the lab at Northwestern University in Chicago who hired me as a research technologist following my undergrad and before I started graduate school. It was here where I developed a keen interest in neuroscience, and I learned proteomics skills which led me to apply and attend the University of Washington Genome Sciences Program. My experience in the lab and skills I acquired prepared me excellently for success in graduate school. And it was also here where I had my first authorship on a scientific publication and several more.

I also owe many thanks to Dr. Randal Tibbetts and Dr. Sang Hwa Kim at the University of Wisconsin-Madison with whom I was largely first introduced to genetic and neuroscience research knowledge and skills during my undergrad. I conducted a senior thesis in the lab, and this jump-started my career in the sciences.

I want to also give thanks to my classmates in UW Genome Sciences including Robin Aguilar, Phoebe Parrish, Sam Regalado, and Chengxiang Qiu. We all started in 2018 in the same class, and I would not have succeeded in grad school without their comradery. I wish all my friends the best in their future careers.

Finally, I would like to thank my family: My mother Jean Smukowski, my father Mark Smukowski, and my brother Ty Smukowski. Their love for, and faith in, me has continuously kept me confident in myself and grateful for the opportunities I have been given.

Nevertheless, there are scores of other people that have all played a role in my professional development. To those whom I haven’t mentioned here by name, I most certainly keep you in my memory and thank you greatly for your generosity.

Table of Contents

Chapter 1: Introduction

1.1 Alzheimer's disease

Alzheimer's disease (AD) is a progressive neurodegenerative disease characterized by the formation of amyloid plaques in the extracellular space and formation of neurofibrillary tau tangles inside the neurons[1]. It is the most prevalent form of dementia accounting for at least 50 million cases worldwide[2]. AD presents in both familial forms (fAD), in which genetic heritability can be identified, and sporadic forms (sAD), in which there is no certain genetic cause. Known causative mutations include those in amyloid precursor protein (*APP*) and two components of the gamma secretase complex, presenilin 1 (*PSEN1*), and presenilin 2 (*PSEN2*), which all play a role in the cleavage of APP into the pathogenic peptide Amyloid beta (Aβ), aggregation of which is the primary hallmark of AD. Other genetic risk factors have been extensively sought out in genome-wide association studies (GWAS)[3,4]. Chief among these is apolipoprotein E (*APOE*) which has been shown to affect several aspects of neural function[5,6].

Although AD pathology has been, and continues to be, exhaustively characterized by its symptoms and molecular profiles, very little success has been made to connect cause and effect, leading to various hypotheses that have yet to be proven[7,8]. It is known that molecular pathology precedes cognitive impairment symptoms up to 20 years beforehand in disease progression[1]. This leads to efforts that can identify and intervene therapeutically before cognitive decline begins, although most attempts have not been fruitful[7]. Critically, we have to understand how amyloid and tau pathology affect synaptic function. Studies to date have characterized how protein composition at the synapse is altered and that, overall, synaptic excitability weakens upon buildup of amyloid in the late stages of disease progression[8]. However, downstream

events from synaptic dysfunction to neurodegeneration and cognitive deficit have yet to be fully elucidated.

In this study, we highlight a cellular phenomenon called localized translation and how it may be impacted in AD and aging. Localized translation is an essential process in synaptic and neural function which facilitates the brain's plastic nature and cognitive ability. In the following sections, we elaborate on how the mechanisms underlying localized translation fit into our understanding of AD and how research into this phenomenon sets forth a novel direction in elucidating AD neuropathology.

1.2 Localized translation in synapse function

Cognitive function in the brain is facilitated by chemoelectrical currents transmitted along circuitries established across a vast network of specialized cells called neurons in a manner analogous to transistors on a computer microchip. Neurons form connections between each other called synapses which receive inputs from neighboring cells and can transmit outputs to subsequent neurons in the network. Neurons are polarized cells and consist of three main anatomical components: The soma, which is the central component of the cell containing the nucleus and main organelles; dendrites, which receive inputs from other cells; and axons, which transmit outputs to other cells. Dendrites contain post-synaptic compartments that pair with pre-synaptic compartments from axons. These neuronal anatomical structures are highly plastic and can adjust their morphology and composition to modify circuits between cells and brain regions.

Synaptic plasticity requires the rapid translation of proteins proximal to synaptic sites. This process is called localized translation[9-11]. When a synapse is stimulated, the axonal pre-synaptic site releases neurotransmitters from synaptic vesicles which

traverse the synaptic cleft and bind to receptors on the dendritic post-synaptic site. When receptors on the post-synapse are activated, ion channels open which causes a shift in local ion concentrations and charge. This change influences the phosphorylation state of nearby proteins as well as the binding of translation initiation factors, translational repressors, and ribosomes to mRNA transcripts localized to the synaptic site. This leads to rapid translation of these transcripts and their protein products that can modify the structure of the synapse create signaling factors that can be transported along neural projections or back to the soma and nucleus, which can influence the transcription of other genes[12-15]. Synaptic signaling can also stimulate the release of extracellular vesicles that can contain additional signaling molecules, proteins, and transcripts to neighboring cells[16].

Synaptic signaling triggers a cascade of protein modifications that drive response. In particular, protein phosphorylation can affect protein action on other substrates. For example, in excitatory neurons, upon synaptic stimulation, CAMKII becomes phosphorylated which in turn activates PKA, CPEB, and mTORC1. This activates translation initiation factors and releases translational repressors that allow for the rapid translation of immediate early genes[17].

One immediate early gene that stands out and was among the first discovered to be locally translated is the activity-related cytoskeletal protein ARC[18]. ARC has been shown to bind its own RNA at synapses and has the capacity to form membrane-bound capsids that exocytose and become internalized by neighboring neurons in a manner akin to retroviruses and has been widely accepted to be a retroviral gene that integrated in vertebrate genomes and became repurposed for synaptic transmission[19-21]. ARC capsids can deliver RNA cargos between neurons that can also undergo localized translation[22]. Locally translated ARC can also undergo retrograde transport back to the nucleus to modulate transcription[12].

Long term structural changes that take place include strengthening of synapses by the synthesis of scaffold proteins including Actin, PSD-95, Homer, Shank1-3 as well as increased

density of synaptic receptors. The extension of additional dendritic (post-synaptic) spines can also take place increasing neuron responsiveness[17].

1.3 Cellular mechanisms that make localized translation possible

The distribution of RNAs in a cell is non-random, and a critical component allowing localized translation to take place is the cytoskeletal transport of target RNAs to distal cellular compartments including synaptic sites. For this to work, RNAs need to bind to RNA-binding proteins (RBPs) that mediate interaction with motor proteins which use energy to “walk” along microtubules. RBPs can bind to specific or non-specific sites in a transcript in which RNA secondary structure creates a complementary interface. Many of these sites are located in the transcripts’ untranslated regions (UTR), most frequently on the 3′ end. 3′ UTRs can contain motifs known as “zip codes” in which unique sequences can drive selective trafficking to target destinations in the cell. UTR content can be modified during the transcription process where alternative splicing and alternative poly-adenylation sites can manipulate transcript length and composition of the same encoded protein[23-25]. It has been found that longer 3′ UTRs also correlate with longer transport distances in neurites. Experiments that splice 3′ UTRs between different genes have been found to differentially affect transport[26,27]. Alternative UTR exons can also control translational efficiency[28,29]. Additional post-transcriptional mechanisms driving RNA transport include RNA modifications such as methylation which make RNA transcripts more stable in the cytoplasm (**Fig 1.1**)[30-32].

These RBP-RNA complexes form what are called biomolecular condensates which are membraneless organelles that distinctly separate from the cytoplasm by liquid-liquid phase separation[33]. Biomolecular condensates are a ubiquitous feature of cell and

neuron function and encompass the nucleolus, stress granules, and synaptic scaffolds[34]. Phase separation is largely mediated by intrinsically disordered regions (IDRs) or low-complexity domains (LCDs)[35]. These motifs tend to have redundant amino acid content that creates flexible protein surfaces that may condense with other proteins or nucleic acids in favorable solute conditions. Examples of proteins harboring LCDs include TDP-43 and FUS which both have C-terminal regions extensively rich in glycine and serine or glutamine. Mutations in these LCDs often result in disease including amyotrophic lateral sclerosis (ALS) and frontotemporal dementia (FTD) because of an increased propensity to phase-separate causing dysregulation of biomolecular condensates[36].

One of the features that makes biomolecular condensates essential for modulating localized translation is their nature to respond rapidly to localized physiological changes in the cytoplasm. An essential component of this is phosphorylation. For example, phosphorylation of the RBP FMRP destabilizes its interaction with RNA and makes the transcript accessible for translation by ribosomes[37]. Targets of both FMRP and TDP-43 are found to be enriched in axons[38]. And FMRP-mRNA granules are enriched in synapses and associate with translational machinery[39].

In addition to RBPs, motor proteins and the cytoskeleton are also essential. In neurons, microtubules extend from the soma and are polarized with a minus end proximal to the nucleus and a plus end growing with the addition of monomers creating distal neural projections including axons and dendrites – Although dendrites can contain microtubules in both orientations. Motor proteins mediate interaction between the microtubules and cargos to be transported and use ATP to traverse along the microtubule. Motor proteins encompass two main families: One is Kinesin (KIFs) which transport cargos from minus-end to plus-end, the other is dynein which transport cargos from plus-end to minus-end. Common cargos that need to be transported include endosomes, mitochondria, proteins, and RNAs[40,41]. Colocalization experiments have found that FMRP-mRNA granules associate with microtubules to traffic

mRNAs to synapses[39]. Knock-down experiments on KIFs have shown reductions in dendritic branching, synaptic density, and neuron firing in neuronal cell culture as well as cognitive deficits in mice largely via the disruption of trafficking synaptic components and translational machinery including mRNAs[42-45]. In contrast, an experiment where KIF5C was overexpressed enhanced these neuronal features and also led to enhanced spatial memory in mice[46].

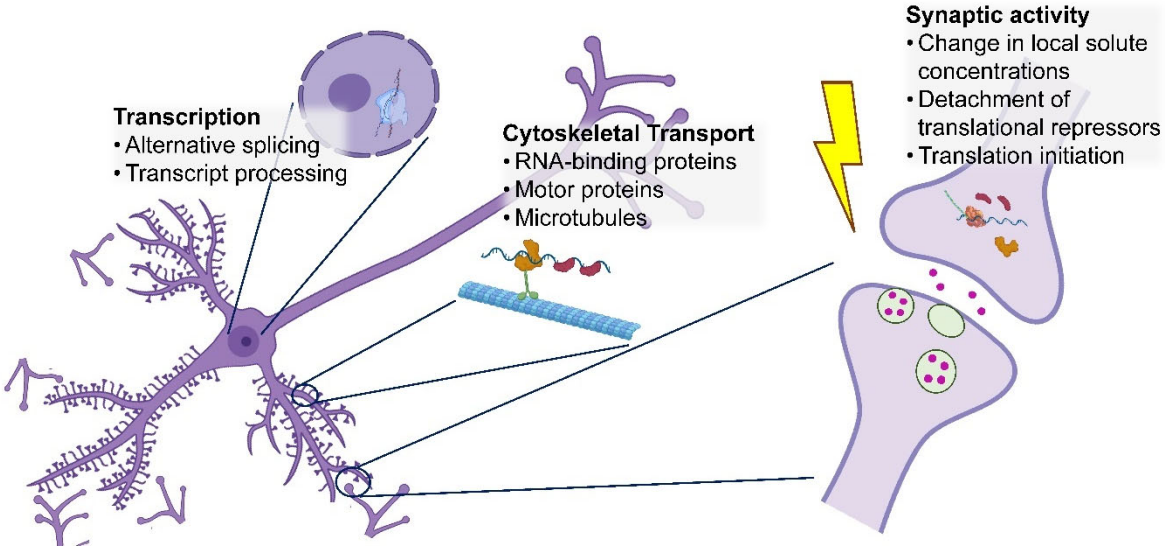

Fig 1.1. The mechanisms of localized translation. First, transcribed mRNAs in the nucleus can undergo alternative splicing or post transcriptional processing to modify sequence content that can drive targeted localization patterns. Next, RNA-binding proteins and motor proteins condense with the transcript to transport it along microtubules to synaptic sites. Finally, upon reaching synaptic locations, synaptic activity can initiate translation by triggering release of translational repressors from the mRNA to synthesize proteins locally at the stimulated synapse. *Figure created using a biorender.com license.*

1.4 Involvement of other RNA species

Given the importance of mRNA 3′ UTRs length and motifs in proper transport and expression at synapses, micro RNAs (miRNAs) have been determined to have critical roles in transcript expression dynamics in subcellular compartments. miRNA's mechanism of action is by binding argonaute (AGO) proteins which form the RNA induced silencing complex (RISC). The miRNA duplex is unwound and one strand is retained which binds to short complementary 7-8bp motifs in 3′ UTRs of mRNA targets. This binding leads to translational repression and/or mRNA degradation. In rare instances, perfect complementarity between the full ~21nt miRNAs and target mRNAs leads to transcript elimination via the endonuclease activity of AGO2. In each of these scenarios, mRNA targets are removed from the pool of local mRNAs that can be translated[47]. It has been shown that miRNAs in addition to the RISC can be selectively transported to synaptic sites. In addition, 3′ UTR miRNA binding sites on synaptic-localized transcripts play a role in facilitating their localized expression dynamics[29].

Circular RNAs (CircRNAs) are a class of non-coding RNAs that are formed by back-splicing a downstream exon to an upstream exon forming a closed loop. CircRNAs have been shown to have various regulatory functions. Examples include serving as microRNA (miRNA) "sponges" whereby a circRNA can include multiple miRNA binding sites that effectually remove miRNAs from binding to other targets. Similarly, circRNAs can include multiple RBP sites which will also reduce their associated RBP's presence in the cytoplasm and affect the expression of other transcripts that they target. Finally, circRNAs are stable molecules that can persist in the cytoplasm longer than their linear counterparts due to exonuclease resistance. CircRNA biology is still a developing area of study, and functional roles of individual isoforms are largely unknown[48].

Given the incredible regulatory potential of circRNAs and the fine-tuned nature of localized translation, it is possible that circRNAs are playing critical roles at synapses regulating the expression of other localized transcripts. Previous research and the research presented in this thesis have demonstrated that circRNAs are enriched at synapses. In addition, circRNAs appear to accumulate in the aging brain in rodent studies[49]. RNA sequencing in AD patient brain samples also revealed significant expression differences of circRNAs in AD.

Long non-coding RNAs (lncRNAs) also play a role in regulating synaptic function and this is an active area of research. These RNAs can serve similar functions to circRNAs by interacting with other components that regulate the expression of mRNAs including interactions with miRNAs and RBPs. lncRNAs interact with RBP-RNA granules as well as translational machinery and perturbations of lncRNAs can thus affect the translation of mRNAs at the synapse and have downstream effects on cognition[50]. lncRNAs have been found to be enriched at synapses and show changes with age[51].

1.5 Ways to study synaptic-localized translation

One approach to studying compartmental mRNA and protein localization in neurons is controlling the growth and physical separation of neurites and the soma using physical barriers. Cell culture plates can be lined with a nylon membrane where the pores are sized such that neurites can penetrate the barrier whilst the larger cellular compartments such as the soma remain on the seeded side of the membrane[52]. Microfluidic chambers can be used in a similar way to drive the growth of axons through structured channels.

A related technique is microdissection. This has been used to separate between the outer layer of somata from the inner layer of neuropil in the CA1 region of the hippocampus due to its distinct anatomy[53-55]. Therefore, the compartmental protein composition can be distinguished within intact tissue.

Among the most robust approaches to studying localized translation and related mechanisms are subcellular fractionation techniques. One of these is the fractionation of intact synaptic particles called “synaptosomes”[56]. Synaptosome fractionation leverages the unique structural morphology of synapses to design approaches that separate them from the rest of the cell body. Specifically, synapses are very protein rich with scaffolds that intercalate within the plasma membrane. These structures of high density can survive homogenization where they remain intact and pinch off from the cell body and reseal to form dense membrane-bound particles encapsulating nearby molecular components. Synaptosomes can then be isolated from the bulk homogenate by passing the homogenate through a density gradient that is centrifuged at high force. This gradient can be composed of a continuous or discontinuous solution of sucrose, percol, or ficol, where the homogenate passes through a column of low density to high density[57]. Particulate matter thus migrates through the gradient and localize to points of matching density. Other techniques to fractionate synaptic particles include successive filtering steps of the homogenate through nylon membranes of decreasing pore size which isolate based on their average size as opposed to density. In the literature, this technique results in particles that are called “synaptoneurosomes” to distinguish between whether the particles were isolated based on size versus density[58,59].

Synaptosomes and synaptoneurosomes have generally been used to study protein compositional differences at synapses in aging and disease. Successful fractionation of synapses can be determined by the enrichment of synaptic markers as well as the visualization the particles under electron microscope. Mass spectrometry techniques have been used to determine and quantify synaptic protein composition in age and in disease[60]. Neuronal cultures

can also be stimulated and changes in protein composition can be measured. Experiments like this have shown that AMPA receptors and scaffold proteins become upregulated at synapses in long-term-potentiation. Visualization techniques have been employed to accompany mass spectrometry and produce three dimensional representations of synaptic organization[61].

A more specific approach to studying differences occurring at synapses includes fluorescent activated synaptosome sorting (FASS). This technique involves tagging specific synapse types using fluorescent antibodies which can then be separated in a manner similar to single-cell sorting[62]. For example, the receptor GLUR1 can be labeled and be used to define the glutamatergic synaptic proteome[63]. Another study used FASS labeling Nectin 3 in conjunction with microdissection to specify the unique synaptic proteome of hippocampal CA1 mossy-fiber synapses[64].

With the increasing technological breakthroughs in next-generation sequencing, studying the RNA composition of synaptosomes has become an emerging area of investigation. RNAseq has been used to determine differences in the transcript composition of neuropil versus soma in mouse hippocampal neurons by culturing in dishes separated by a nylon membrane[52]. RNAseq has also been used to determine specific differences in UTR composition of transcripts that are selectively transported to neurites[27]. Ribo-seq is a technique in which ribosomes can be crosslinked to mRNA and therefore measure ribosome occupancy on actively translating mRNAs; this has been termed the “translatome”[54]. This can be used to determine what transcripts become locally translated upon neuronal stimulation. Crosslinking can also be used in conjunction with immunoprecipitation to sequence the targets of RNA binding proteins such as FMRP and KIF3C[46].

Creative sequencing techniques have been employed to study synaptic-localized transcriptomes or other subcellular compartments. One of these is an APEX proximal

labeling approach to tag localized transcripts nearby compartmental protein markers which can then be isolated by conjugation and the isolated transcripts sequenced. This approach has been used to elucidate the localized transcriptome of the mitochondria, endoplasmic reticulum, nuclear lamina, among other compartments[65]. These localized transcriptomes can then be compared to the cytoplasm to determine enriched transcripts. Single-cell sequencing approaches are also being adapted to separate synapse and cell types in brain tissue and cell culture[66,67].

In neurons cultured *in vitro*, localized translation can be studied by stimulating neurons and measuring newly synthesized proteins. This can be measured even more precisely by glutamate uncaging experiments where light can be used to release glutamate at specific locations along neural projections thereby isolating localized translation activity to an area less than 50nm. Experiments of this type have shown that stimulation and localized translation in one synapse can affect other synapses nearby to strengthen connections[68].

In addition to quantitative protein measurement techniques, several visual techniques have also been developed to study localized translation. RNA localization can be measured using fluorescent in situ hybridization[69]. Ribosome occupancy can be measured using electron microscopy. Newly synthesized proteins can also be measured in neuronal culture by pulsing in an amino acid analogue that facilitates click chemistry of fluorophores[70,71]. And proteins undergoing active translation can be identified by colocalization with ribosomes[52].

In summary, a wide selection of techniques has been developed over the past several decades to delve deeper into the phenomenon of localized translation. Each of these techniques helps explore and appreciate different facets of the complex regulatory nature of localized translation in neurons to respond to stimulation to elicit structural changes facilitating synaptic plasticity and cognition.

1.6 Relationship of localized translation to neurodegenerative disease

Given the complexity of mechanisms involved in facilitating synaptic localized translation and their essential role in cognitive function, it stands to reason that perturbations in this delicate process can elicit disease phenotypes resulting in cognitive impairment or neurodegeneration. Studies into the genetic etiology of various neurological diseases have revealed connections to mutations or differential expression of genes coding for RNA binding proteins, miRNAs, and alternative splicing. Therefore, understanding the impact these deficits can have on the process of localized translation can bridge the gap between genetics and cognitive impairment or neurodegeneration.

Fragile X syndrome

One of the most comprehensively studied neurological diseases related to defects in localized translation is Fragile X syndrome. Fragile X syndrome (FXS) is a genetic disease inherited in an X-linked dominant manner. Therefore, the disease is more severe in males than females. The disease is clinically characterized as an autism spectrum disorder (ASD) and typically diagnosed within 3-4 years after birth, or it can be determined by perinatal genetic testing. Symptoms include cognitive delays accompanied with hyperactivity, anxiety, and heightened sensitivity to sensory stimuli. Individuals with FXS may also display physical abnormalities related to changes in connective tissue resulting in hyperextensible joints and susceptibility to dislocations[72].

FXS is genetically characterized by a repeat expansion in the 3′ region of the Fragile X mental retardation 1 gene (*FMR1*) severely reducing the expression of the

Fragile X mental retardation protein (FMRP) which, as mentioned earlier, is an RNA-binding protein essential for RNA trafficking to synapses and localized translation. FMRP coordinates the translation of several proteins in post-synaptic compartments and glutamatergic synapses in particular. The loss or decreased expression of FMRP therefore leads to an overall increase in localized translation at synapses resulting in an excitatory/inhibitory imbalance in the brain[72]. Target and impacted proteins include AMPA receptors, GABA receptors, translation initiation factors, ERK signaling, MMP9, GSK3, AKT, and mTOR. Downstream effects include altered dendritic spine morphology. In *FMR1* knock-out mouse models, translational repressors are being explored as therapeutic options. Pharmaceuticals targeting some of the downstream overexpressed proteins controlled by FMRP are also showing promise at mitigating FXS symptoms including metformin, minocycline, JQ1, antibiotics, and bumetanide.

FMRP is RNA-binding, however a consensus motif has not been identified, but there is evidence that it binds to G-quadruplexes[73]. Coimmunoprecipitation experiments and ribosome profiling have identified several FMRP mRNA targets including *CAMK2A*, *ANKRD11*, *KIF5A*, and *GRIN2A*[38,74]. Although it is hypothesized that these account for only a small fraction of all potential targets. FMRP is known to directly interact with ribosome subunits and translation initiation factors by way of a binding partner, CYFIP1. FMRP has also been shown to preferentially interact with m^6A modified RNA as well as the RNA-editing enzyme ADAR. Thus, studies centered on FMRP and FXS have demonstrated extraordinary complexity of RNA and translational regulation mediating synaptic plasticity.

Overall, FXS is an important example of localized translation going awry. Study of the disease offers an essential platform for studying how RBPs and translational repressors play critical roles in regulating synaptic plasticity and downstream morphological and phenotypic outcomes of their loss or differential expression. Though FXS is a monogenic disease, its study also serves as a basis for addressing other neurological diseases, such as other developmental disorders that do not have a clear genetic cause, since many of the molecular and synaptic

pathologies overlap. FMRP could be a common therapeutic target among many of these diseases.

Amyotrophic lateral sclerosis

Studies of synaptic localization deficits in amyotrophic lateral sclerosis (ALS) have been gaining more attention. ALS is characterized by progressive degeneration of motor neurons leading to spasticity, limb weakness, and fatality by respiratory failure within 2-5 years of initial symptom onset. ALS can be either familial or sporadic and has been linked to genetic variants in more than 60 different genes. Two of the most well-studied genes, which were identified via autosomal dominant inheritance patterns, are Fused in Sarcoma (*FUS*), which encodes an RNA-binding protein, and TAR DNA binding protein (*TARDBP*), which encodes the protein TDP-43. These two proteins harbor low-complexity domains which make them prone to pathogenic aggregation. Ubiquitin-positive TDP-43 inclusions, which can include various other proteins and nucleic acids, are seen as an essential hallmark of ALS and observed in almost all cases. The notable exception to this is ALS related to genetic variants in superoxide dismutase 1 (*SOD1*) which also leads to pathogenic aggregates that can propagate in a prion-like manner.

Several cases of ALS have been linked to mutations in other RNA-binding proteins. This includes EWS RNA Binding Protein 1 (*EWSR1*), heterogeneous nuclear ribonucleoproteins A1 and A2B1 (*hnRNPa1*, *hnRNPa2b1*), Ataxin 2 (*ATXN2*), Matrin 3 (*MAT3*), and TIA1 cytotoxic granule associated RNA binding protein (*TIA1*). Other groups of genes implicated in ALS are those involved in the cytoskeleton or proteostasis including Kinesin Family Member 5A (*KIF5A*), Dynactin subunit 1 (*DCTN1*), Valosin Containing Protein (*VCP*), and Optineurin (*OPTN*)[75]. Taken together, perturbations

among any of these genes may result in disruption of the essential mechanisms supporting synaptic-localized translation.

Analogous to how dysregulation of the RNA-binding protein FMRP is the central mechanism of FXS, dysregulation of TDP-43 appears to be the central explanatory component behind most forms of ALS revealing similar complexity in its interactions. TDP-43 is a common component of RNP granules and can bind to motifs within mRNA 3′ UTRs. TDP-43 also interacts with other transport proteins including FMRP, kinesin proteins, Staufen, and SMN. RNA targets regulated by TDP-43 include itself, *CAMK2A*, *HNRNPA1*, *MAPT*, *STMN2*, and *UNC13A*. TDP-43 plays essential roles in the nucleus such as alternative splicing. In ALS, TDP-43 forms cytoplasmic aggregates which interrupt cytoskeletal transport and sequester other critical RNA and protein factors in pathological cytoplasmic phase-separated aggregates which increase over time. TDP-43 sequestration in the cytoplasm also prevents the protein from performing its essential roles in the nucleus. Motor neurons are uniquely susceptible to these pathologies given their extraordinary length where cytoskeletal transport of essential factors to the neuromuscular junction takes substantial time. Although these pathologies are also not exclusive to ALS, and the related disease of frontotemporal dementia (FTD), which sometimes co-occurs with ALS, show similar neuronal aggregates. It is also becoming more appreciated that TDP-43 cytoplasmic aggregation is a co-pathology in some cases of AD and has been found to exacerbate tau pathology[76,77]. Given the connection between ALS and AD pathologies, a common mechanism could be sequestering essential factors required by synapses, including both proteins and RNAs, thus preventing their transport.

Our understanding of ALS suggests that inappropriate aggregation of proteins reduces the capacity of cells to transport RNA and proteins to synapses resulting in deficits in localized translation and neuron degeneration. Central factors in ALS pathology include a wide variety of RNA-binding proteins which are inhibited from carrying out their normal functions and affect downstream processes. Given that aggregation is largely driven by the same mechanisms

behind liquid-liquid phase separation in biomolecular condensates, therapeutic options being tested include ways of dissolving the aggregates as well as gene therapies.

1.7 Localized translation in Alzheimer's disease, aging, and rationale for this study

Given this evidence and the essential role localized translation has in synaptic plasticity and observations in other neurological diseases, it stands to reason that this process could be perturbed in AD. Furthermore, identifying changes in localized translation has the potential to create a connection between AD molecular hallmarks and the resulting neurodegeneration. Tying localized translation into the study of AD mechanisms is starting to gain traction in the field with studies in 5xFAD mice, a mouse model that harbors mutations in humanized *APP* and *PSEN1*, showing an upregulation of inflammatory gene mRNAs in synaptosomes including complement components which were not upregulated in nuclei[67]. A microarray RNA profile of human AD synaptosomes showed an upregulation of synaptic and intracellular transport genes and a downregulation of cell cycle genes[78]. In this collection of research, we explore the RNA localization differences that are taking place in disease and in aging including mRNAs, circRNAs, and miRNAs.

There is substantial evidence supporting an exploration into localized translation in AD. Some of the risk loci indicated by GWAS are in genes that code for proteins involved in vesicle trafficking such as *SORL1*[79]. Transcriptomic studies have shown that genes involved in protein metabolism were frequently perturbed in AD suggesting a subsequent dysregulation of localized translation[80]. And single-cell RNAseq has shown

that genes related to myelination are regulated specifically in oligodendrocytes, astrocytes, and glia which can impact the efficiency of neuronal communication[81]. Another important piece of evidence is tau pathology, which is a ubiquitous feature of AD, and the protein has the ordinary function of stabilizing microtubules. With its pathogenic aggregation in the cytoplasm, transport of RNAs, proteins, and other cargos along the cytoskeleton becomes impaired. It has also been found that enlarged endosomes also occur in disease furthermore blocking normal transport functions[82,83]. These studies have thus led to the proposal of the “traffic jam” hypothesis of AD pathology[84].

AD pathology has also been found to incorporate TDP-43 inclusions, similar to those seen in ALS, and the TDP-43 inclusions have been shown to interact with tau[76,77,85]. Given TDP-43 pathological impacts in ALS, this suggests that the RNA splicing and transport functions the protein normally facilitates are disrupted. Indeed, splicing changes have been observed in AD among several genes including *EIF5B*, *EIF3K*, *ANXA2*, *VPS48*, *DNAJC7*, *MAP1B*, *DYNLRB1*, and *DCTN2*[86].

Another important line of evidence includes proteomic studies in AD brains that have showed differences in RNA-binding and motor proteins as well as changes in mitochondrial proteins, cell adhesion proteins, and cytoskeletal proteins[86,87]. An essential takeaway from proteomic studies is that differentially expressed proteins do not necessarily align with differentially expressed mRNAs which shows that there are critical regulatory steps that are perturbed between transcription and translation in neurons[88]. Proteomic studies in AD synaptosomes observed increases in immune response proteins and decreases in proteins related to long-term potentiation and oxidative phosphorylation[60]. Altogether these studies suggest that there could be other mechanisms driving the differences in protein composition at synapses.

One common feature of AD progression is a stage of neuronal hyperexcitability[89-92]. This stage also leads some patients to develop seizures. Studies in localized translation have shown

that perturbing its underlying mechanisms affects neuronal excitability. This could mean that disruptions in localized translation in AD are contributing towards this phenotype.

Collectively, these lines of evidence suggest that RNA trafficking to, and its regulation at, synapses could be affected by AD cellular pathologies. The research presented in this thesis explores how mRNAs could be mislocalized to synapses in AD and aging. In our study, we use the term mislocalized to mean that the differences in mRNA at synapses occur independently of global transcriptional changes. This provides a new line of evidence that can be used to hypothesize mechanisms of causation among various hypotheses and suggest opportunities for therapeutic intervention.

Chapter 2: mRNA and circRNA mislocalization at synapses are key features of Alzheimer's disease

This chapter comes from the text of the manuscript currently under review at PLOS Genetics as of 5/22/2024:

Smukowski SN, Danyko C, Somberg J, Kaufman EJ, Course MM, Postupna N, Barker-Haliski M, Keene CD, and Valdmanis PN. mRNA and circRNA mislocalization to synapses are key features of Alzheimer's Disease. *PLOS Genetics*. 2024. *–Under Re-review*

2.1 Abstract

Proper transport of RNAs to synapses is essential for localized translation of proteins in response to synaptic signals and synaptic plasticity. Alzheimer's disease (AD) is a neurodegenerative disease characterized by accumulation of amyloid aggregates and hyperphosphorylated tau neurofibrillary tangles followed by widespread synapse loss. To understand whether RNA synaptic localization is impacted in AD, we performed RNA sequencing on synaptosomes and brain homogenates from AD patients and cognitively healthy controls. This resulted in the discovery of hundreds of mislocalized mRNAs in AD among frontal and temporal brain regions. Similar observations were found in an APP^{swe}/$PSEN1^{dE9}$ mouse model. Furthermore, major differences were observed among circular RNAs (circRNAs) localized to synapses in AD including two overlapping isoforms of *circGSK3β,* one upregulated, and one downregulated. Expression of these distinct isoforms affected tau phosphorylation in

neuronal cells substantiating the importance of circRNAs in the brain and pointing to a new class of therapeutic targets.

2.2 Introduction

For years, AD research has centered upon the formation of amyloid plaques which is the most distinguishable event before downstream pathologies and cognitive impairment are observed[1]. Yet, it remains to be explained whether amyloid plaques themselves result in neurodegeneration or simply precipitate other events that ultimately cause cognitive dysfunction. This has led to several lines of research dedicated to specific hypotheses of AD mechanisms including neuroinflammation, tau neurofibrillary tangles, excitotoxicity, and metabolic dysfunction[7]. It has also been found that some patients are cognitively resilient to some of the characteristic pathologies making amyloid plaques necessary, but not sufficient, for AD dementia[1,93].

Synapse loss is one of the cardinal features of AD pathology and precedes Aβ deposition and tau neurofilament tangles. Therefore, maintaining synaptic integrity is important to prevent cognitive decline. A key component of this integrity is the localized translation of mRNAs at the synapse in rapid response to stimuli that modify synaptic structure and connections that are essential for synaptic plasticity[10,94,95]. For localized translation to take place, mRNAs need to be properly trafficked to synaptic destinations. This is orchestrated by a combination of localization signals in the untranslated regions of mRNA and formation of complexes with RNA binding proteins (RBPs) and motor proteins that shuttle RNA-protein biomolecular condensates along microtubules in the neurites to reach synaptic destinations[23,27,30,33,54,66,69,74,96-99]. Given the importance and complexity of this process for cognition, it remains to be seen how RNA transport and

synaptic-localized translation is impacted by AD pathologies. Previous research has shown that retrograde transport of transcriptional factors in neurons further propagates pathology throughout the brain[13]. Additional studies have revealed that cytoskeletal transport is impacted in AD including roles for SORL1 and Dyneins[82,100]. The observed dysfunctions of these and other proteins involved in cytoskeletal transport and the endocytic cycle has led to hypotheses describing that at least some of the downstream AD pathology is propagated by impaired vesicle transportation along the cytoskeleton causing a “traffic jam” along transportation conduits[41,84]. Given that RNA, proteins, and vesicles are transported along the same cytoskeletal network, competition may arise for transportation among all these cargos, and disruption of this critical system can impact cellular function as a whole. Thus, impacting RNA localization and translation thereof to elicit synaptic dysfunction and cognitive impairment.

To better understand questions pertaining to synapse biology and integrity, techniques have been optimized to collect synapses in the form of synaptosomes[56,57]. Synaptosomes are particles of synaptic material that form from the sheering forces during brain tissue homogenization. During homogenization, the dense, protein-rich membranes of synapses remain intact and pinch off from the larger plasma membrane allowing for the synapses to reseal and form individual particles and can be purified via gradient ultracentrifugation. The synaptosome model has frequently been used to analyze synaptic protein changes in AD[58-60,101,102]. This has led to discoveries including an upregulation of immune response pathways and downregulation of synaptic-signaling pathways[60]. Microarray analysis on AD human patient synaptosomes previously demonstrated an increase in localized synaptic genes and a decrease in metabolic genes. However, this data was not compared against expression changes in a brain homogenate background, and the analysis was limited to known mRNAs, precluding discovery and analysis of novel RNA species[78]. A study on mouse hippocampal synaptosomes derived from the 5xFAD model (bearing pathogenic variants in *APP* and *PSEN1*) that were droplet sequenced and compared to single nuclei sequencing showed synaptic mRNA

localization differences in inflammatory pathway related genes[67]. Thus, synaptosomes offer an unparalleled opportunity to investigate the localized regulatory processes and mRNA expression differences in the context of brain aging and AD.

It is well-appreciated that several species of non-coding RNAs exist that fine-tune RNA and protein expression, including locally at the synapse. Circular RNAs (circRNAs) are non-coding RNAs serving regulatory functions that have been gaining more appreciation in the study of AD. CircRNAs are produced by back-splicing a downstream exon's 3′ end, the "Donor", to a preceding exon's 5′ end, the "Acceptor", creating a closed-loop structure. CircRNAs are primarily formed from conserved exon junctions, are stable due to exonuclease resistance, and can exceed linear counterparts in abundance by an order of magnitude[48,103-105]. Several properties of circRNAs lend themselves as unique regulators in neurobiology. Some circRNAs are translated and others can act as sponges for microRNAs[106-108]. Their expression is highest in the brain, especially synaptic vesicles and exosomes and accumulate during rodent postnatal development[109,110]. However, the role of circRNAs in synapses and in neurodegeneration and AD remains poorly understood.

To fill this gap, we herein utilized brain tissue from human AD samples and a transgenic mouse model of fAD to identify mislocalized coding and non-coding RNAs in synaptosomes. We discovered significant mRNA localization differences in AD brains compared to cognitively healthy controls. We also identified major differences among circRNAs localized to synapses in AD. Among our data, we discovered two unique isoforms of *circGSK3β* that are differentially expressed in AD. These differential expression changes among non-coding RNAs may reveal novel mechanisms of synaptic regulation critical to the development of AD and neurodegeneration.

2.3 Methods

2.3.1 Human brain samples

Human brain tissue samples used in this study were derived from brains donated for research by participants in the UW ADRC and the Kaiser Permanente Washington (KPW) ACT study, including 11 donors with neuropathologically-confirmed AD dementia, and 12 cognitively healthy individuals with no or low AD neuropathologic change (**S2.1 Table**). The ACT study is a community-based cohort study in Seattle, WA in which KPW patients 65 years or older are randomly invited to join the ACT study and, if cognitively normal, are enrolled and undergo cognitive screening every two years until they convert to dementia, withdraw from the study, or die; a subset of ACT participants consent to donate their brains for research[111]. The UW ADRC is a mostly clinic-based study of participants with varying levels of cognitive impairment who are followed annually with a battery of neuropsychometric tests until they withdraw from the study or die, and most consent to donate their brains for research. In selecting donors for this study, cognitive status and AD and related dementias neuropathologies were considered, with donors with AD dementia carefully matched with non-demented controls for age, sex, and post-mortem interval (PMI). All samples were collected following approved protocols with informed consent as approved by the University of Washington Institutional Review Board (IRB). Tissues were collected during rapid brain autopsy and flash frozen in liquid nitrogen or supercooled isopentane. For 16 of the samples, we acquired tissues from both the frontal lobe (middle frontal gyrus – dorsolateral prefrontal cortex) and temporal lobe (middle temporal gyrus) which were preserved in 0.32M sucrose, 25mM tris buffer. Other samples we collected were from the frontal lobe which were preserved by flash-freezing in isopentane.

2.3.2 Mouse brain samples

The University of Washington Institutional Animal Care and Use Committee (IACUC) approved all mouse studies (protocol 4387-01). Mice were maintained on an irradiated diet and provided free access to filtered water, with housing conditions maintained as previously described[112]. Following CO_2 asphyxiation according to AVMA guidelines, brains were dissected from a mouse line bearing the APP Swedish mutation (K595N/M596L) and deletion of *PSEN1* exon 9 in the C57BL/6J background with WT littermates used as controls[113]. Brains were sectioned based on brain regions, of which the frontal cortex was used for sequencing.

2.3.3 Synaptosome Isolation and RNA extraction

We adapted established protocols to isolate synaptosomes[56,57]. Approximately 300 mg of brain tissue was homogenized using a glass douncer in 1.5 mL of homogenization buffer: 0.32 M sucrose, 1 mM sodium bicarbonate, 1 mM magnesium chloride, 0.5 mM calcium chloride, 100 µM aurintricarboxylic acid, 24 U/mL NEB Murine RNAse inhibitor, and 0.5x Thermo HALT protease and phosphatase inhibitor cocktail. Following homogenization, 120 µL of homogenate was set aside for RNA extraction and sequencing and additional analyses. The remaining homogenate was spun down at 750 × g for 10 min at 4ºC to remove debris. Next the supernatant was centrifuged at 13,800 × g to produce a pellet of crude synaptosomes. The supernatant was collected as the cytoplasmic fraction. The crude synaptosome pellet was resuspended in 1 mL of homogenization buffer. A discontinuous sucrose gradient was prepared in a 4.2 mL ultracentrifuge tube with a 1 mL bottom layer of 1.2 M sucrose + 1 mM sodium

bicarbonate, 1 mL middle layer of 1.0 M sucrose + 1 mM sodium bicarbonate, and a 1 mL top layer of 0.85 M sucrose + 1 mM sodium bicarbonate. The 1 mL of resuspended crude synaptosome was layered on top of the gradient. The samples were then spun using a swinging bucket rotor in an ultracentrifuge at 28,000 rpm (~82,000 × g). The purified synaptosomes were collected from the interface between the 1.2 M and 1.0 M layers. RNA was subsequently extracted from 500 µl of the collected synaptosomes with Trizol/chloroform. We validated synaptosome isolation by western blot.

2.3.4 Synaptosome protein analysis

Protein from the homogenate, crude P2 pellet, cytoplasm S2, and isolated synaptosome fractions were precipitated using methanol/chloroform extraction. Proteins were resolubilized in 1% SDS, 100 mM triethylammonium bicarbonate and 15 min bath sonication. Protein concentrations were estimated using Qubit (Thermo) and equal amounts were set aside for western blot loading. Blot quantification conducted with FIJI software (Image J). Antibodies: Mouse anti-actin (mAbGEa) (Invitrogen: MA51-744), Rabbit anti-NeuN (Invitrogen: PA5-78499), Rabbit anti-synaptophysin (SP11) (Invitrogen: MA5-14532), Mouse anti-IBA1 (Proteintech: 66827-1-Ig). IR dye 680 goat anti-rabbit (LI-COR: 926-68071), IR dye 800 goat anti-mouse (LI-COR: 926-32210).

2.3.5 Sequencing

100 ng of RNA from synaptosome and pre-fractionated homogenate fractions were aliquoted for library preparation using the Illumina stranded total RNA with rRNA removal (human). Samples were barcoded and pooled into batches of twelve for sequencing submission

to GeneWiz (Azenta) using 2 x 150 bp reads, on an Illumina NovaSeq S4 instrument. Data was delivered as fastq files pertaining to each sample. Prior to data analysis, sequencing data quality was evaluated using the fastp tool available on the Galaxy online platform. All samples passed accepted thresholds (examples in **S2.16A** and **S2.16B Fig**).

2.3.6 Data analysis for localization

Transcriptome mapping and quantification was conducted with Salmon[114]. Transcriptome references were retrieved from Gencode (version 33 Homo sapiens, and version M31 Mus musculus). Salmon quant files for each sample were imported into R for differential expression analysis using the DESeq2 package and workflow[115,116]. Expression analysis was normalized based on default DESeq2 parameters which takes into account the total number of reads as well as the length of each gene. We first ran DESeq2 on a dataset of all samples with (design = ~ Fraction + Condition). We filtered our gene list by having ten counts in at least nine samples. From this, we used sample clustering and multidimensional scaling analysis to identify outliers and hierarchical clustering and weighted gene correlation analysis (WGCNA) to identify confounding variables[117]. WGCNA parameters included all defaults with adjustments as follows: maxblocksize=10500, power=9, corType = "bicor", networkType = "signed", TOMType = "signed", deepSplit = 3, minModuleSize = 24, stabilityCriterion = "Individual fraction", reassignThreshold = 0.00001, and mergeCutHeight = 0.15. The single variable that stood out most was the way in which the brain tissue was preserved. Some frontal lobe samples were sucrose preserved, while some samples were preserved by isopentane; all temporal lobe samples were sucrose preserved. If we ran DESeq2 using

"preservative" as our variable of comparison in synaptosome data, we saw substantial differences in RNA expression. We successfully corrected for this phenomenon using the software ComBat-Seq treating "preservative" as a batch variable[118]. This correction nearly eliminated the variation as seen before (**S2.17A** and **S2.17B Fig**). After batch correction and removing outliers, clustering of sample distances and multidimensional scaling analysis showed robust separation and clustering of synaptosomes vs homogenate and modest separation and clustering of disease status (**Fig 2.1D** and **S2.1B**). A minor confounding variable determined by WGCNA was age. We did not correct for age or incorporate it into our interpretation of results. PMI, RIN score, sex, and *APOE* genotype did not show significant effects on data clustering and not considered as confounding variables.

To conduct localization analysis on a brain region, we first created four separate datasets corresponding to control samples, AD samples, homogenate samples, and synaptosome samples. We ran DESeq2 independently on each dataset. We filtered our gene list by having ten counts in at least nine samples. Next, we applied batch correction using ComBat-Seq based on preservative for frontal lobe samples; we did not apply batch correction for temporal lobe nor mouse frontal lobe samples[118]. To identify synaptosome enriched transcripts, we ran DESeq2 differential expression analysis on either the control dataset or AD dataset using results ("Fraction", "Synaptosome", "Homogenate"). To identify differentially expressed genes between AD and control in either the homogenate or synaptosome datasets we ran results ("Condition", "AD", "Control").

To determine mislocalized transcript differences, we first made a ratio-of-ratios comparing the synaptosome results fold change to homogenate results fold change as such:

$$Fold\ Change = \log_2 \frac{\left(\frac{AD}{Control}\right)_{Synaptosome}}{\left(\frac{AD}{Control}\right)_{Homogenate}}$$

To construct a *p* value, we assumed a normal distribution of the synaptosome $\log_2$ fold change versus homogenate $\log_2$ fold change values from a y=x (i.e. 1:1) trendline as pictured in **Fig 2.2D**. We therefore calculated a difference of $\log_2$ fold changes of AD vs control between the synaptosome value and the homogenate value weighted by their standard error for each measured transcript. We calculated the weighted $\log_2$ fold change differences across all measured transcripts to produce a T-statistic based on the assumption that the weighted $\log_2$ fold change differences follow a normal distribution along y=x. A *p* value was drawn from a two-tailed normal distribution with N-1 degrees of freedom and setting an FDR cutoff of 0.001 for the frontal lobe and 0.01 for the temporal lobe and mice due to differences in sample sizes. Our formula for calculating a T-statistic per gene is represented by:

$$T = \frac{R_w}{\frac{\sqrt{\frac{\sum_{i=1}^{number\ of\ genes} {R_w}^2}{number\ of\ genes}}}{\sqrt{Number\ of\ Samples}}}$$

Where:

$$R_w = \frac{1}{SE} \times \log_2 \left(\frac{AD}{Control}\right)_{Synaptosome} - \frac{1}{SE} \times \log_2 \left(\frac{AD}{Control}\right)_{Homogenate}$$

R_w represents the difference in $\log_2$ fold changes of AD vs control weighted by their respective standard errors between. Since DESeq2 calculates differential expression using a Wald statistic, our approach could be interpreted as simply taking a T-statistic between the Wald statistics. This resulted in a selection of significantly measured mislocalized mRNAs representing the expected fraction of a transcript's reads found in synaptosomes compared to homogenate is different in AD versus control. This

could represent errors specifically in RNA transport or degradation dynamics within the neurites independent of global expression changes.

Gene ontology analysis was conducted using GOpanther “biological process complete”[119]. Genome alignments for visualization were conducted using RNA-STAR[120]. Human genomes were aligned to GRCh38 and mouse genomes were aligned to GRCm39 acquired from Ensembl.

2.3.7 CircRNA identification

We generated a custom back-spliced junction database by adding all possible permutations of exon combinations in which a downstream exon’s 3′ end, the “Donor”, is joined to the 5′ end of an upstream exon, the “Acceptor”. Next, we generated bowtie2 indexes for both the back splice junction file and the Gencode v. 33 reference transcriptomes. The samples’ fastq files were first mapped to the reference canonical transcriptome using bowtie2[121]. Unmapped reads were extracted from the resultant alignment files using samtools[122]. The unmapped read files were then converted into fastq files using bedtools[123]. Next these fastq files were mapped to the back splice junction index with bowtie2. CircRNA read alignments were counted for each sample producing a count matrix. This count matrix was then appended to the count matrix of linear canonical transcript unnormalized counts and imported back into R to run DESeq2 differential expression analysis on the combined counts to normalize in context of the rest of the transcriptome. We filtered our circRNA list by having four counts per unique circRNA in at least five samples. To test our approach against DCC, we used the standard workflow and settings including the preliminary alignment using RNA-STAR[124].

2.3.8 miRNA site analysis

To identify miRNA binding sites, the biomaRt package was used to obtain 3′UTR sequences for all genes we measured which were then input into Targetscan producing a result table counting all miRNA binding sites within each UTR across the transcriptome[125,126]. To predict miRNA binding site enrichment among significantly mislocalized mRNAs, the UTRs were retrieved for our short-list and using Targetscan v. 7.0, and we produced a count table of all miRNA binding sites. Using our transcriptome-wide miRNA site index as a background, we calculated the expected values for each miRNA binding site distributed among our short-lists. We calculated a $\log_2$ fold change based on the ratio of observed vs expected fraction each miRNA was represented out of the total number of identified binding sites (i.e. the fraction of total binding sites for a miRNA found within our short list versus the fraction of total binding sites for said miRNA throughout the entire transcriptome). We calculated significance of miRNA binding site enrichment using a χ^2 test.

2.3.9 PCR validation

PCR amplicons for circRNAs were designed with primers that would amplify the back splice junction. We then Sanger sequenced these amplicons to validate the junctions. Primers are listed in **S2.32 Table**.

2.3.10 Circ plasmids

We ordered custom synthesized plasmids from Genscript designed with *GSK3β* exon inserts between Alu elements in the pcDNA3.1+ backbone designed, proven, and published to coax RNA circularization (Addgene #60648)[127].

2.3.11 Transfections

SH-Sy5y cells, obtained from ATCC, were differentiated into neurons using an abbreviated protocol based on Shipley et al[128]. Undifferentiated cells were cultured in a 50/50 mixture of DMEM/F12 media supplemented with 15% heat inactivated fetal bovine serum (FBS) plus 1% penicillin/streptomycin solution. Undifferentiated cells were passaged into T25 flasks to begin differentiation on day 0. On day 1, media was swapped to 3% FBS solution supplemented with 10 μM all-trans retinoic acid. On day 3, media was swapped to 1% FBS solution supplemented with 10 μM all-trans retinoic acid. On day 5 cells were passaged onto Geltrex (Gibco) coated 6 well plates, 120,000 cells each. On day 6, media was refreshed, and transfections took place using lipofectamine using 1.5 μg plasmid with 5 μl per well in 250 μl Opti-MEM. On day 7, media was swapped to Neurobasal plus media supplemented with 1x B27 plus, 2 mM Glutamax, 1% penicillin/streptomycin, 20 mM potassium chloride, 50 ng/mL BDNF, 2 mM dibutyryl cyclic AMP, and 10 μM all-trans retinoic acid. Media was refreshed on day 9, day 11, and day 12. Cells were harvested on day 13 with 1 mL RIPA buffer and sonicated in a bath at 4ºC for 15 min. Protein was quantified with qubit for equal loading in western blot. Blot quantification conducted with FIJI software (Image J) We validated circular RNA formation using PCR and Sanger sequencing where we confirmed bands associated with the complete circle and proper splicing (data not shown). Antibodies include: rabbit anti-GSK3β (Cell systems:

D5C5Z), rabbit anti-pS9-GSK3β (Cell systems: D85E12), mouse anti-pS202,T205-tau (AT8) (Invitrogen: MN1020), mouse anti-tau (Tau5) (Invitrogen: AHB0042), rabbit anti-GAPDH (Cell Systems: 14C10), Mouse anti-beta tubulin (BT7R) (Invitrogen: MA5-16308), Rabbit anti-NeuN (Invitrogen: PA5-78499), Rabbit anti-synaptophysin (SP11) (Invitrogen: MA5-14532), IR dye 680 goat anti-mouse (LI-COR: 926-68070), IR dye 680 goat anti-rabbit (LI-COR: 926-68071), IR dye 800 goat anti-mouse (LI-COR: 926-32210), IR dye 800 goat anti-rabbit (LI-COR: 926-32211).

2.3.12 BaseScope in situ hybridization

Custom BaseScope probes spanning the *GSK3β* circRNA exon 10-to-9 and exon 9-to-7 junctions of NM_002093.4 were designed and ordered by ACD. In addition, we designed a similar probe to the mRNA sequence of *GSK3β* that is not part of the circRNA. The BaseScope duplex reagent kit and protocol was used for hybridization. Brain slices of a square area approximately 0.3 cm x 0.3 cm from our frontal lobe sample collection were sectioned via cryostat into 20 µm sections onto Superfrost Plus slides. Brain tissue slides were fixed using chilled 4% formaldehyde in PBS for 15 min. Next, the slides were dehydrated by a 5 min wash with 50% ethanol, a 5 min wash with 70% ethanol, and two 5 min washes in 100% ethanol. Slides were dried at room temp before proceeding with the BaseScope Duplex protocol. The only modification to the protocol was extending the AMP step [11] to 40 min instead of 30 min. *CircGSK3β* exon 9-to-7 and *CircGSK3β* 10-to-9 were visualized using Fast-Green chromogenic reagent. Linear *GSK3β* visualized using Fast-Red chromogenic reagent. Nuclear and membrane stained using 0.5x Gil's hematoxylin. Slides were imaged in brightfield on a Nikon Ti-2 microscope. Quantification was done by research scientists uninvested in the final

outcome whereby mRNA molecules were counted and summed among 8 images per tissue.

2.3.13 Synaptosome confocal microscopy

We followed a modified protocol previously utilized for synaptosome immunohistochemistry [61]. First, bovine serum albumin coated slides were prepared by immersing the slides in 3% BSA, PBS and sodium azide overnight at 4ºC. Slides were subsequently washed with PBS and left to dry. 0.5 cm x 0.5 cm squares were drawn on the slides with nail polish. 250 µL synaptosomes were diluted 5x in PBS in microcentrifuge tubes. They were spun down at 12,000 × g for 20 min at 4ºC. The synaptosome pellet was resuspended in 50ul PBS. 5ul of resuspended synaptosomes were added to each outlined square on the BSA coated slides. This was followed by the addition of 5 µl of PBS. Next, 10 µl of 8% formaldehyde was added to the synaptosomes on the square. Synaptosomes were allowed to fix at room temperature for 1 hour. Next, excess liquid was aspirated from the squares leaving synaptosomes fixed on the slides. Excess formaldehyde was quenched with 35 µl of 100 mM glycine. Excess liquid was aspirated. Synaptosomes were stained with the lipophilic fluorophore FM1-43, 20 µl at 5 µg/mL concentration for 5 min at room temperature. Excess stain was aspirated. Stained synaptosomes were washed with 35 µl PBS for 10 min at room temperature. Excess liquid was aspirated. Drops of Vectashield mounting media were placed within the squares and coverslips placed on top. Coverslips were sealed with nail polish. Slides were imaged on an Olympus FV-1000 confocal in the GFP channel.

2.4 Results

2.4.1 Synaptosome sequencing identifies mRNAs enriched and localized to synapses.

We obtained post-mortem human brain samples from participants in the University of Washington (UW) Alzheimer's Disease Research Center (ADRC) and the Adult Changes in Thought (ACT) Study based at Kaiser Permanente Washington[111]. We acquired frontal lobe (prefrontal cortex) samples from 23 individuals including donors with late-onset sAD and healthy controls. For 16 of these individuals, we also studied tissue samples from the temporal lobe (middle temporal gyrus). Patient samples were carefully selected to match for age, postmortem interval, and neuropathological features. A benefit from the ADRC and ACT programs is that the post-mortem interval (PMI) for collection is less than eight hours substantially reducing the impact of PMI as a confounding variable (**Table 2.1; S2.1 Table**).

We isolated synaptosomes from frontal lobe brain samples using a well-established sucrose gradient protocol (**Fig 2.1A**)[56,57]. We validated our technique by western blot of common markers demonstrating enrichment of synaptophysin in the synaptosome fraction and depletion of the neuronal marker NeuN as well as the robust elimination of the glial marker IBA1 in control samples (**Fig 2.1B** and **2.1C**). Fractionation was similar in the AD samples (**S2.1A Fig**). Furthermore, for a visual confirmation, we imaged particles in the synaptosome fraction using a fluorescent lipophilic stain by confocal microscopy. We observe particles of the expected 0.5-1.5μm size, several of which appear as bipartite structures indicative of joined pre-synaptic and post-synaptic terminals (**S2.1B Fig**). After synaptosome isolation, we extracted RNA from the bulk synaptosome fraction as well as from the pre-fractionated homogenate that served as a background with which to compare the expression at synapses. We subsequently

performed RNA sequencing using a ribo-removal stranded total RNA kit to capture coding RNAs and non-coding RNAs lacking poly-A tails, such as circRNAs. After measuring read counts, we analyzed sample variability using sample distance clustering and multidimensional scaling analysis (**Fig 2.1D** and **S2.1C**). This analysis revealed robust clustering distinctly separating synaptosome and homogenate fractions as well as between AD and control albeit with more variability among the AD samples compared to the control samples. We ran hierarchal clustering on the expression data and discovered no other confounding variables except a possible contribution from patient age (**S2.1D Fig**). Critically, we did not identify PMI, RNA integrity number (RIN), sex, or *APOE* alleles, to be confounding variables. The lack of any other variables confounding our analyses of interest on Fraction, and Condition after batch correction was confirmed by weighted gene correlation analysis (see methods and **S2.14 Fig**). We repeated multidimensional scaling analysis focusing on groups of samples including only control (**S2.2A Fig**) and only AD (**S2.2B Fig**) which substantiated robust separation of homogenate vs. synaptosome in both groups. We also looked at only homogenate (**S2.2C Fig**) and only synaptosome (**S2.2D Fig**) which showed more distinct profiles among AD vs. control in the synaptosome fraction compared to the homogenate.

To identify RNAs enriched at synapses in the frontal lobe, we first compared RNA abundance differences between synaptosomes versus the pre-fractionated homogenate in control samples. This resulted in 3,402 significantly enriched mRNAs at synapses ($p < 0.01$). Notably, synaptically-enriched mRNAs are still a minority of all measured mRNAs detected in control tissue while most mRNAs were still preferentially localized elsewhere in the bulk homogenate including in the cytoplasm, nucleus, and non-neuronal cells (**Fig 2.1E**; **S2.2 Table**). We similarly analyzed the synaptosome transcriptome in the frontal lobe AD samples (**S2.1E Fig**; **S2.3 Table**). We observed a very strong correlation between the control and AD samples ($R^2 = 0.9266$) (**Fig 2.1F** and **2.1G**). Successful synaptic-transcriptome enrichment was validated by high expression of PSD-95 (Discs Large MAGUK scaffold protein 4; *DLG4*) in synaptosomes

vs. homogenate. Other notable synaptic transcripts we observe include activity related cytoskeleton associated protein (*ARC*), calcium/calmodulin dependent protein kinase II alpha (*CAMK2A*), and SH3 and multiple ankyrin repeat domains 3 (*SHANK3*). Another telltale signature of synaptosome fractionation is the alternative splicing of fused in sarcoma (*FUS*) mRNA where we observe intron retention isoforms specifically in nuclear transcripts (**S2.3 Fig**). We also analyzed GO biological process enrichment in the synaptic transcriptome and discovered that synaptic-localized mRNAs are significantly enriched in translation, metabolic functions, and organelle organization processes (**Fig 2.1H**). To this end, some notable gene families are represented among our synapse-enrichment data including several eukaryotic translation initiation factors (*EIF1-EIF6*). We also observed an enrichment of motor proteins including dyneins and kinesins, as well as RNA-binding proteins including Fragile-X mental retardation protein (*FMR1*).

Table 2.1 Human brain sample properties.

Brain tissue donors including sAD patients and cognitively healthy controls were recruited by the University of Washington Alzheimer's Disease Research Center and the Kaiser Permanente Adult Changes in Thought (ACT) study. Brain tissue was collected from the frontal lobe (dorsolateral prefrontal cortex) of 23 individuals and temporal lobe (middle temporal gyrus) from 16 of the aforementioned 23 individuals. PMI: Postmortem Interval.

Group	Samples (n)	PMI (hrs)	Age (yrs)	Sex	Thal Phase	Braak Stage
Frontal Lobe:						
Control	12	4.8 ± 1.8	87.6 ± 6.7	11F, 1M	0 – 3	I - III
Sporadic AD	11	5.4 ± 1.4	86.0 ± 9.0	10F, 1M	4 – 5	V - VI
Temporal Lobe:						
Control	8	4.3 ± 0.8	87.3 ± 7.7	7F, 1M	0 – 3	I - III
Sporadic AD	8	5.6 ± 1.0	86.5 ± 4.1	7F, 1M	4 – 5	V - VI

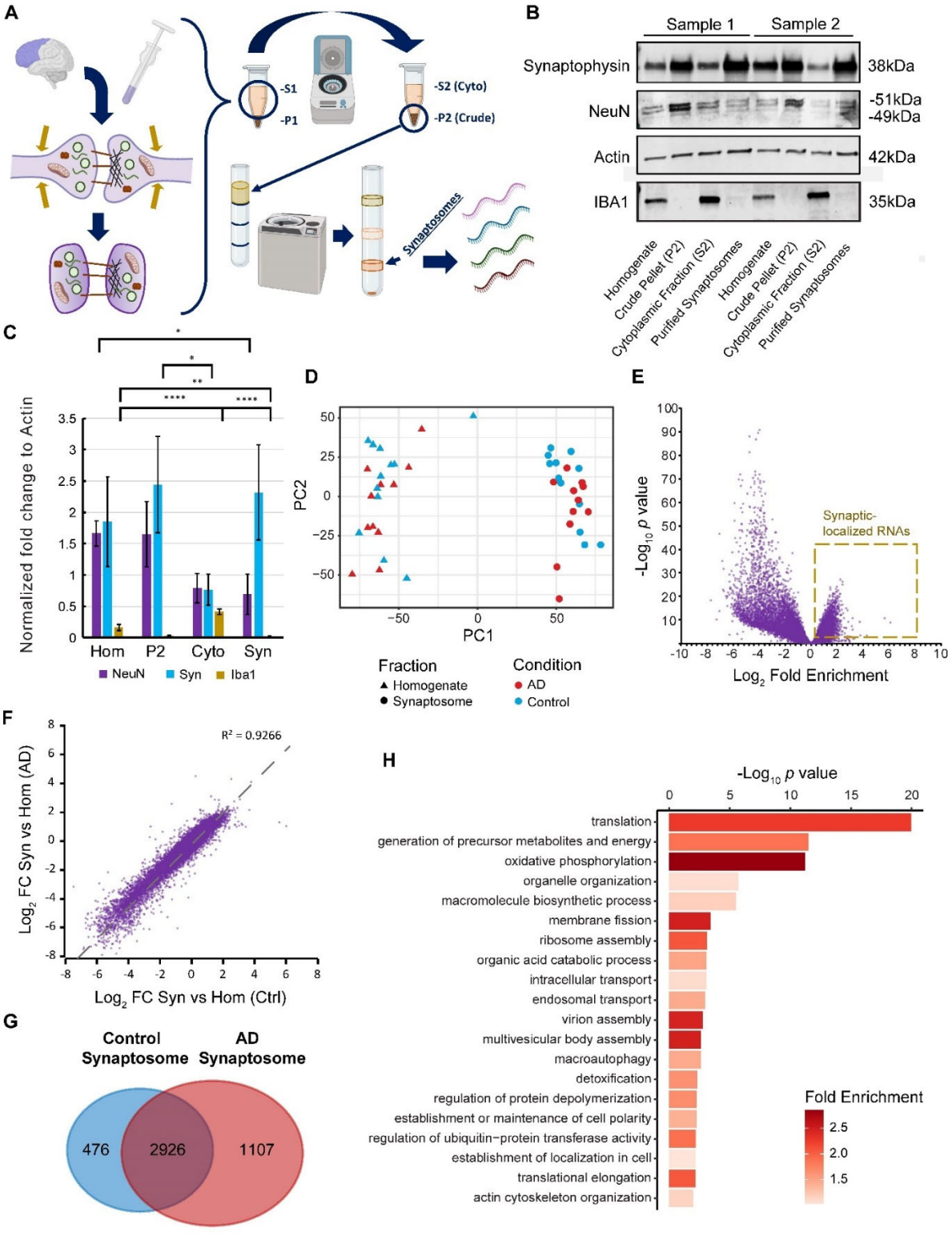
A
-S1
-P1
-S2 (Cyto)
-P2 (Crude)
Synaptosomes
B
Sample 1
Sample 2
Synaptophysin
38kDa
NeuN
-51kDa
-49kDa
Actin
42kDa
IBA1
35kDa
Homogenate
Crude Pellet (P2)
Cytoplasmic Fraction (S2)
Purified Synaptosomes
C
Normalized fold change to Actin
Hom
P2
Cyto
Syn
NeuN
Syn
Iba1
D
PC2
PC1
Fraction
Homogenate
Synaptosome
Condition
AD
Control
E
-Log10 p value
Synaptic-localized RNAs
Log2 Fold Enrichment
F
R² = 0.9266
Log2 FC Syn vs Hom (AD)
Log2 FC Syn vs Hom (Ctrl)
G
Control Synaptosome
AD Synaptosome
476
2926
1107
H
-Log10 p value
translation
generation of precursor metabolites and energy
oxidative phosphorylation
organelle organization
macromolecule biosynthetic process
membrane fission
ribosome assembly
organic acid catabolic process
intracellular transport
endosomal transport
virion assembly
multivesicular body assembly
macroautophagy
detoxification
regulation of protein depolymerization
establishment or maintenance of cell polarity
regulation of ubiquitin−protein transferase activity
establishment of localization in cell
translational elongation
actin cytoskeleton organization
Fold Enrichment
2.5
2.0
1.5

Fig 2.1. RNA sequencing of synaptosomes is an effective strategy for identifying localized RNA transcripts in the human frontal lobe. A. Schematic of synaptosome isolation, which are particles formed during the shearing forces of brain tissue homogenization whereby synaptic terminals pinch-off and reseal to form intact bipartite particles consisting of pre- and post-synaptic compartments. Based on their density, synaptosomes can be purified by sequential centrifugation steps concluding with gradient ultracentrifugation. After purification, the RNA contents of synaptosomes can be isolated and sequenced. *Figure created using a biorender.com license.* **B.** Western blot of a synaptic marker, synaptophysin, a nuclear marker, NeuN, and a microglial marker, IBA1, for the different fractionation steps during synaptosome preparation in control samples. **C.** Quantification of the blot in (**B**). N=4 per group. Significance calculated via T-test. *: $p < 0.05$, **: $p < 0.01$, ****: $p < 0.0001$. **D.** Multidimensional scaling analysis demonstrating separation between mRNA counts of homogenate and synaptosome fractions as well as variability between sporadic AD samples and controls. **E.** Volcano plot comparing synaptosome vs homogenate mRNA enrichment in only control samples. A distinct minority of mRNAs are significantly enriched at synaptic terminals ($p < 0.01$, gold box). **F.** Correlation between the fold change/enrichment of synaptosome vs homogenate between AD and control ($R2 = 0.9266$). **G.** Venn diagram demonstrating overlap of synaptosome enriched genes between AD and control samples. **H.** GO biological process analysis of synaptosome-enriched genes.

2.4.2 Significant mRNA localization differences occur at AD synapses

First, we analyzed the frontal lobe sequencing data from synaptosomes and homogenate separately and compared AD and control in each case (**Fig 2.2A** and **2.2B**; **S2.4** and **S2.5 Table**). We saw substantially more differentially expressed mRNAs (2,998; $p < 0.05$)

in the synaptosome data, compared to the homogenate (380; $p < 0.05$). 134 of these mRNAs overlapped and 98% were concordant in their direction of $\log_2$ fold-change expression differences (**Fig 2.2C**). Given the high concordance between synaptosome and homogenate fractions, it may be the case that significantly differentially expressed mRNAs at synapses are merely a result of global expression changes. Therefore, we wanted to understand the extent to which mRNA differences at the synapse in AD occurred as a result of changes in how mRNAs were transported and localized to the synapse in addition to global expression changes. We refer to this as "mislocalization" in which the expected fraction of a transcript's reads sequenced within the synaptosome fraction compared to the homogenate is different in AD versus control. The exact mechanism by which an mRNA becomes mislocalized in AD has yet to be determined, though it could be hypothesized this is a result of errors in cytoskeletal transport or the degradation dynamics of mRNAs within neurites.

To identify mislocalized mRNAs at synapses in AD, we compared the $\log_2$ fold change between AD and control of each mRNA in synaptosomes to that of AD vs control in homogenate (**Fig 2.2D**). This analysis showed that mRNA expression differences between AD and control in synaptosomes are largely uncorrelated with global expression changes and deviates from a 1:1 trendline ($R^2 = 0.2327$). To identify mislocalized RNAs, we calculated the ratio of $\log_2$ fold change of AD to control in the synapse to the $\log_2$ fold change of AD to control in the homogenate to determine the fold change of mislocalization. We calculated a *p* value based on the deviation from a 1:1 (i.e. y = x) trendline by assuming a normal distribution while also accounting for the standard error of the respective $\log_2$ fold change measurements (see methods for additional details). This analysis resulted in the identification of 1,198 significantly mislocalized mRNAs in the frontal lobe synapses of AD brains (FDR < 0.001), 712 of which were upregulated and 483 were downregulated (**S2.6 Table**). We found that by clustering results and visualizing them in a heatmap, these mislocalized mRNAs form distinct blocks

representing independent expression changes in synaptosomes versus homogenate (**S2.4A Fig**). Gene ontology analysis of the upregulated mRNAs revealed enrichment of anatomical structure morphogenesis, developmental process, cell differentiation, and cell-adhesion biological processes (**Fig 2.2E**). The downregulated mRNAs showed enrichment of vascular endothelial cell proliferation, response to osmotic stress, signaling, and ion import across the plasma membrane (**Fig 2.2F**).

Next, we compared results from frontal lobe to results from the temporal lobe. First, we ran sample distance clustering and multidimensional scaling analysis. Similar to the frontal lobe, we observed robust separation between the synaptosome and homogenate fractions as well as between AD and control (**S2.5A** and **S2.5B Fig**). We then ran multidimensional scaling analysis in 3D to compare the frontal lobe samples to the temporal lobe samples (**Fig 2.3A**). This analysis revealed that principal component 1 distinctly separated the synaptosome and homogenate fractions among both frontal lobe and temporal lobe samples, principal component 2 appeared to explain variation between AD and control, while principal component 3 appeared to distinguish between the frontal lobe and temporal lobe brain regions, notably with less variation that of the other components. Sample distance clustering similarly reflected these observations (**S2.5C Fig**). Via heatmap, it appeared that clustering of disease status defined sample mRNA expression patterns preceding the clustering of brain regions, and most importantly synaptosome versus homogenate took overall precedence (**S2.6A Fig**).

Next, we analyzed synaptic enrichment of mRNAs in the temporal lobe. There was a similar pattern where a minority of mRNAs were synaptosome enriched (**S2.7A Fig; S2.7 Table**). This was also observed in the AD temporal lobe tissue with a strong correlation between AD and control (R^2 = 0.8955) (**S2.6B** and **S2.7C Fig; S2.8 Table**). Comparing synaptic enrichment between temporal lobe and frontal lobe among our control samples also showed a strong correlation (R^2 = 0.886) (**Fig 2.3B** and **2.3C**). We analyzed AD versus control in the temporal lobe separately between the homogenate and synaptosome fractions and discovered

many more significant differences in mRNA expression between them ($p < 0.05$). 568 of these differentially expressed mRNAs overlapped between the fractions with 99% having a concordant directionality in $\log_2$ fold change (**S2.7D-F Fig; S2.9** and **S2.10 Tables**).

We repeated our mislocalization analysis on the temporal lobe samples. We found a moderately stronger (41% larger) correlation between synaptosome and homogenate expression differences between AD and control ($R^2 = 0.3281$) (**Fig 2.3D**). Given a stronger correlation, there were fewer mislocalized genes in the temporal lobe versus the frontal lobe with very little overlap between the two brain regions (**Fig 2.3E**). This showed only 351 upregulated mRNAs and 222 downregulated ones (FDR < 0.01; **S2.11 Table**). GO analysis indicated enrichment of trans-synaptic signaling, cell surface receptor signaling, neurotransmitter secretion, and protein localization to the presynapse biological processes among upregulated mRNAs (**Fig 2.3F**). Among downregulated mRNAs there was an enrichment of microtubule-based movement regulation, regulation of calcium-mediated signaling, and neuron projection guidance (**Fig 2.3G**). As was the case for the frontal lobe, hierarchical clustering of mRNA expression showed distinct blocks representing disproportional expression changes between AD and control between the synaptosome and homogenate fractions (**S2.7G Fig**).

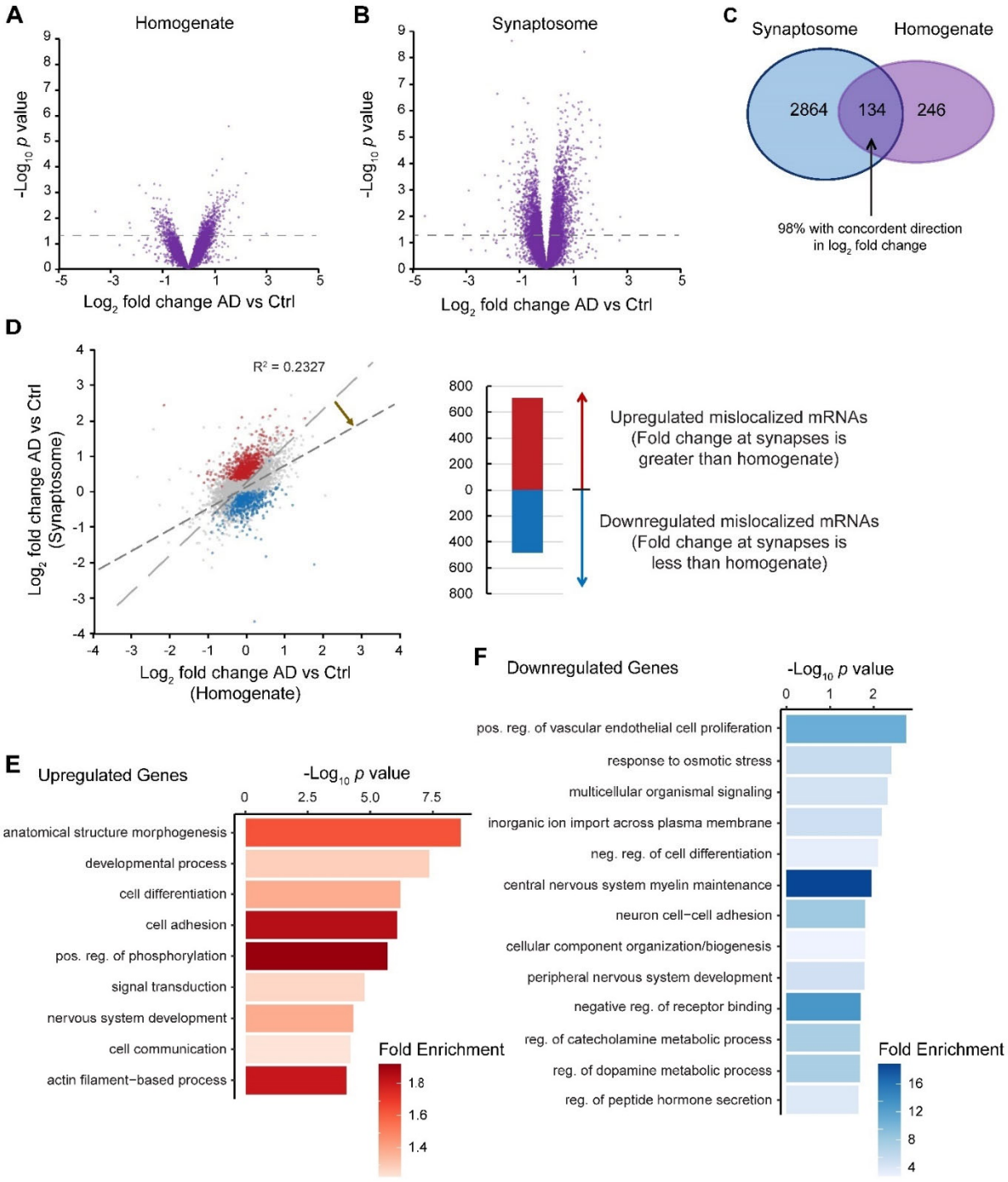
A
Homogenate
-Log10 p value
Log2 fold change AD vs Ctrl
B
Synaptosome
-Log10 p value
Log2 fold change AD vs Ctrl
C
Synaptosome
Homogenate
2864
134
246
98% with concordent direction in log2 fold change
D
R² = 0.2327
Log2 fold change AD vs Ctrl (Synaptosome)
Log2 fold change AD vs Ctrl (Homogenate)
Upregulated mislocalized mRNAs (Fold change at synapses is greater than homogenate)
Downregulated mislocalized mRNAs (Fold change at synapses is less than homogenate)
E
Upregulated Genes
-Log10 p value
anatomical structure morphogenesis
developmental process
cell differentiation
cell adhesion
pos. reg. of phosphorylation
signal transduction
nervous system development
cell communication
actin filament−based process
Fold Enrichment
F
Downregulated Genes
-Log10 p value
pos. reg. of vascular endothelial cell proliferation
response to osmotic stress
multicellular organismal signaling
inorganic ion import across plasma membrane
neg. reg. of cell differentiation
central nervous system myelin maintenance
neuron cell−cell adhesion
cellular component organization/biogenesis
peripheral nervous system development
negative reg. of receptor binding
reg. of catecholamine metabolic process
reg. of dopamine metabolic process
reg. of peptide hormone secretion
Fold Enrichment

Fig 2.2. Comparison between AD and control in synaptosomes vs homogenate reveals mislocalized transcripts in the human frontal lobe. A. Volcano plot comparing expression differences between AD and control in the bulk, unfractionated homogenate. **B.** Volcano plot comparing expression differences between AD and control just within the synaptosome particles. **C.** Venn diagram comparing the significant expression differences in homogenate (**A**) and synaptosome (**B**). **D.** Comparison of the fold changes of AD vs control between synaptosomes and homogenate (R^2 = 0.2327). Genes that have a T-statistic most distant from a y=x trendline are significantly mislocalized, independent of global expression changes (FDR < 0.001, see methods). **E.** GO biological process analysis of upregulated genes in (**D**). **F.** GO biological process analysis of downregulated genes in (**D**).

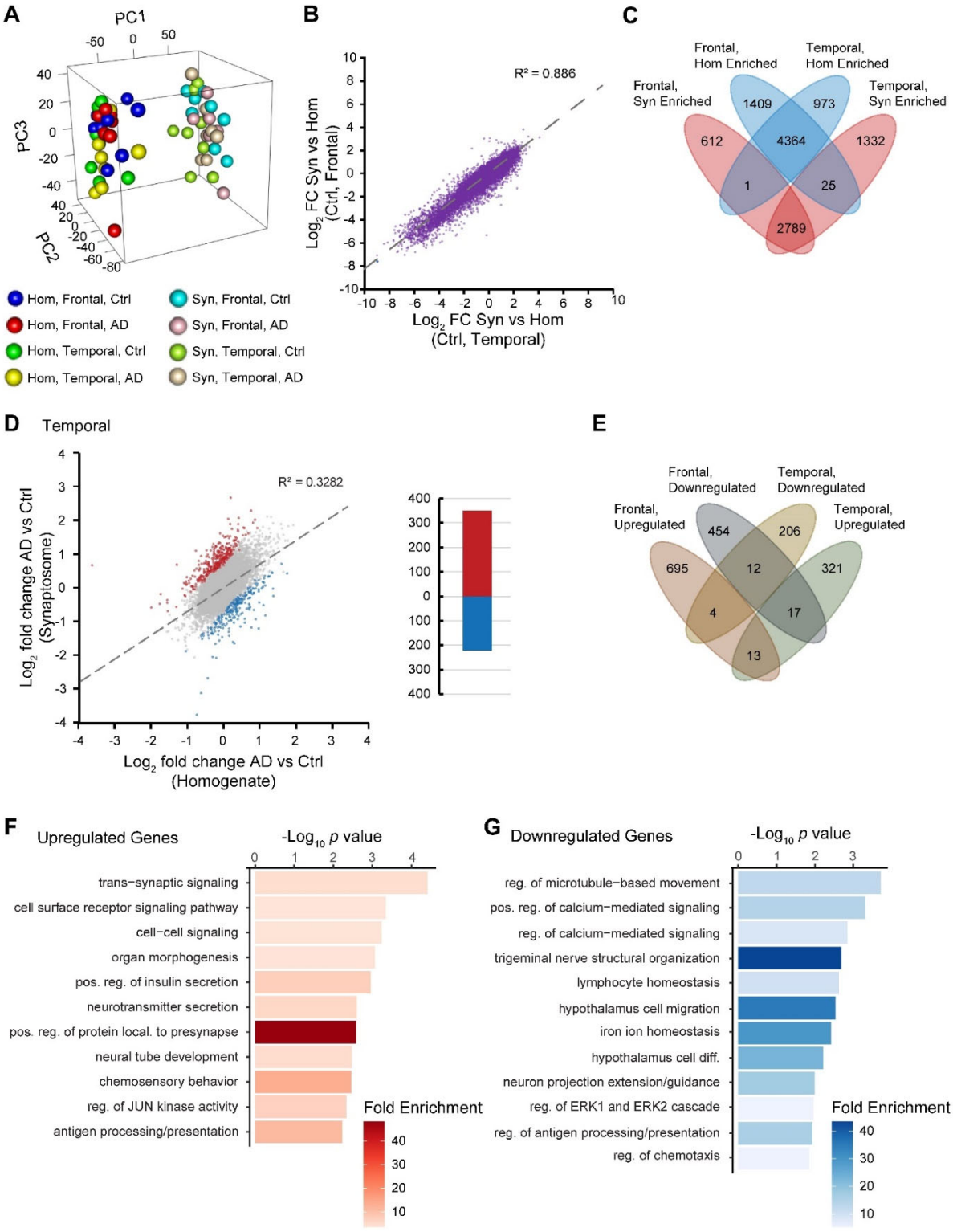
A
PC1
PC3
PC2
Hom, Frontal, Ctrl
Hom, Frontal, AD
Hom, Temporal, Ctrl
Hom, Temporal, AD
Syn, Frontal, Ctrl
Syn, Frontal, AD
Syn, Temporal, Ctrl
Syn, Temporal, AD
B
R² = 0.886
Log2 FC Syn vs Hom (Ctrl, Frontal)
Log2 FC Syn vs Hom (Ctrl, Temporal)
C
Frontal, Hom Enriched
Temporal, Hom Enriched
Frontal, Syn Enriched
Temporal, Syn Enriched
1409
973
612
4364
1332
1
25
2789
D
Temporal
R² = 0.3282
Log2 fold change AD vs Ctrl (Synaptosome)
Log2 fold change AD vs Ctrl (Homogenate)
E
Frontal, Downregulated
Temporal, Downregulated
Frontal, Upregulated
Temporal, Upregulated
454
206
695
12
321
4
17
13
F
Upregulated Genes
-Log10 p value
trans−synaptic signaling
cell surface receptor signaling pathway
cell−cell signaling
organ morphogenesis
pos. reg. of insulin secretion
neurotransmitter secretion
pos. reg. of protein local. to presynapse
neural tube development
chemosensory behavior
reg. of JUN kinase activity
antigen processing/presentation
Fold Enrichment
G
Downregulated Genes
-Log10 p value
reg. of microtubule−based movement
pos. reg. of calcium−mediated signaling
reg. of calcium−mediated signaling
trigeminal nerve structural organization
lymphocyte homeostasis
hypothalamus cell migration
iron ion homeostasis
hypothalamus cell diff.
neuron projection extension/guidance
reg. of ERK1 and ERK2 cascade
reg. of antigen processing/presentation
reg. of chemotaxis
Fold Enrichment

Fig 2.3. Synaptosome sequencing in the human temporal lobe reveals similarities among synaptosome-enriched transcripts and differences in mislocalized transcripts. A. Multidimensional scaling analysis among the frontal lobe and temporal lobe samples. **B.** Comparison of synaptosome-enriched transcripts between frontal and temporal lobe samples (R^2 = 0.886). **C.** Venn diagram showing overlap of synaptosome-enriched transcripts between frontal and temporal lobe samples (p < 0.01). **D.** Comparison of the fold changes of AD vs control between synaptosomes and homogenate in temporal lobe samples (R^2 = 0.3282). Genes that have a T-statistic most distant from a y=x trendline are significantly mislocalized, independent of global expression changes (FDR < 0.01, see methods). **E.** Venn diagram showing minimal overlap of mislocalized transcripts between frontal and temporal lobe samples. **F.** GO biological process analysis of upregulated genes in (**D**). **G.** GO biological process analysis of downregulated genes in (**D**).

2.4.3 Synaptosome sequencing findings in the APP/PSEN1 mouse model are poorly correlated with findings from human samples.

Finally, given the difficulties with studying functional consequences of mislocalized RNAs in human samples, we wanted to examine whether the well-studied APP^{swe}/$PSEN1^{dE9}$ mouse model recapitulated the differences we observed in our human datasets[113]. We sequenced homogenates and synaptosome fractions from mouse frontal cortex tissue including six WT control and eight APP/PSEN1 aged mutant mice matched closely for age (**S2.8A Fig**). Using sample distance clustering and multidimensional scaling analysis, we found more robust separation and less variation between AD and WT compared to the human samples in addition to the distinct separation between the synaptosome and homogenate fractions (**S2.8B** and **S2.8C Fig**).

When we analyzed the sequencing data between synaptosome and homogenate in mouse frontal lobe, we also found a small selection of mRNAs that were synaptic enriched, which was also strongly correlated between AD and control (R^2 = 0.8913) (**Fig 2.4A**, **S2.9A**, and **S2.9B**; **S2.12** and **S2.13 Tables**). However, we did not find this model to reflect the differences we observed among our human frontal lobe samples. Comparing synaptic enriched mRNAs between control mouse and human frontal lobe tissue, we observed a weak correlation (R^2 = 0.2164) with very little overlap between the two species (**Fig 2.4B** and **2.4C**). Next, we looked at significant expression differences between AD and control separately in homogenate and synaptosome. We found that 105 mRNAs overlapped between the fractions with 92% having concordant directionality in $\log_2$ fold change (**S2.9C-E Fig**; **S2.14** and **S2.15 Tables**).

We conducted our mislocalization analysis and found 280 upregulated and 268 downregulated mRNAs. Only 13 of these mRNAs overlapped with our human frontal lobe data (**Fig 2.4D** and **2.4E**; **S2.16 Table**). GO analyses seemed to contrast with the human data as well with upregulated mRNAs being enriched for immune-related biological processes and cell projection assembly (**Fig 2.4F**). In addition, downregulated mRNAs were enriched for extracellular structure organization, carbohydrate transmembrane transport, transforming growth factor beta activation, and (interestingly) response to amyloid-beta (**Fig 2.4G**).

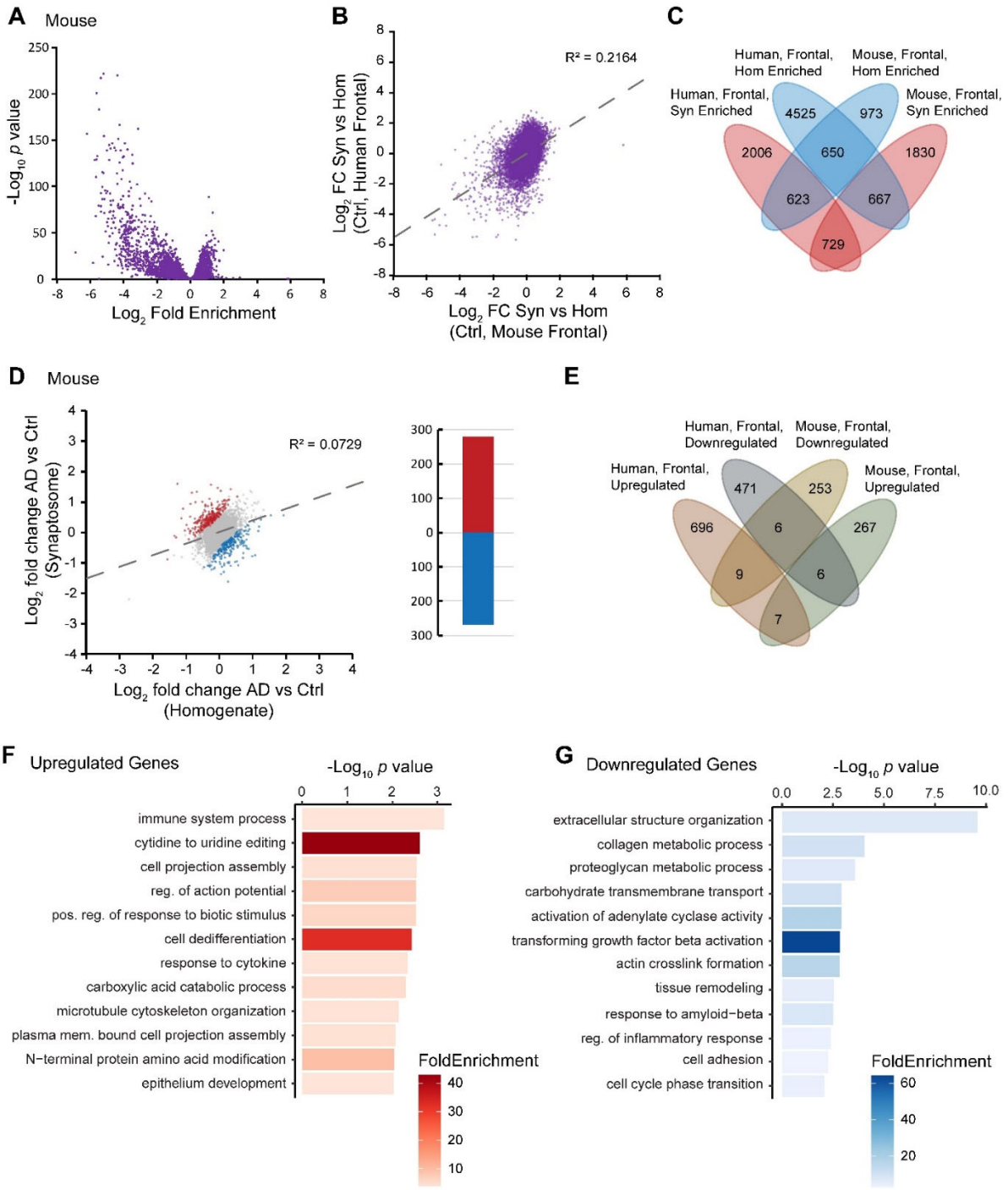
A
Mouse
-Log10 p value
Log2 Fold Enrichment
B
R² = 0.2164
Log2 FC Syn vs Hom (Ctrl, Human Frontal)
Log2 FC Syn vs Hom (Ctrl, Mouse Frontal)
C
Human, Frontal, Hom Enriched
Mouse, Frontal, Hom Enriched
Human, Frontal, Syn Enriched
Mouse, Frontal, Syn Enriched
4525
973
2006
650
1830
623
667
729
D
Mouse
R² = 0.0729
Log2 fold change AD vs Ctrl (Synaptosome)
Log2 fold change AD vs Ctrl (Homogenate)
E
Human, Frontal, Downregulated
Mouse, Frontal, Downregulated
Human, Frontal, Upregulated
Mouse, Frontal, Upregulated
471
253
696
6
267
9
6
7
F
Upregulated Genes
-Log10 p value
immune system process
cytidine to uridine editing
cell projection assembly
reg. of action potential
pos. reg. of response to biotic stimulus
cell dedifferentiation
response to cytokine
carboxylic acid catabolic process
microtubule cytoskeleton organization
plasma mem. bound cell projection assembly
N-terminal protein amino acid modification
epithelium development
FoldEnrichment
G
Downregulated Genes
-Log10 p value
extracellular structure organization
collagen metabolic process
proteoglycan metabolic process
carbohydrate transmembrane transport
activation of adenylate cyclase activity
transforming growth factor beta activation
actin crosslink formation
tissue remodeling
response to amyloid-beta
reg. of inflammatory response
cell adhesion
cell cycle phase transition
FoldEnrichment

Fig 2.4. Synaptosome sequencing of frontal lobe samples from the APP^{swe}/PSEN1^{dE9} AD and wild-type mouse models reveals substantial differences in transcript localization patterns from that of human samples. A. Volcano plot comparing synaptosome vs homogenate in wild-type mouse samples (FDR < 0.001). **B.** Comparison of synaptosome-enriched transcripts between mouse and human frontal lobe samples (R^2 = 0.2164). **C.** Venn diagram showing overlap of synaptosome-enriched transcripts between human and mouse frontal lobe samples (p < 0.01). **D.** Comparison of the fold changes of AD vs control between synaptosomes and homogenate in temporal lobe samples (R^2 = 0.0729). Genes that have a T-statistic most distant from a y=x trendline are significantly mislocalized, independent of global expression changes (FDR < 0.01, see methods). **E.** Venn diagram showing minimal overlap of mislocalized transcripts between mouse and human and mouse frontal lobe samples. **F.** GO biological process analysis of upregulated genes in (**D**). **G.** GO biological process analysis of downregulated genes in (**D**).

2.4.4 Synaptic-localized RNAs in mouse aligns with independent studies

Recently, a study was published in which individual 5xFAD and control mouse hippocampus synaptosomes and nuclei were sorted into droplets and sequenced[67], though concerns have been raised regarding the study's methodology and synaptosome purity[129]. We conducted a comparison analysis between our data and Niu et al's to highlight differences in our approaches.

There are notable differences between our methods presented here and Niu et al.'s approach. The most significant is that instead of using bulk pre-fractionated homogenate as the background, Niu et al. used single nuclei RNAseq as their background to compare synaptosome localization. The drawback is that this approach would only identify nascent mRNAs while the

benefit being that cell type diversity, specificity, and clustering can add new dimensions to interpreting the data. Remarkably we found substantial similarity in synaptic-localized mRNAs with a modest correlation of $R^2 = 0.58$ and an overlap of 1155 genes (**S2.10A** and **S2.10B Fig**) while a minority of mRNAs show opposite compartmental enrichment.

We repeated our mislocalization analysis on their data and discovered an entirely different repertoire of mislocalized mRNAs within the mouse hippocampus reflecting tissue differences akin to the differences observed between human frontal and temporal lobes as well as differences between the 5xFAD and APP/PSEN1 mouse models (**S2.10C Fig**). We found that 147 genes were upregulated including *Nrxn1/3*, *Calm3*, and *Camk2a/b*, as well as 21 downregulated including *Mef2c* and *Septin7*.

2.4.5 Mislocalized mRNAs are enriched for particular microRNA (miRNA) binding sites

Another recent publication presented a study in which miRNA abundance was quantified in AD and control human synaptosomes which found an upregulation of miR-502-3p, miR-103a-3p, and miR-501-3p among AD synaptosomes[130]. In an attempt to postulate mechanisms relating to mislocalized mRNAs, we analyzed miRNA binding sites in the 3′UTRs of differentially expressed mRNAs and found striking patterns. Among the frontal cortex upregulated mislocalized mRNAs, we observed an enrichment of 241 miRNA binding sites compared to background frequencies (FDR < 0.05) including miR-101, miR-203, and miR-501-5p (**S2.11A Fig**; **S2.17 Table**). We found 309 binding sites that were enriched among the frontal lobe downregulated mRNAs including miR-10, miR-22, miR-138, and miR-503 (**S2.11B Fig**; **S2.18 Table**). A notable observation is that miRNAs that are enriched among the upregulated mRNAs are correspondingly de-enriched among the downregulated mRNAs and vice versa. In the temporal upregulated

mislocalized mRNAs, we saw an enrichment of 360 sites including miR-22, miR-138, miR-151, and miR-503 (**S2.11C Fig**; **S2.19 Table**). In the temporal downregulated mRNAs, we saw an enrichment of only 8 miRNA binding sites including miR-296-3p, miR-145 and miR-181 (**S2.11D Fig**; **S2.20 Table**). These data can support the hypothesis that these miRNAs are also mis-expressed in AD and contribute towards mRNA stability at synapses suggesting a mechanism behind their mislocalization.

2.4.6 CircRNAs are enriched at synapses and show significant localization differences in AD

Despite considerable advances in circRNA biology, the primary mechanistic role(s) of most circRNAs are still uncertain (**Fig 2.5A**). We wanted to understand whether there are differences among circRNA species localized to synapses in AD. To identify circRNAs, we analyzed our sequencing data for reads mapping to back-splice junctions by an alignment strategy where we first mapped our RNA sequence reads to canonical transcripts and subsequently extracted the unmapped reads. From there, we aligned the reads to a file containing all possible back splice junctions including 150 bp on either side within each canonical transcript (**Fig 2.5B**).

First, we calculated expression differences between synaptosomes and pre-fractionated homogenate from human frontal lobe control samples (**Fig 2.5C**; **S2.21 Table**). We found that the overwhelming majority (2,276) of circRNAs are enriched and localized to synapses compared to unfractionated homogenate ($p < 0.001$). An identical pattern was seen in the frontal lobe AD samples, and correlation between AD and control was moderate ($R^2 = 0.3928$) (**S2.12A** and **S2.12B Fig**; **S2.22 Table**). This is consistent with observations from previous studies in rodents demonstrating that circRNAs are enriched at synapses[49,51,104,110]. Next, we

compared circRNA expression differences between AD and control in the frontal lobe homogenate samples (**Fig 2.5D**; **S2.23 Table**). Here we found 20 upregulated and 90 downregulated circRNAs ($p < 0.05$). Given the observation of high synaptic enrichment of circRNAs, we focused on differences between AD and control among the synaptosome data. We found more substantial differences in circRNA synaptic expression including 87 upregulated and 220 downregulated circRNAs (**Fig 2.5E**; **S2.24 Table**). Only 9 of these differentially expressed circRNAs overlapped between the homogenate and synaptosome fractions (**Fig 2.5F**). We visualized these circRNA expression trends by hierarchical clustering (**Fig 2.5G**). From this we confirmed that expression changes in circRNAs between AD and control take place exclusively at the synapse independent of changes in the unfractionated homogenate. To visualize how circRNA expression varies across the samples, we conducted multidimensional scaling analysis exclusive to circRNA counts (no linear counts). We observed more variation among the synaptosome samples between AD and control, and more uniformity among the homogenate samples (**S2.12C Fig**). Another intriguing observation was the predicted length of circRNAs we observed. The majority of circRNAs have back-splice junctions that are between 2 and 4 exons apart (**S2.12D Fig**). Furthermore, a number circRNAs consist of only a single exon spliced back on itself.

One of the most noteworthy discoveries from the frontal lobe synaptosome circRNA data was the observation of isoform switches within the same genes between AD and control (**Table 2.2**). For example, *ATF6* showed an exon 9-to-2 isoform that is downregulated in AD synapses while simultaneously there is an exon 15-to-10 isoform that was upregulated.

When analyzing the human temporal lobe data, there was a similar trend where circRNAs are substantially enriched in the synaptosome fraction (**S2.13A Fig**; **S2.25 Table**). We also observed a moderate correlation of circRNA synaptic enrichment between temporal and frontal lobes ($R^2 = 0.4843$) (**S2.13B Fig**). We similarly conducted a multidimensional scaling analysis among the temporal lobe samples exclusive to circRNA counts. This showed similar

trends to the frontal lobe circRNA clustering (**S2.13C Fig**). In the temporal lobe homogenate fraction, we observed 99 upregulated and 35 downregulated circRNAs in AD versus control (**S2.13D Fig**; **S2.26 Table**). In the temporal lobe synaptosome fraction, we found 218 upregulated and 52 downregulated circRNAs (**S2.13E Fig**; **S2.27 Table**). Between the temporal lobe synaptosome and homogenate fractions, only 10 of these circRNAs overlap as differentially expressed between AD and control (**S13F Fig**). Finally, between temporal lobe synaptosomes and frontal lobe synaptosomes, 17 circRNAs overlap with only 65% as being similarly differentially expressed between AD and control (**S2.13G Fig**).

CircRNAs among our mouse frontal lobe samples demonstrated little similarity to what we observed in the human samples. Though we found that circRNAs are still prominently enriched in synaptosomes, these identifications were less abundant and pronounced, encapsulating only 200 circRNAs ($p < 0.01$) (**S2.14A Fig**; **S2.28 Table**). Among mouse frontal lobe synaptosomes, between AD and control, we saw upregulation of 83 circRNAs and downregulation of 83 circRNAs (**S2.14B Fig**; **S2.29 Table**).

We sought to benchmark our novel approach to identifying circRNAs against another popular software, DCC[124] which has been used previously in AD research[131]. In contrast to the DCC method which relies on the chimeric junction files produced by RNA STAR, we create a custom fasta junction reference which substantially narrows the search space and boosts sensitivity to identify unique splice isoforms of coding exons (**Fig 2.5B**). We tested DCC on our human frontal lobe RNA seq data following standard DCC workflow and settings, and the software detected 2374 total circRNAs, while our approach detected 3999 circRNAs. We repeated our synaptosome analysis using the DCC data and found 1080 circRNAs significantly enriched in synaptosomes, 752 of which aligned with our data where we discovered 2,276 (**S2.30 Table**). Next, we compared AD synaptosomes to control synaptosomes and DCC found 296 significant differentially expressed circRNAs, 45 of these overlapped with our finding of 307 circRNAs (**S2.31 Table**).

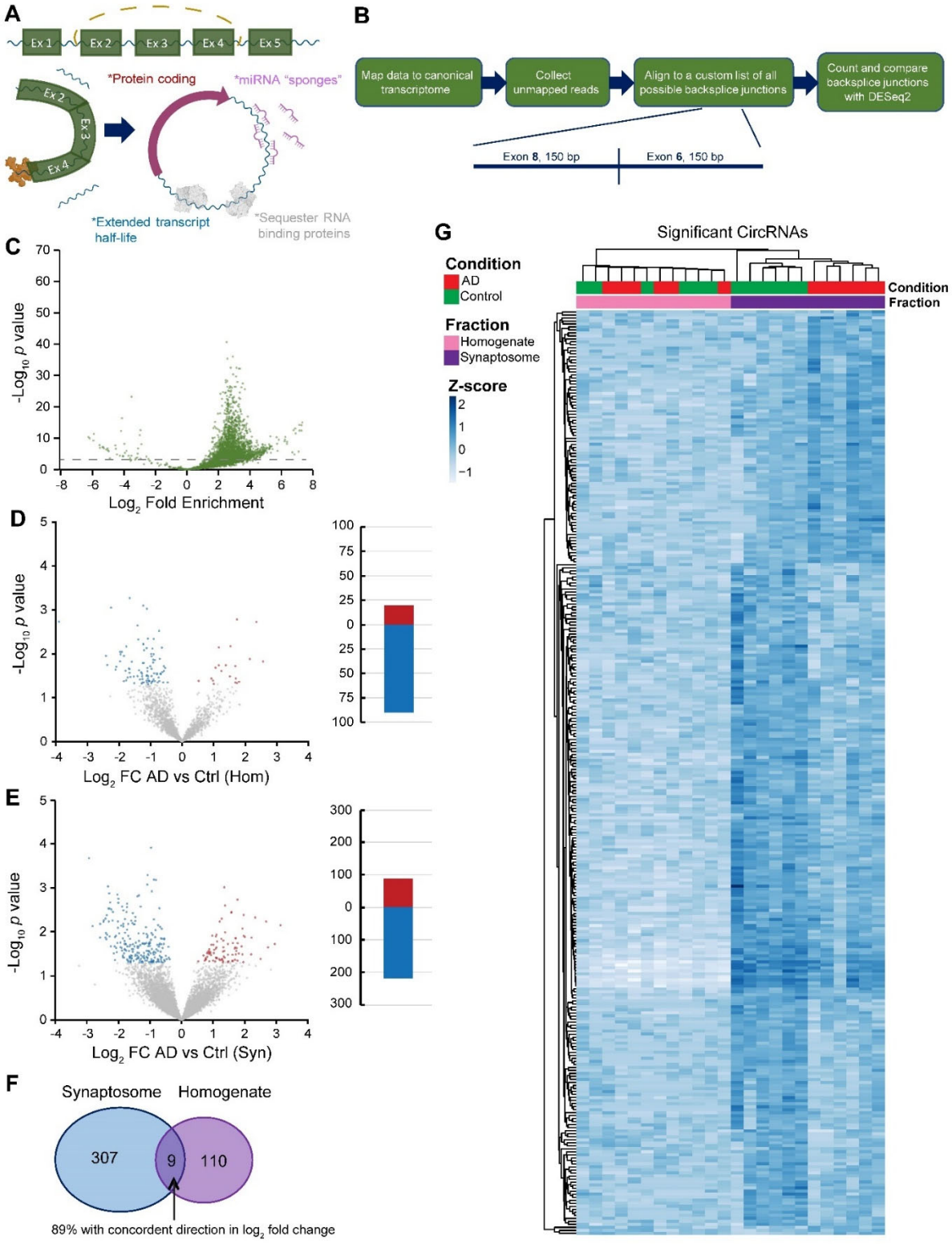
A
Ex 1
Ex 2
Ex 3
Ex 4
Ex 5
*Protein coding
*miRNA "sponges"
*Extended transcript half-life
*Sequester RNA binding proteins
B
Map data to canonical transcriptome
Collect unmapped reads
Align to a custom list of all possible backsplice junctions
Count and compare backsplice junctions with DESeq2
Exon 8, 150 bp
Exon 6, 150 bp
C
-Log10 p value
Log2 Fold Enrichment
D
-Log10 p value
Log2 FC AD vs Ctrl (Hom)
E
-Log10 p value
Log2 FC AD vs Ctrl (Syn)
F
Synaptosome
Homogenate
307
9
110
89% with concordent direction in log2 fold change
G
Significant CircRNAs
Condition
AD
Control
Fraction
Homogenate
Synaptosome
Z-score
Condition
Fraction

Fig 2.5. Analysis of circular RNAs in synaptosomes shows their preferential localization to synapses and substantial differences in AD samples. A. Schematic of circular RNAs (circRNAs) that are formed by back-splicing a later exon onto a preceding exon. *Figure created using a biorender.com license.* **B.** Workflow for analyzing circRNAs includes first mapping the sequencing data to the canonical transcriptome. Second, unmapped reads are extracted from the alignment file. Third, unmapped reads are aligned to a custom list of all possible back-splice junctions within genes including 150bp flanking each side. Finally, reads mapping to back splice junctions are counted and differential expression is evaluated using DESeq2. **C.** Volcano plot comparing circRNAs in synaptosome vs homogenate in control frontal lobe samples. The overwhelming majority of circRNAs are significantly enriched at synaptic terminals. **D.** Volcano plot comparing circRNAs in AD vs control in the unfractionated homogenate ($p < 0.05$). **E.** Volcano plot comparing circRNAs in AD vs control in the synaptosome fraction ($p < 0.05$). **F.** Venn diagram showing overlap of AD vs control differentially expressed circRNAs between the homogenate and synaptosome fractions. **G.** Heatmap of differentially expressed circRNAs between AD vs control in synaptosomes. Differential expression is both independent of, and substantially greater than, the bulk homogenate.

Table 2.2 Examples of circRNA isoform switches between sAD and control in frontal lobe synaptosomes.

Comparing RNA sequencing data mapped to circRNA back-splice junctions between AD and control synaptosomes revealed that significant expression changes often arose from multiple circular isoforms originating from the same gene and would show contrasting fold changes. “Donor” refers to the downstream exon by which its 3′ end is spliced back onto the upstream “Acceptor” exon’s 5′ end. We report the raw *p* value.

Gene	Donor	Acceptor	Log_2 Fold Change	*p* value
ATF6	9	2	-2.81	0.00740
ATF6	15	10	1.94	0.00860
ATF6	14	10	-1.25	0.0363
ANKS1B	4	2	1.21	0.000585
ANKS1B	8	2	-1.01	0.0170
GSK3β	9	7	1.58	0.00370
GSK3β	10	9	-1.68	0.00666
UBA2	16	9	-1.84	0.00755
UBA2	16	10	1.49	0.0473

2.4.7 *CircGSK3β* isoforms show contrasting expression changes at AD synapses and can regulate protein and phosphorylation levels including for tau

One of the most intriguing discoveries from our human data concerned two distinct isoforms of *GSK3β*. A *circGSK3β* exon 9-to-7 isoform was upregulated in AD with a log_2 fold change of 1.58, while a *circGSK3β* exon 10-to-9 isoform was downregulated in AD with a log_2 fold change of -1.68 (**Fig 2.6A**). Importantly, these isoforms have not been previously established nor associated with AD. The GSK3β protein plays a well-established role in AD pathology given it is among the chief proteins that phosphorylate tau [111,132,133]. We validated the back-splice junctions using PCR and Sanger sequencing with an exon 9 forward primer and an exon 7 reverse primer and an exon 10 forward primer and an exon 9 reverse primer respectively (**Fig 2.6B**), and used similar methods to confirm another significant circRNA present in *HOMER1* (**S2.15A Fig**). To validate synapse localization and sequencing quantitative measurements we

probed human frontal cortex brain sections using BaseScope RNA *in situ* hybridization. We discovered that, indeed, these *circGSK3β* isoforms have a propensity to localize in neurites distal from the soma while the linear *GSK3β* isoform tends to be localized more proximal to the nucleus (**Fig 2.6C** and **S2.15B Fig**). We confirmed neurite enrichment by quantifying relative distance from the soma as marked by the nucleus (**S2.15C Fig**). We also discovered supporting evidence confirming the AD versus control expression differences of *circGSK3β* isoforms by analyzing BaseScope images (**S2.15D Fig**).

To investigate the biomolecular impacts of the *circGSK3β* isoform expression, we utilized a plasmid vector that coerces circRNA splicing by inserting circRNA-producing exons between two Alu elements (**Fig 2.6D**) [127]. We used this vector to transfect neuron-differentiated SH-Sy5y cells with *circGSK3β* isoforms and subsequently measured protein expression. We used a differentiation protocol incorporating retinoic acid and BDNF. We confirmed neural morphology as visualized under a light microscope (**S2.15E Fig**).We also validated successful neural differentiation by the enrichment of neural markers including NeuN and synaptophysin using western blot (**S2.15F** and **S2.15G Fig**) [128].

Compared to transfection with a control plasmid, we found that transfection of both the *circGSK3βx9-7* and *circGSK3βx10-9* isoforms resulted in reduced phospho-tau with the *circGSK3βx10-9* isoform impacting phospho-tau significantly more so than *circGSK3βx9-7* (**Fig 2.6E** and **S2.15H**). We also found transfection of both isoforms to result in reduced total GSK3β abundance and the *circGSK3βx10-9* isoform resulted in decreased phospho-Serine 9 GSK3β. When we compared the ratio of phosphorylated protein to total protein, we found that transfection of both *circGSK3β* isoforms resulted in reduced tau phosphorylation compared to control. However, *circGSK3βx10-9* in particular reduced tau phosphorylation significantly more than *circGSK3βx9-7* (**Fig 2.6F**). We did not find any significant differences in phosphorylated GSK3β. Taken together, these results demonstrate that these *circGSK3β* isoforms have contrasting impacts on tau and its phosphorylation.

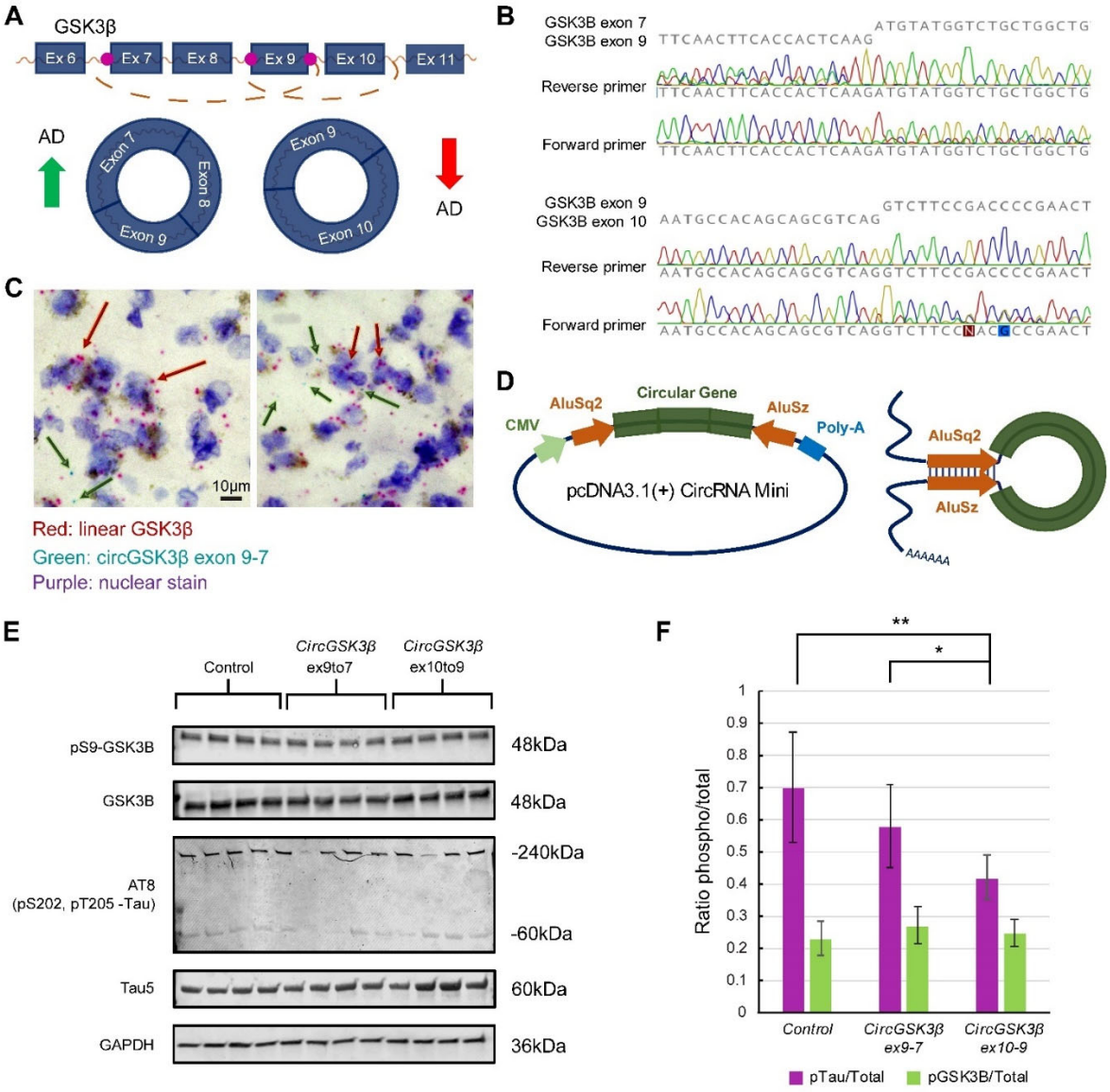

Fig 2.6. *CircGSK3β* isoforms show contrasting expression differences between AD and control and may play regulatory roles related to AD pathologies. A. Two distinct isoforms of *circGSK3β* with contrasting expression differences in AD. An isoform where exon 9 is back-spliced onto exon 7 is upregulated in AD, while an exon 10 spliced onto exon 9 isoform is downregulated. *Figure created with a biorender.com license.* **B.** Confirmation of *circGSK3β* isoform back-splice junctions by Sanger sequencing using primers flanking the splice junction. **C.** BaseScope RNA hybridization probes show that *circGSK3β* isoforms (green) are more

frequently distal to the nucleus than the linear *GSK3β* transcript (red) in human control frontal lobe brain slices. Tissue and nuclei were stained with hematoxylin. **D.** A specialized plasmid containing Alu elements coerces circular back-splicing of gene insert [127]. **E.** Western blot of neuron-differentiated SH-Sy5y cells transfected with either a control plasmid, a *circGSK3β exon 9-7* plasmid, or a *circGSK3β exon 10-9* plasmid. Cell lysates were probed for total Tau (Tau5), phospho-Tau (AT8), GSK3β, phospho-S9 GSK3β, and GAPDH. **F.** Quantification of the ratios between phospho-Tau and total Tau as well as between phospho-S9 GSK3β and total GSK3β in each of the transfection conditions in (**E**). N=8 samples per group. Significance calculated by T-test. *: $p < 0.05$, **: $p < 0.01$, ***: $p < 0.001$.

2.5 Discussion

Synaptosome sequencing reveals RNA mislocalization as a key feature of Alzheimer's disease. When a synapse is stimulated, rapid, local changes result in the activation of translational machinery on relevant, proximal RNAs[10,94,95]. Past studies have established synaptic-localized transcriptomes in cell culture and healthy models[52,54,55]. In this study, we sequenced the synaptic-localized transcriptomes of human brain tissue, and we discovered remarkable differences between AD patients and cognitively healthy, age-matched controls. We furthermore identified differences among different brain regions (frontal and temporal lobes), as well as differences from a popular mouse model of fAD. Therefore, our study reveals that the synaptic-localized transcriptome is perturbed in AD independent of global expression changes, which can impact proper localized translation and synaptic plasticity.

There may be several mechanisms responsible for this observation. One could be that there are differences in the abundance of RNA binding proteins to shuttle their respective RNA targets or that help protect mRNAs at the synapse from degradation[38,39,74,134-136]. It has been

shown that dysfunction of motor proteins such as the kinesin family affects the transport of mRNAs in neurons[46]. Another could be errors in alternative splicing and post-transcriptional processing that dictate RNA destinations[24,30,137]. There is substantial evidence that alternative 3′UTRs facilitate mRNA localization[23,27,54,66,97-99]. Although our ability to detect this phenomenon was limited, we nevertheless identified enrichment of particular microRNA binding sites within the 3′UTRs of mislocalized mRNAs suggesting that the interaction between 3′UTRs and microRNAs contributes to mRNA mislocalization. Alternatively, it could be that the efficiency of RNA cytoskeletal transport itself is impaired[41,82,84]. There is evidence that each of these mechanisms are impacted in AD, though it has been unknown how they could be connected to localized translation despite observations that localized translation was impaired in AD mouse synaptosomes[138]. We show that there is at least an impact of RNA localization to synapses in AD and a collection of specific transcripts that are common among sAD patients. This finding is underscored by the fact that changes in synaptic transcripts between AD and control are not correlated to homogenate differential expression between AD and control (**Fig 2.2D**, **2.3D**, and **2.4D**), thus indicating that transport of RNAs play a more critical role than global differential expression in synaptic function and degeneration.

The data produced from this study adds a new dimension to our understanding of neurodegeneration and AD. Overall, synaptic localized transcripts are largely congruent between AD and control, and between different brain regions. Importantly, hierarchical clustering methods continuously differentiate synaptosome expression from homogenate expression (**S2.2 Fig**). The difference is the ability of these transcripts to be properly trafficked and localized to the synapse independent of global expression changes in AD. Inefficiently localized RNAs may not be translated at their expected levels thereby impacting functions taking place at the synapse[52,54,138]. For example, GO analysis among the frontal lobe

mislocalized genes postulates that cell adhesion processes are largely affected (**Fig 2.2F** and **2.2G**). In addition, transcripts related to ion transport are downregulated which could provide a means of interpreting synaptic dysfunction in AD. On the other hand, GO terms among upregulated mislocalized transcripts in both the human frontal and temporal lobes relate to signaling, cell communication, and development. This finding could substantiate theories of neuronal overexcitability in AD[1,7]. Another finding is that the frontal lobe appears to be impacted differently than the temporal lobe. This is reflective of our understanding of the development and spread of AD pathology in the brain.

Something that stands out from this research is that this mouse model does not faithfully recapitulate our findings from human sAD brain tissue. There are stark contrasts between synaptic localized transcripts between wild type mice and non-demented humans, as well as contrasts in mislocalized transcripts between AD and control, perhaps reflecting species or mouse model differences. It is worth noting that the AD mouse model is more representative of fAD, as opposed to the sAD patients from which tissue was obtained considering that pathological and non-pathological features are more heterogeneous in sAD. Although mouse models have been extremely beneficial at studying hallmark aspects of AD, they may not be entirely suited for studying the complexity of mRNA transport and subsequent localized translation[139]. PMI and cause of death may also play a substantial role in transcript differences. Human samples were collected <8 hrs postmortem, while mice were euthanized via CO_2 and dissected within 2 hrs.

Our circRNA analysis reveals novel insights into possible mechanisms behind synaptic dysfunction. We discovered circRNAs are key regulatory molecules at synapses likely impacting protein expression. We find more than 200 circRNAs are misregulated in AD both in the frontal and temporal lobes. There are also stark differences between the brain regions. We compared our circRNA findings to the data produced from Dube et al. which was obtained from bulk homogenate[131]. We discovered considerable overlap between the data sets including

circHOMER1, which has previously been shown to be misregulated in AD, as well as *circATRNL1*, *circMAP7*, *circRTN4*, *circMLIP*, *circFMN1*, and *circICA1*[140]. A noteworthy finding from our data is that a selection of circRNAs show contrasts in the differential expression of different isoforms arising from the same gene, including two isoforms of *circGSK3β*: an exon 9-to-7 isoform that is upregulated and a 10-to-9 isoform that is downregulated in AD. These isoforms also have contrasting regulatory effects on tau phosphorylation when expressed in neural cell culture. This finding, in the context of a study demonstrating oligomeric tau can be spread by way of synaptic junctions, suggests that proper balance of these circRNA isoforms may slow the spread of tau pathology between neurons[141].

Future directions. Our discovery of two unique *circGSK3β* isoforms with differential expression in AD presents new targets for the development of AD therapeutics. We present evidence suggesting that these two isoforms play contrasting regulatory roles in the expression and phosphorylation of proteins relevant to AD progression including GSK3β and tau. Previously, attempts have been made to target GSK3β as a treatment for AD, though trials have been unsuccessful thus far[142,143]. Indeed, administration of the FDA-approved GSK3β inhibitor, valproic acid, may even worsen disease course in people with AD[92,144,145]. Therefore, innovative attempts to carefully restore the balance of these two isoforms may represent a potential treatment strategy. In addition, we identify hundreds of other circRNAs to be misregulated in AD, all of which could be playing consequential regulatory roles at the synapse. Our *circGSK3β* delivery experiments demonstrate successful expression and correct splicing of designed circular RNAs using a specialized plasmid created by Liang et al[127]. This paves the way for the design of viral payloads that could express circRNAs as gene therapies.

Our results also open a new avenue to test neuron and synaptic dysfunction in AD and neurodegenerative disease. Although we identify mislocalized RNAs, it remains

to be seen whether these mislocalized RNAs are also improperly translated upon synaptic stimulation. A follow-up study could include a Ribo-Seq approach to identify what transcripts are being actively translated[146,147]. Ideally, metabolically active synaptosomes could be isolated and stimulated, subsequently measuring protein translation over time [138].

In conclusion, we put forth a novel RNA-seq analysis of AD from human sAD brain synaptosomes and in the APP^{swe}/$PSEN1^{dE9}$ fAD mouse model. We highlight a rigorous approach to identify mislocalized synaptic RNAs. This includes both mRNAs, as well as many circRNAs, which could both be contributing to synaptic dysfunction and loss in AD or related neurodegenerative diseases. These datasets present a launching point for additional studies into the mechanisms by which RNAs become mislocalized and their corresponding impact on localized translation and synaptic function. Finally, we provide evidence that novel therapeutic strategies could be established to express circRNAs to regulate proteins at the level of synaptic translation.

2.6 Supplemental Data

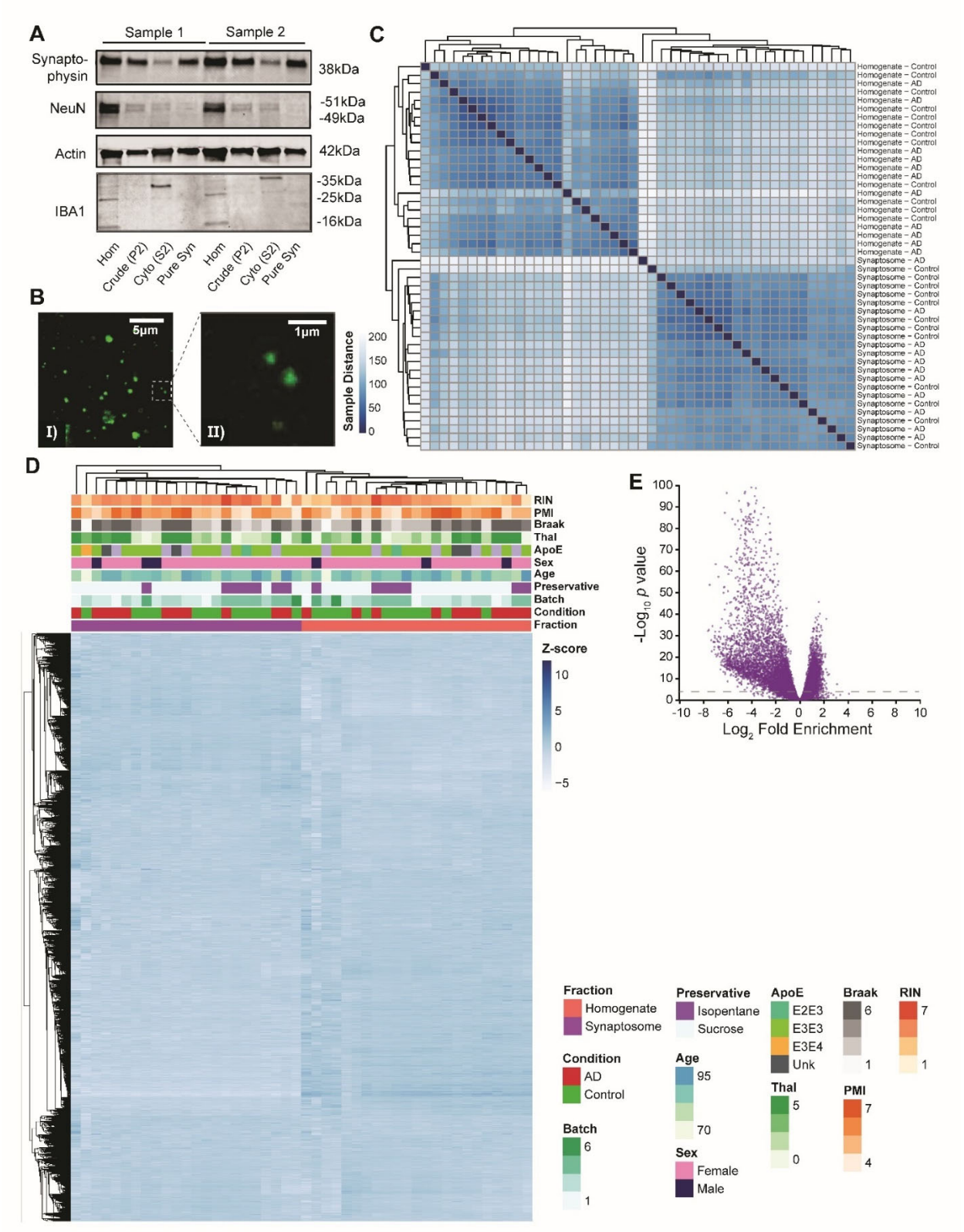

S2.1 Fig. Extended data for Fig 2.1; Human frontal lobe sample properties. A. Western blot

of a synaptic marker, synaptophysin, a nuclear marker, NeuN, and a microglial marker, IBA1, for the different fractionation steps during synaptosome preparation in AD samples. **B.** Fluorescent membrane staining and confocal imaging of the synaptosomal fraction shows intact bipartite structures of expected size. **C.** Sample distance heatmap showing robust clustering of synaptosome and homogenate fractions among AD and control frontal lobe samples. **D.** Heatmap substantiating robust clustering of synaptosome and homogenate fractions as well as minimal impact of other variables after batch correction including PMI, RIN, sex, and *APOE* alleles. **E.** Volcano plot comparing synaptosome vs homogenate in AD samples shows the same pattern as control samples in (See **Fig 2.1E**).

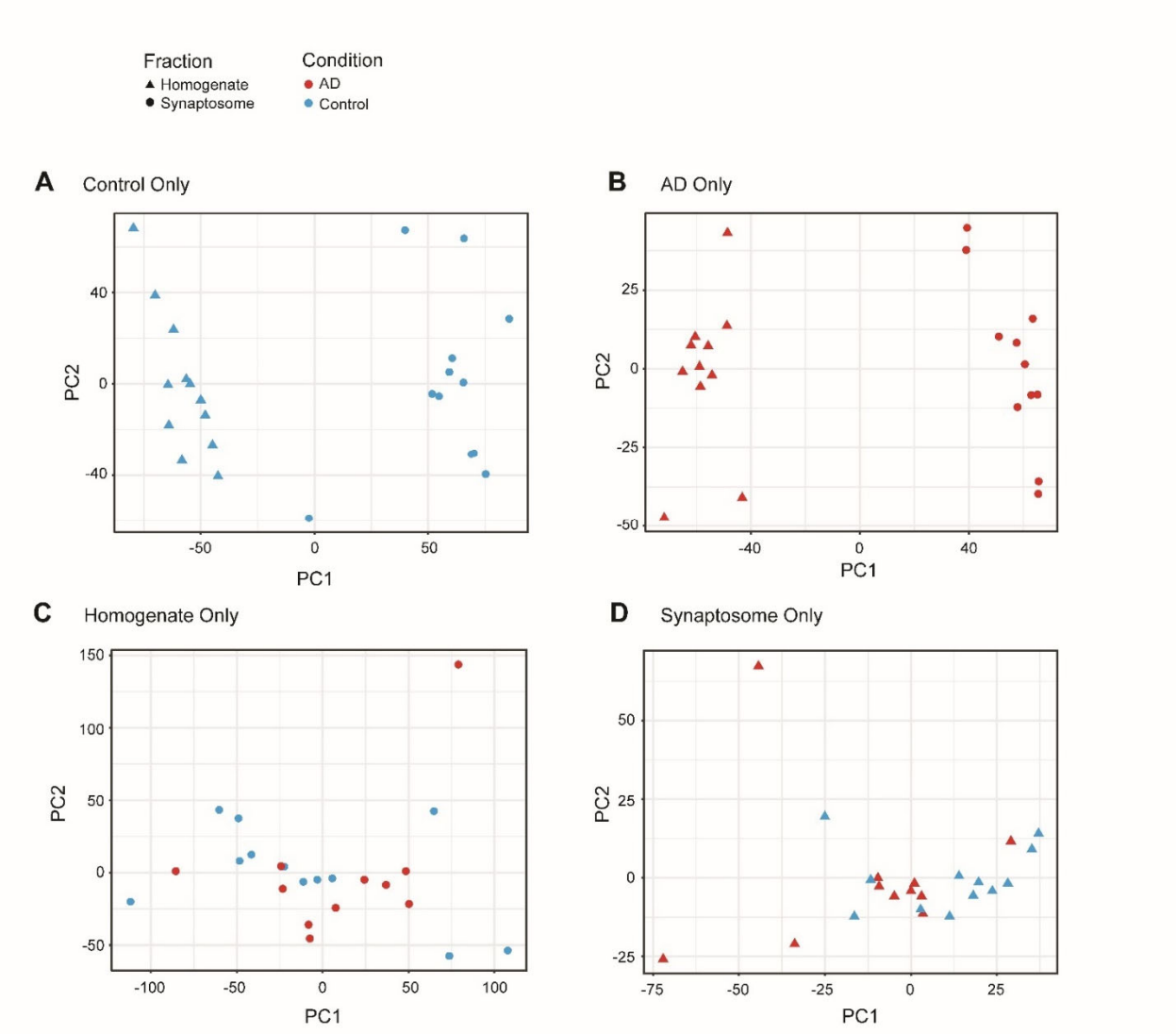

S2.2 Fig. Extended data for Fig 2.1; Additional PCA (multidimensional scaling) plots. A. Multidimensional scaling analysis among control samples only substantiating that most sample variation is determined by synaptosome vs. homogenate fraction. **B**. The same phenomenon is apparent among only AD samples. **C-D**. Multidimensional scaling analysis among only homogenate, and only synaptosome, respectively, reveals greater separation between control and AD among the synaptosome fraction compared to homogenate.

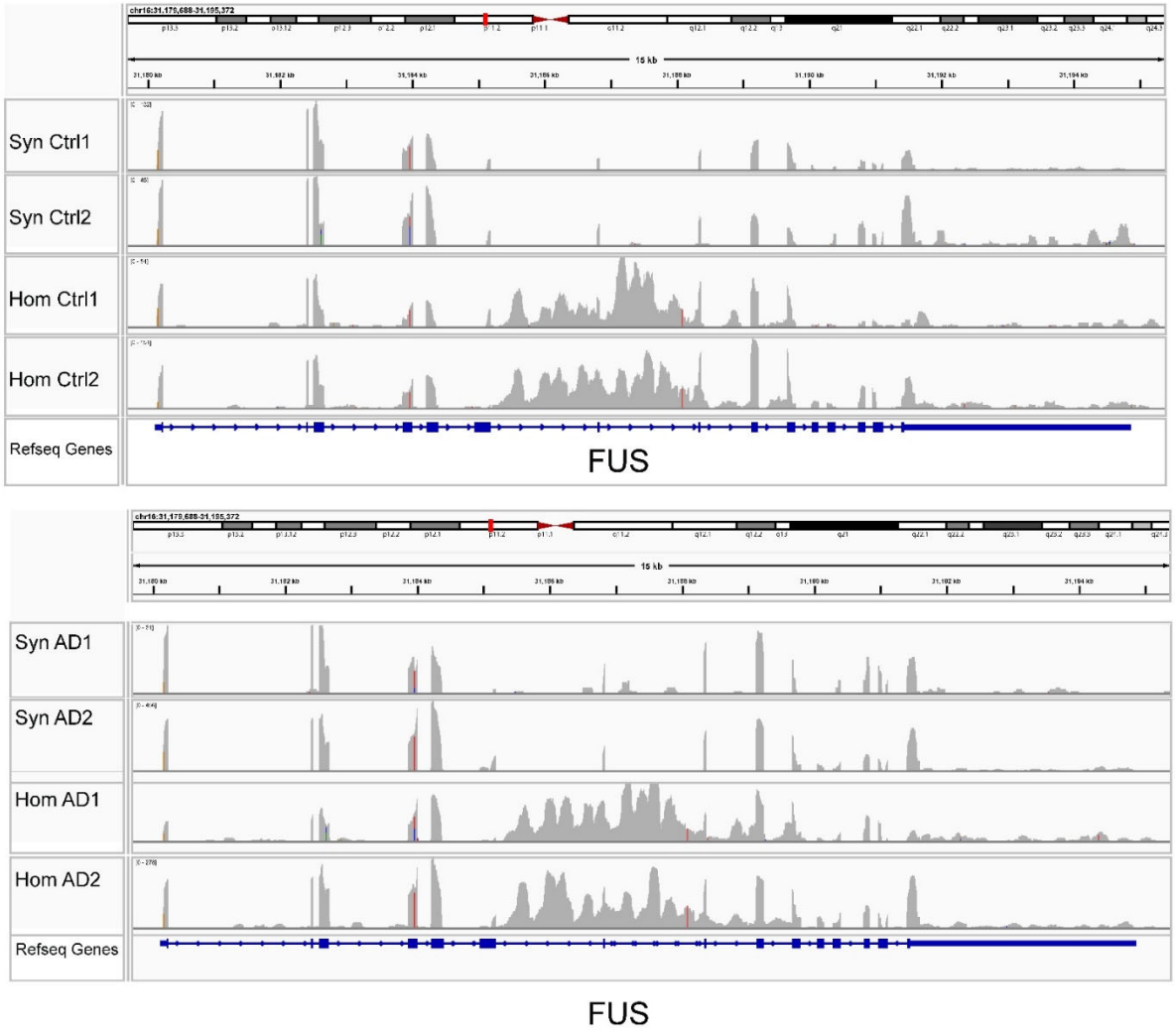

S2.3 Fig. Extended data for Fig 2.1; Fus alternative splicing in synaptosomes. Integrated genome viewer (IGV) version 2.16.2 image of control and AD homogenate and synaptosome RNA-seq tracks spanning the Fused in Sarcoma (FUS) locus (GRCh38 chr16:31,179,688-31,195,372) and demonstrating intron 6 and intron 7 retention events specific to homogenate samples.

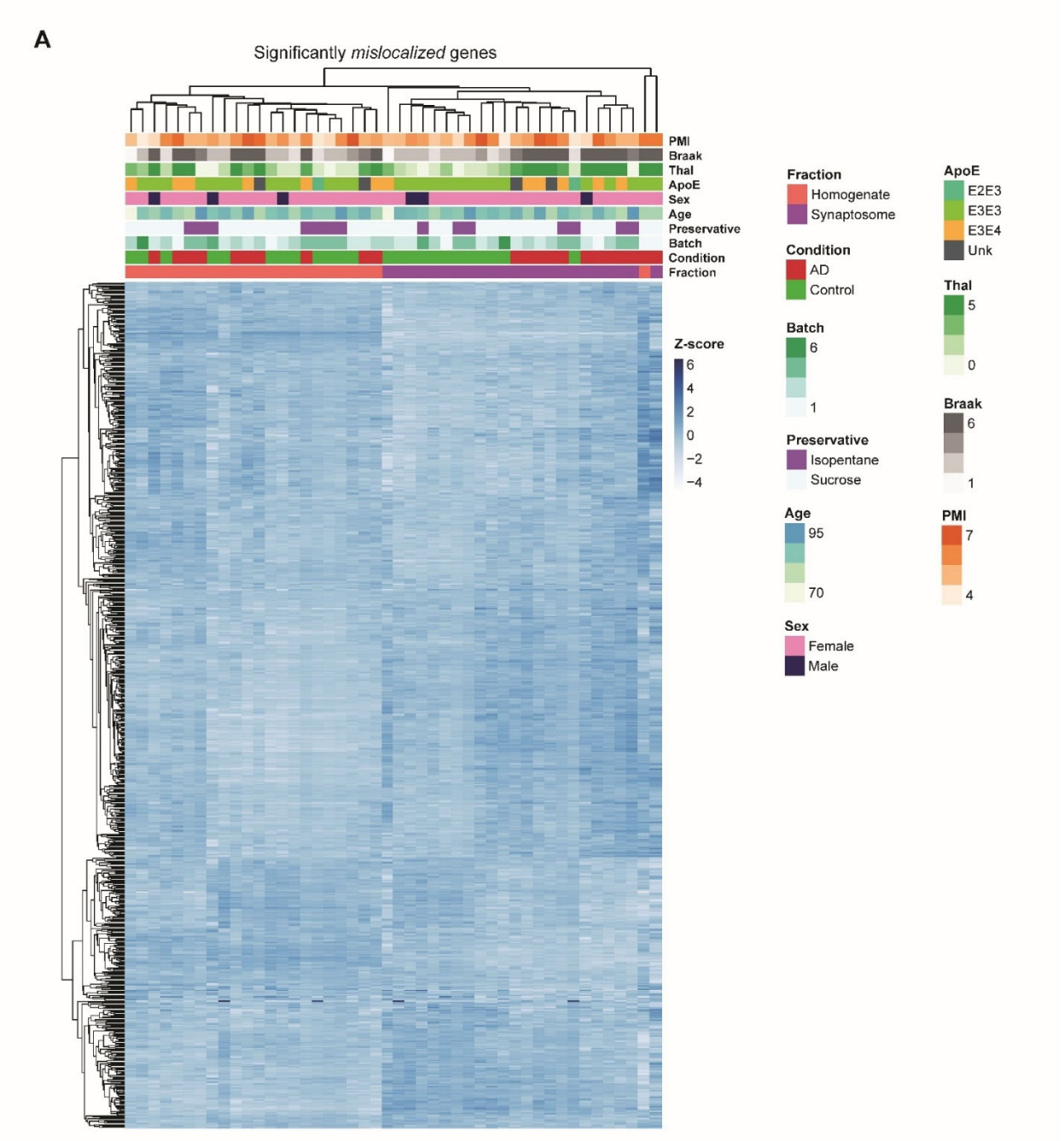

S2.4 Fig. Extended data for Fig 2.2; Expression patterns of mislocalized mRNAs in the human frontal lobe. A. Heatmap of significantly mislocalized mRNAs in the frontal lobe (see **Fig 2.2D**). Expression patterns reveal that mislocalized mRNAs in the synaptosome fraction cluster disease condition more robustly than expression patterns in the homogenate fraction

demonstrating independence from global expression changes. Furthermore, other variables seem to have minimal bearing on clustering.

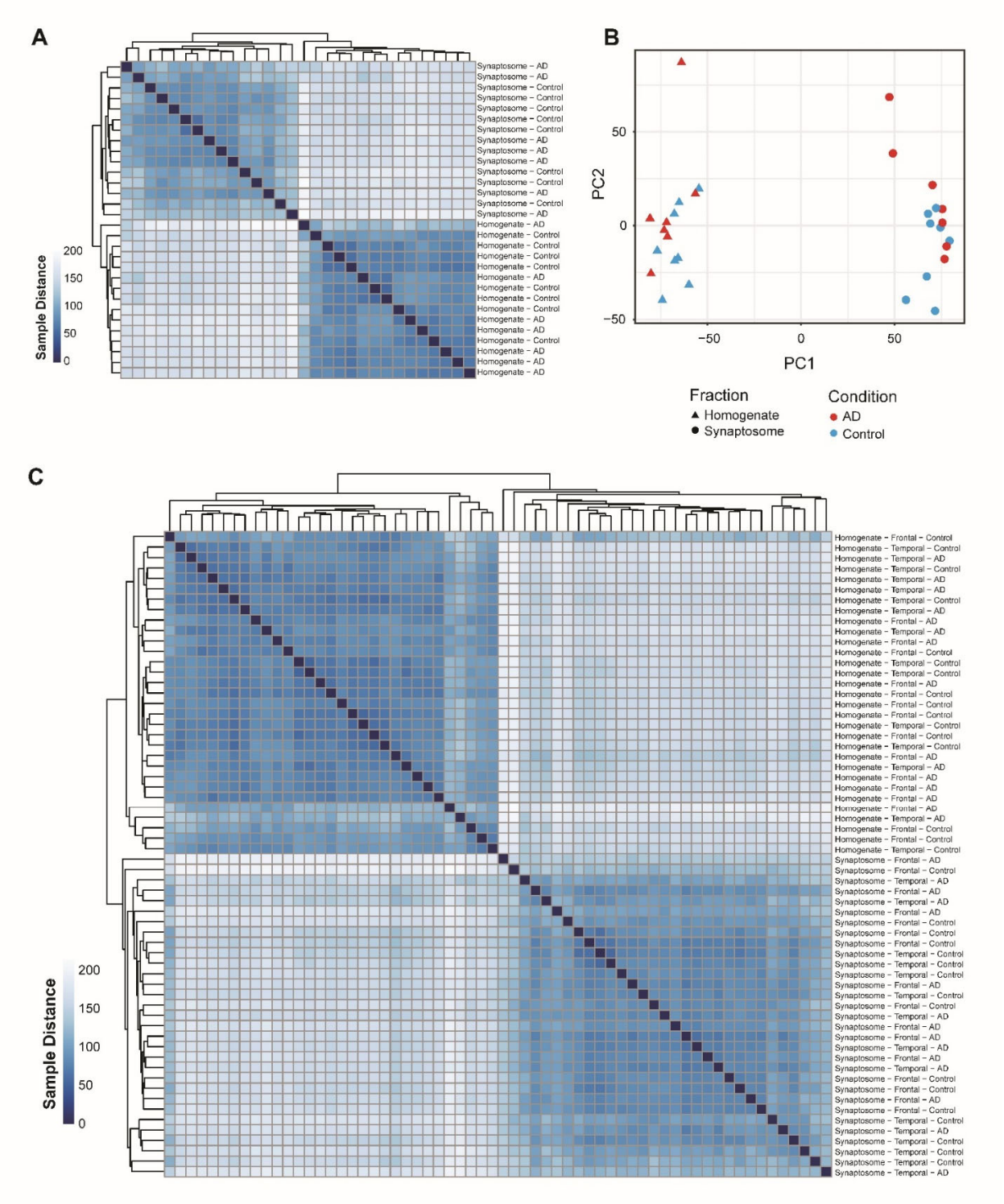

S2.5 Fig. Extended data for Fig 2.3; Human temporal lobe sample properties. A. Sample distance heatmap showing robust clustering of synaptosome and homogenate fractions among AD and control temporal lobe samples. **B.** Multidimensional scaling analysis shows robust

separation between mRNA counts of homogenate and synaptosome fractions among temporal lobe samples as well as moderate separation between disease condition. **C.** Sample distance heatmap including both frontal and temporal lobe samples showing more similarity between fractions than either tissue or disease condition.

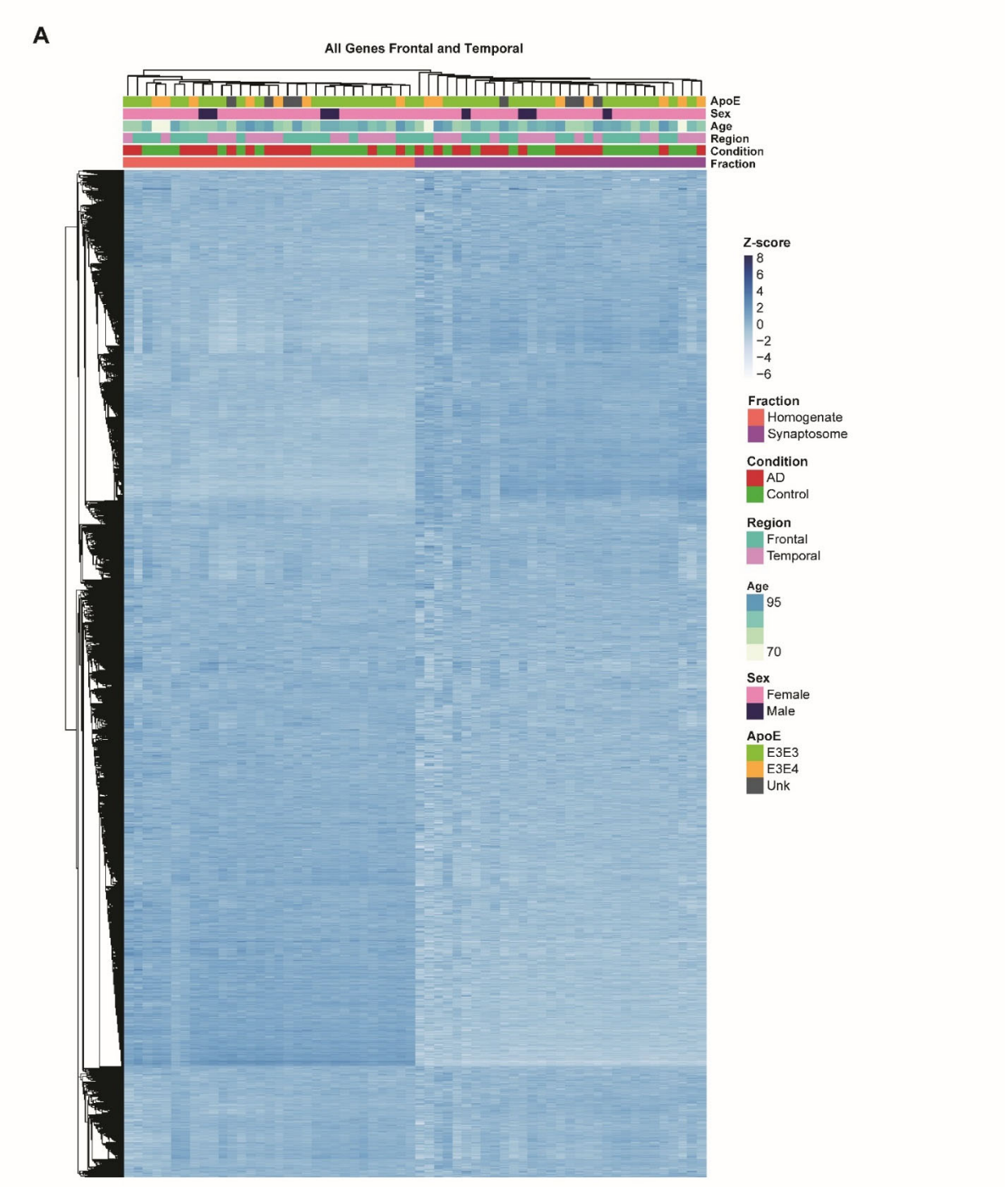

S2.6 Fig. Extended data for Fig 2.3; Heatmap of human temporal lobe gene expression. A. Heatmap including both frontal and temporal lobe samples (sucrose preservative only) showing

that fraction and disease condition precedes brain region in clustering impact with minimal effects from other variables.

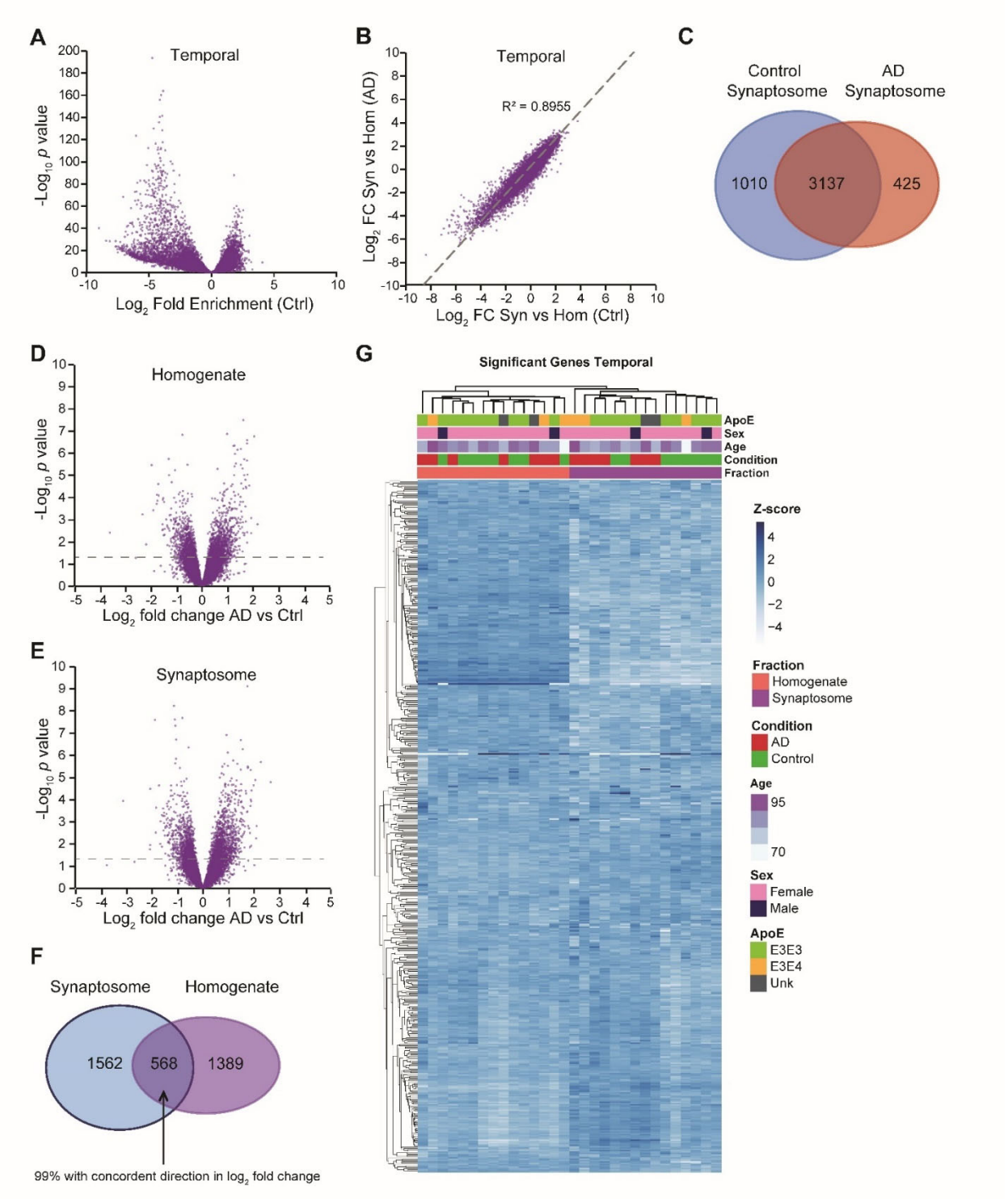

S2.7 Fig. Extended data for Fig 2.3; Expression patterns in the human temporal lobe. A. Volcano plot of synaptosome-enriched mRNAs in control temporal lobe samples. **B.**

Comparison of synaptosome-enrichment between AD and control temporal lobe samples shows strong correlation (R^2 = 0.8955). **C.** Venn diagram showing substantial overlap of synaptosome-enriched mRNAs between AD and control temporal lobe samples (p < 0.01). **D.** Volcano plot comparing expression differences between AD and control in the bulk, unfractionated homogenate. **E.** Volcano plot comparing expression differences between AD and control just within the synaptosome particles. **F.** Venn diagram showing minimal overlap of differentially expressed mRNAs in temporal lobe synaptosome and homogenate fractions (p < 0.05). Those that do overlap have 99% concordant $\log_2$ fold change. **G.** Heatmap of significantly mislocalized mRNAs in the temporal lobe (See **Fig 2.3D**). Expression patterns reveal that disease condition has a stronger bearing on mislocalized mRNAs in the synaptosome fraction compared to the homogenate fraction demonstrating independence from global expression changes. Additionally, other variables seem to have minimal bearing on clustering.

A

Group	Samples (n)	PMI (hrs)	Age (months)	Sex
Mouse Frontal Lobe				
Control	6	< 2	10 ± 1	1F, 5M
APP/PSEN1 mutant (AD)	8	< 2	10 ± 1	4F, 4M

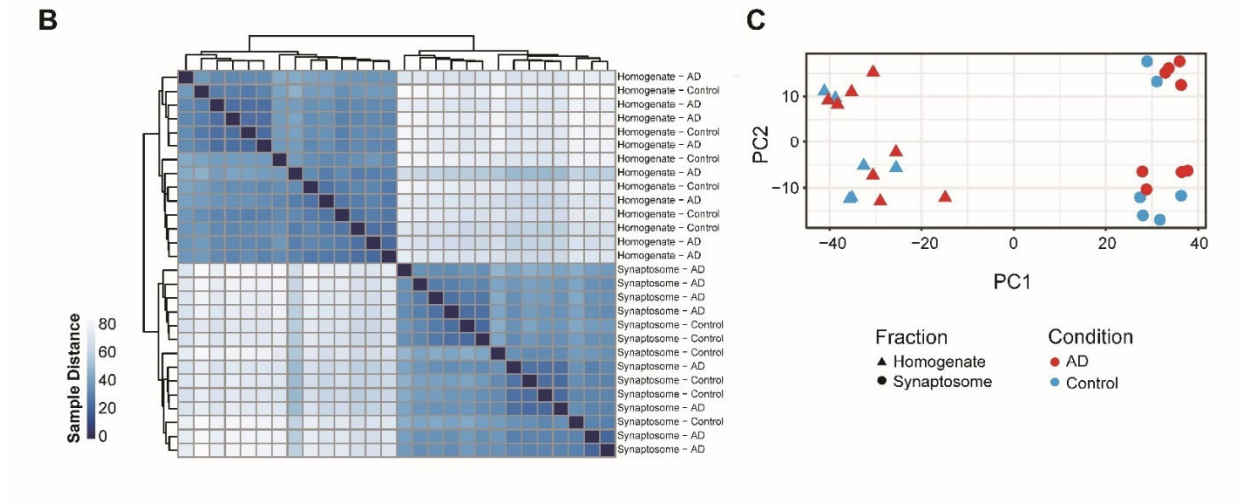

S2.8 Fig. Extended data for Fig 2.4; Mouse frontal lobe sample properties. A. Table showing sample properties of mice used for synaptosome sequencing. **B.** Sample distance heatmap shows robust separation between synaptosome and homogenate fractions. **C.** Multidimensional scaling analysis also shows robust separation between synaptosome and homogenate fractions, yet minimal separation between AD and wild-type samples.

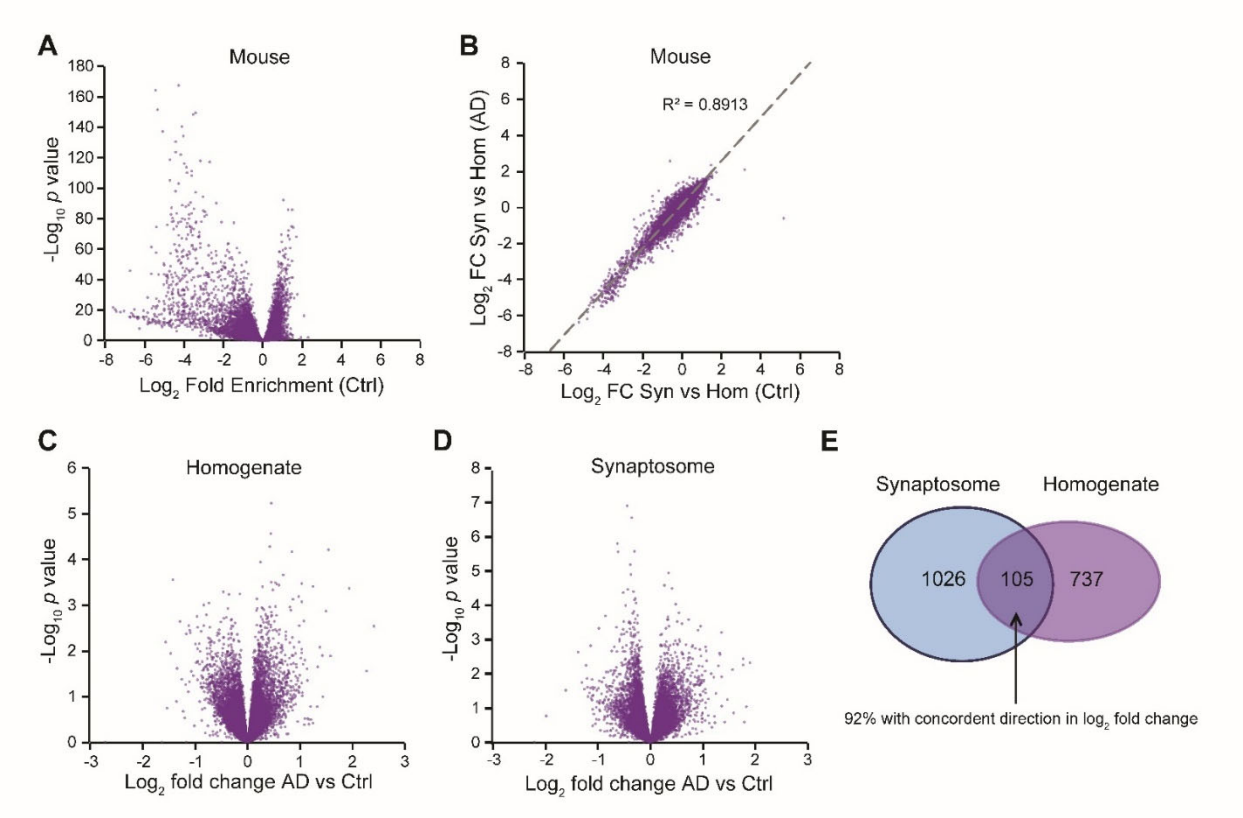

S2.9 Fig. Extended data for Fig 2.4; Expression patterns in the mouse frontal lobe. A. Volcano plot showing synaptosome-enriched mRNAs in control mouse frontal lobe samples. **B.** Comparison of synaptosome-enrichment ($p < 0.01$) between AD and control mouse frontal lobe samples shows strong correlation ($R^2 = 0.8913$). **C.** Volcano plot comparing expression differences between AD and control in the bulk, unfractionated homogenate. **D.** Volcano plot comparing expression differences between AD and control just within the synaptosome particles. **E.** Venn diagram showing minimal overlap of differentially expressed mRNAs in mouse frontal lobe synaptosome and homogenate fractions ($p < 0.05$). Those that do overlap have 92% concordant $\log_2$ fold change.

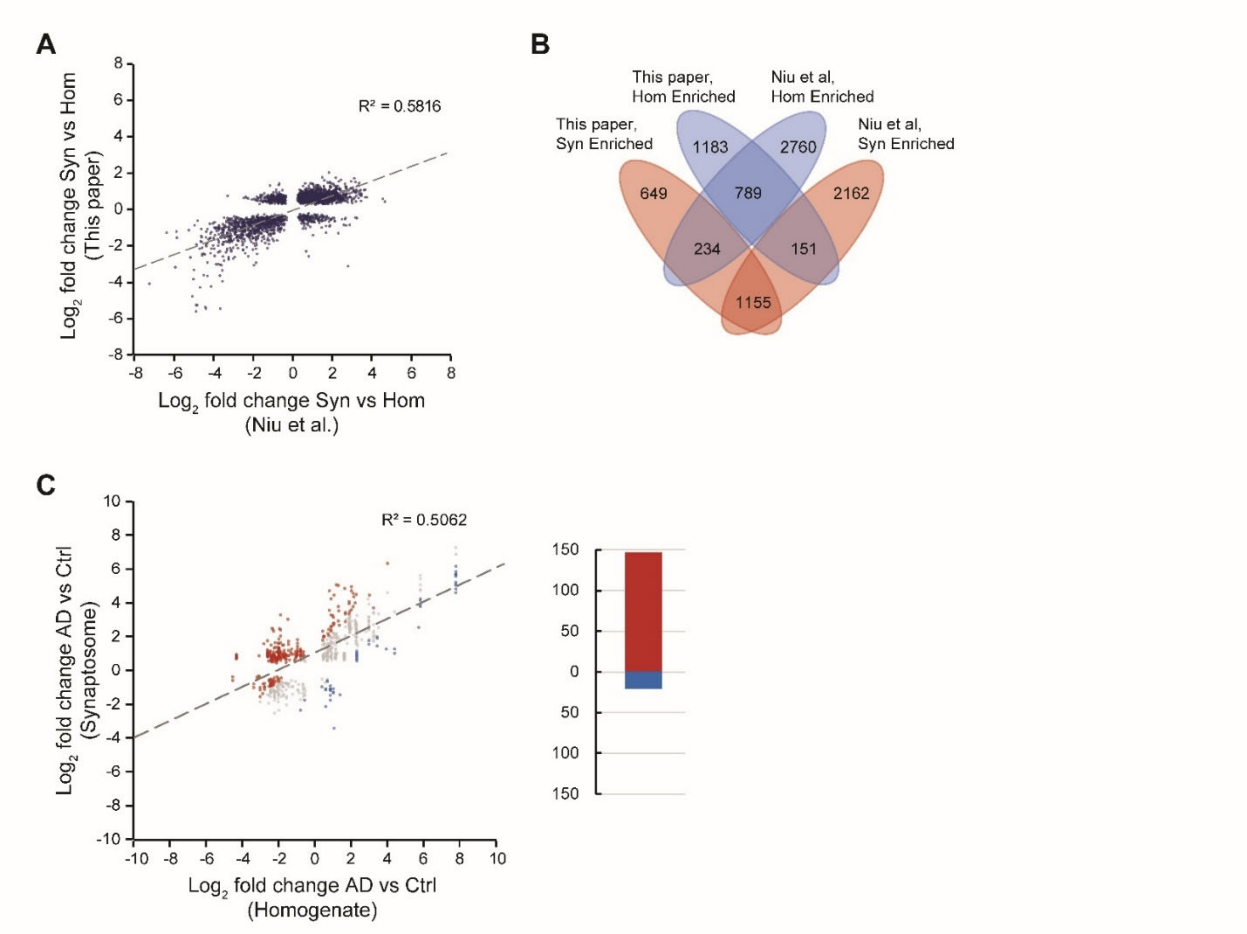

S2.10 Fig. Comparison of mouse synaptosome data with a previous study from Niu et al [67]. A. Comparing the fold changes/enrichment of synaptosome vs homogenate between our data and Niu et al. shows a moderate correlation ($R^2 = 0.5816$). **B.** Venn diagram shows plenty of synaptosome enriched genes overlap between our data and Niu et al. **C.** Comparing the fold changes of AD vs control between synaptosomes and homogenate in Niu et al.'s data shows moderate correlation ($R^2 = 0.5062$). Genes that have a T-statistic most distant from a y=x trendline are significantly mislocalized, independent of global expression changes ($p < 0.05$).

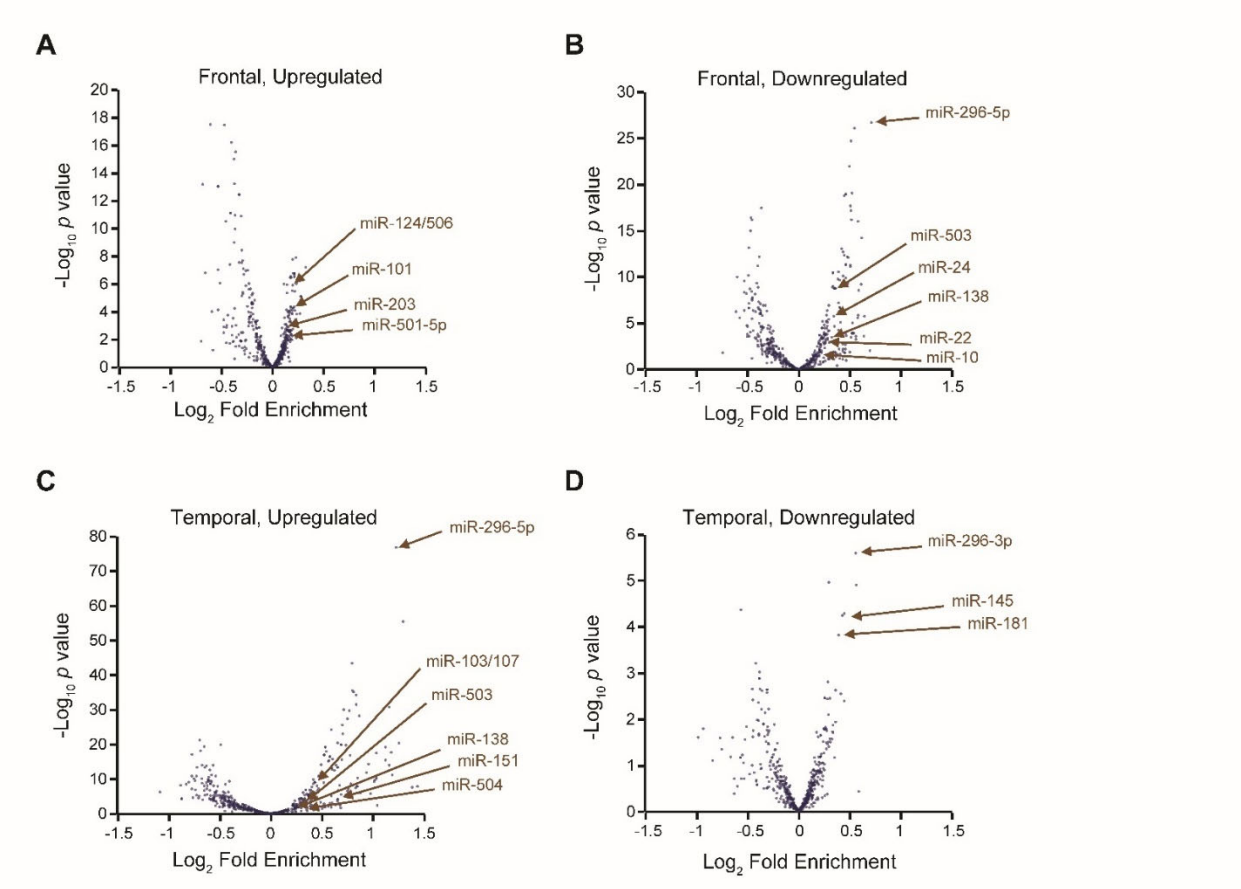

S2.11 Fig. Mislocalized mRNAs show specific enrichment and de-enrichment of microRNA binding sites. A. Volcano plot showing enrichment of microRNA binding sites among the upregulated mislocalized mRNAs in the human frontal lobe ($p < 0.05$, see **Fig 2.2D**). **B.** Volcano plot showing enrichment of microRNA binding sites among the downregulated mislocalized mRNAs in the human frontal lobe ($p < 0.05$, see **Fig 2.2D**). **C.** Volcano plot showing enrichment of microRNA binding sites among the upregulated mislocalized mRNAs in the human temporal lobe ($p < 0.05$, see **Fig 2.3D**). **D.** Volcano plot showing enrichment of microRNA binding sites among the downregulated mislocalized mRNAs in the human temporal lobe ($p < 0.05$, see **Fig 2.3D**).

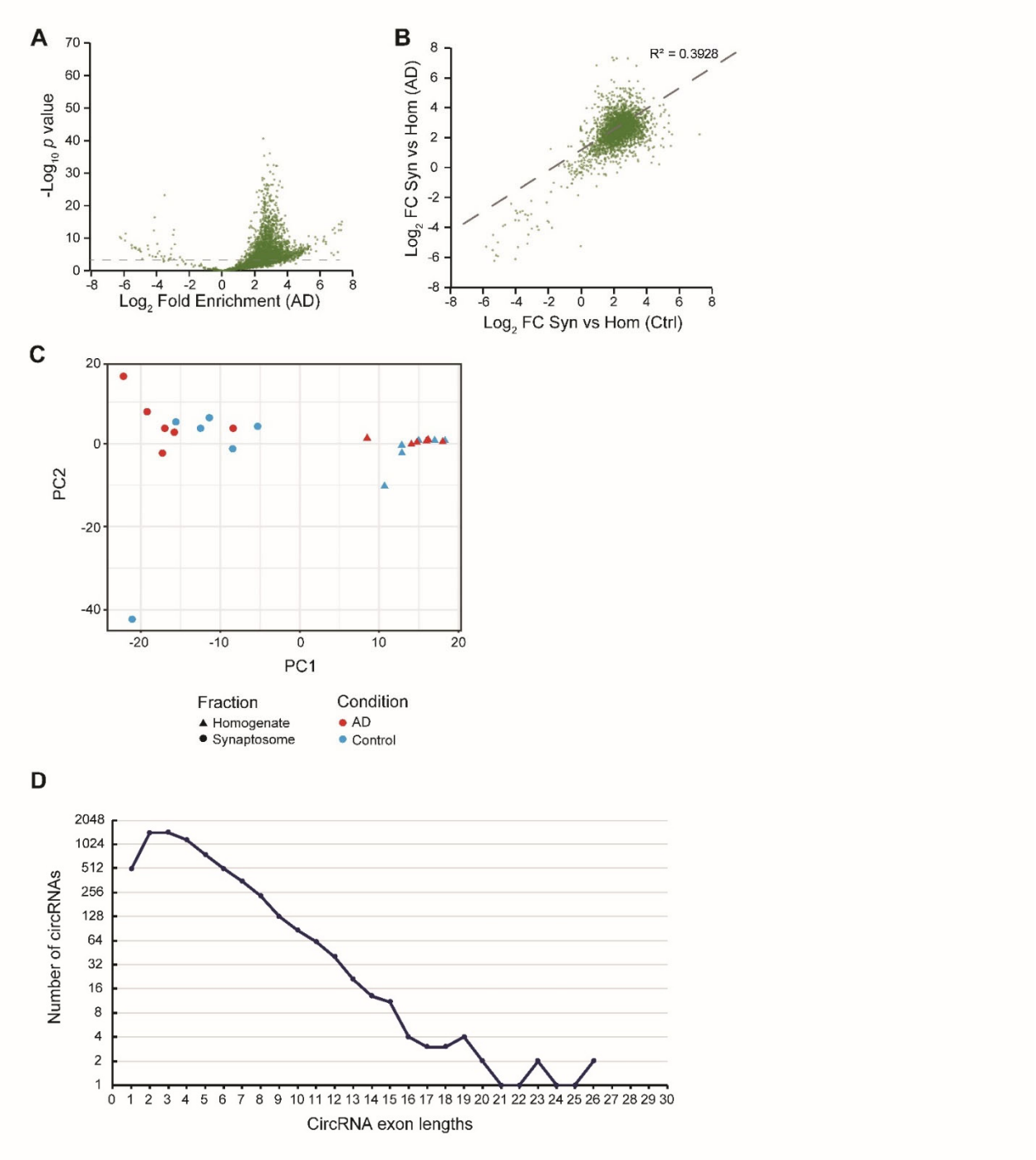

S2.12 Fig. Extended data for Fig 2.5; CircRNA expression and properties in the human frontal lobe. A. Volcano plot comparing circRNAs in synaptosome vs homogenate in AD frontal lobe samples shows that the majority of circRNAs are significantly enriched at synaptic terminals. **B.** Comparing circRNAs in synaptosome vs homogenate in both AD and control

frontal lobe samples shows that synaptic enrichment of circRNAs is a shared phenomenon. **C.** Multidimensional scaling plot of samples used for circRNA analysis representing the variation exclusively among circRNA reads (this is separate from the differential expression analysis where the combination of linear and circular reads were used for normalization). **D.** Analyzing the difference between the donor and acceptor exons involved in back-splicing shows that the majority of circRNAs consist of 2-3 exons.

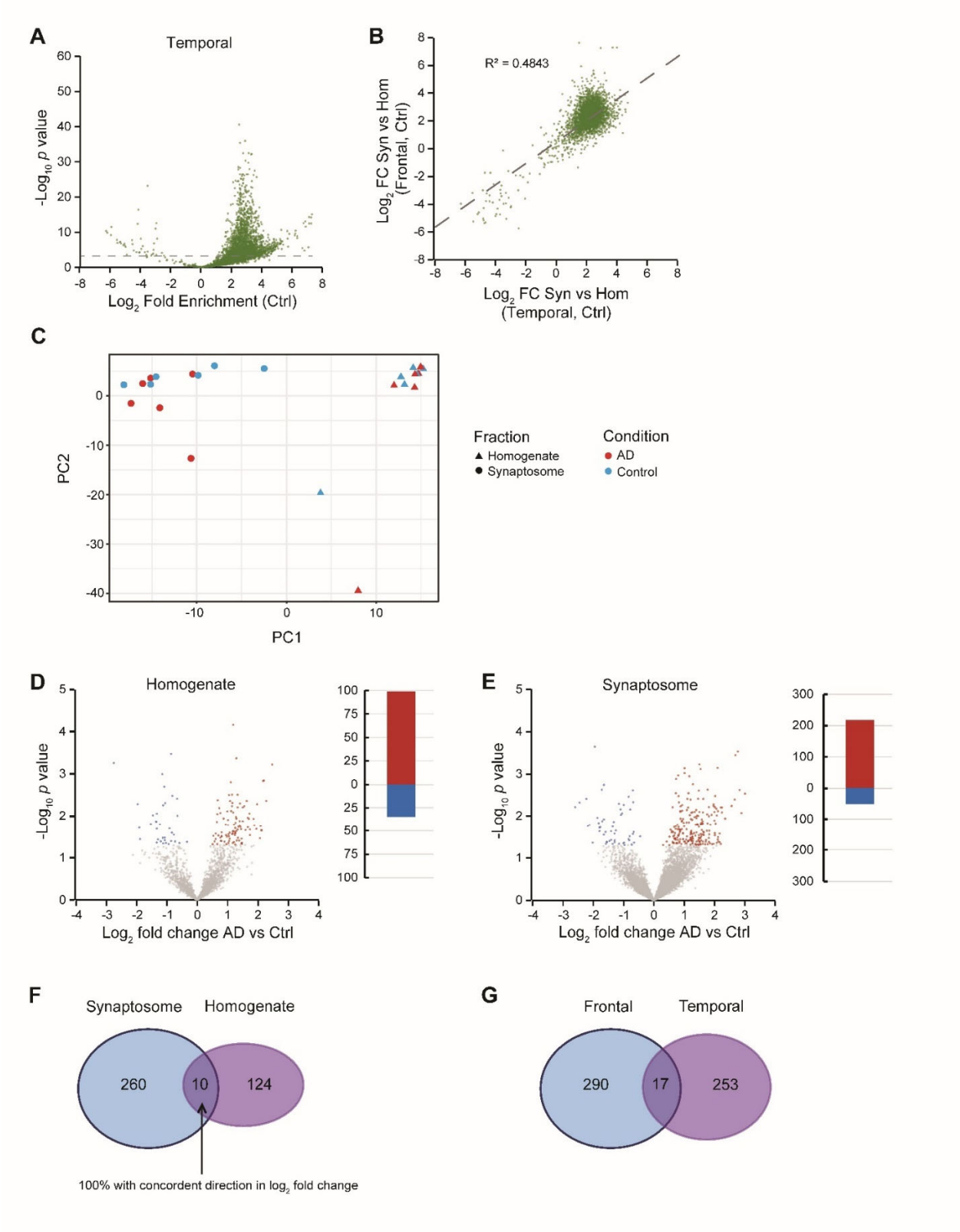
A
Temporal
-Log10 p value
Log2 Fold Enrichment (Ctrl)
B
R² = 0.4843
Log2 FC Syn vs Hom (Frontal, Ctrl)
Log2 FC Syn vs Hom (Temporal, Ctrl)
C
PC2
PC1
Fraction
Homogenate
Synaptosome
Condition
AD
Control
D
Homogenate
-Log10 p value
Log2 fold change AD vs Ctrl
E
Synaptosome
-Log10 p value
Log2 fold change AD vs Ctrl
F
Synaptosome
Homogenate
260
10
124
100% with concordent direction in log2 fold change
G
Frontal
Temporal
290
17
253

S2.13 Fig. Extended data for Fig 2.5; CircRNA expression in the human temporal lobe. A. Volcano plot comparing circRNAs in synaptosome vs homogenate in control temporal lobe samples shows that the majority of circRNAs are significantly enriched at synaptic terminals. **B.** Comparing circRNAs in synaptosome vs homogenate in both control frontal lobe and temporal lobe samples shows that synaptic enrichment of circRNAs is similar in both tissues. **C.** Volcano plot comparing circRNAs in AD vs control in the unfractionated homogenate ($p < 0.05$). **D.** Volcano plot comparing circRNAs in AD vs control in the synaptosome fraction ($p < 0.05$). **E.** Venn diagram shows minimal overlap of differentially expressed circRNAs between synaptosome and homogenate fractions with more occurring in the synaptosome fraction ($p < 0.05$). Those that do overlap show 100% concordant Log_2 fold change. **F.** Venn diagram shows minimal overlap of differentially expressed circRNAs in the synaptosome fraction between human frontal and temporal lobes ($p < 0.05$).

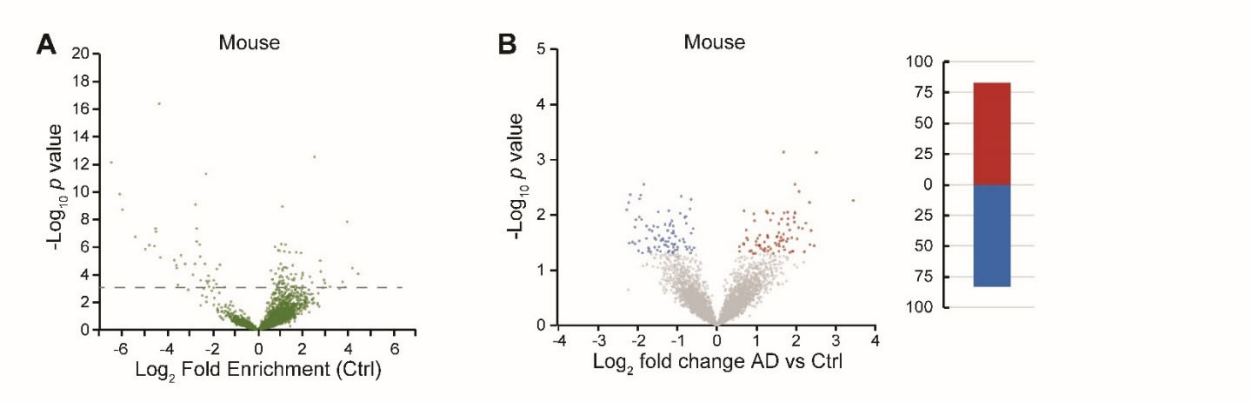

S2.14 Fig. Extended data for Fig 2.5; CircRNA expression in the mouse frontal lobe. A. Volcano plot comparing circRNAs in synaptosome vs homogenate in control mouse samples continues to show synaptic enrichment of circRNAs. **B.** Volcano plot comparing circRNAs in AD vs control in mouse synaptosomes (p <0.05).

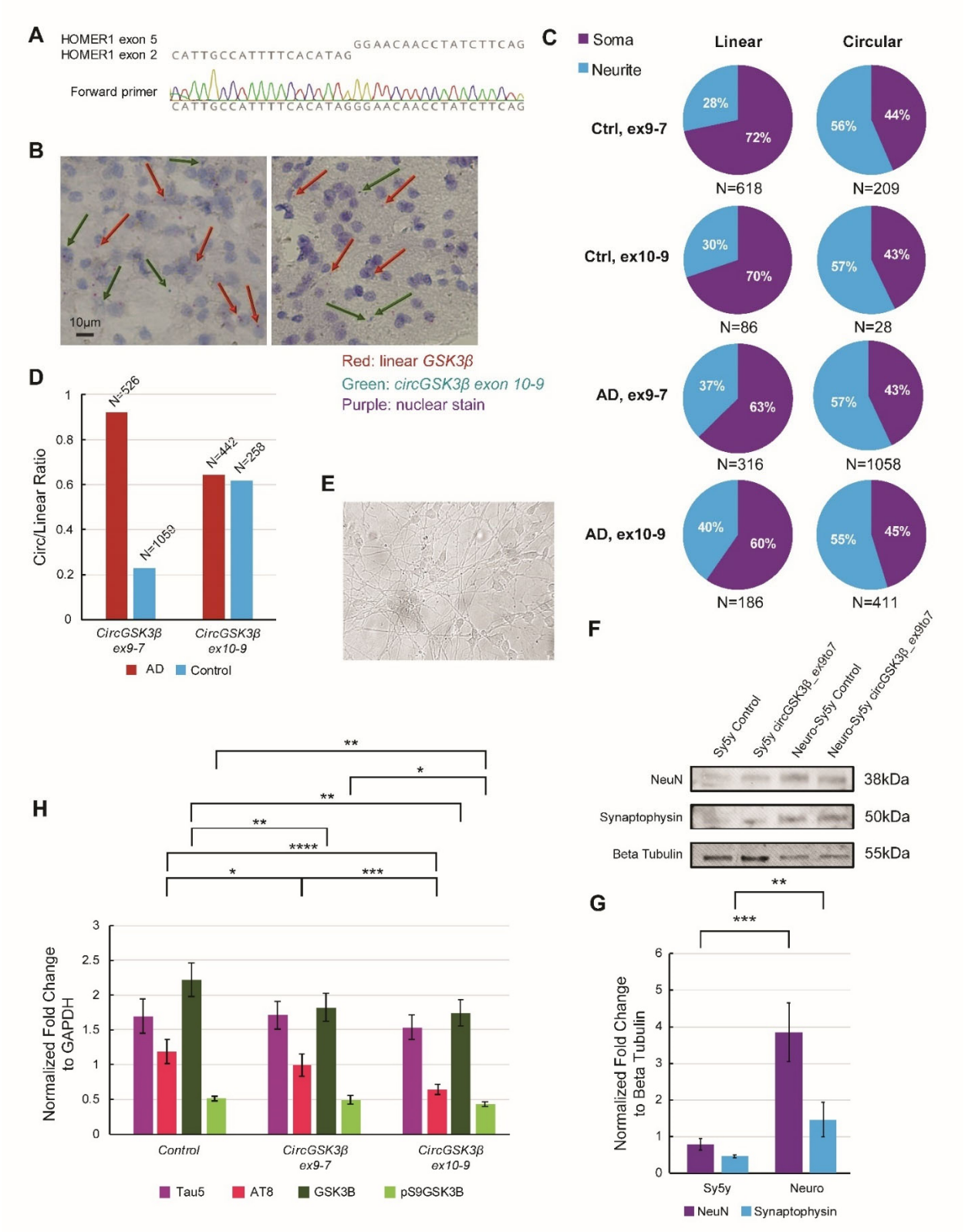
A
HOMER1 exon 5
HOMER1 exon 2
CATTGCCATTTTCACATAG
GGAACAACCTATCTTCAG
Forward primer
CATTGCCATTTTCACATAGGGAACAACCTATCTTCAG
B
10μm
Red: linear GSK3β
Green: circGSK3β exon 10-9
Purple: nuclear stain
C
Soma
Neurite
Linear
Circular
Ctrl, ex9-7
28%
72%
N=618
56%
44%
N=209
Ctrl, ex10-9
30%
70%
N=86
57%
43%
N=28
AD, ex9-7
37%
63%
N=316
57%
43%
N=1058
AD, ex10-9
40%
60%
N=186
55%
45%
N=411
D
Circ/Linear Ratio
N=526
N=1059
N=442
N=258
CircGSK3β ex9-7
CircGSK3β ex10-9
AD
Control
E
F
Sy5y Control
Sy5y circGSK3β_ex9to7
Neuro-Sy5y Control
Neuro-Sy5y circGSK3β_ex9to7
NeuN
38kDa
Synaptophysin
50kDa
Beta Tubulin
55kDa
G
Normalized Fold Change to Beta Tubulin
Sy5y
Neuro
NeuN
Synaptophysin
H
Normalized Fold Change to GAPDH
Control
CircGSK3β ex9-7
CircGSK3β ex10-9
Tau5
AT8
GSK3B
pS9GSK3B

S2.15 Fig. Extended data for Fig 2.6; SH-Sy5y differentiation into neurons and *CircGSK3β* transfections. A. Sanger Sequencing confirmation of back-splice junction between exons 5 and 2 of *HOMER1*. **B.** BaseScope RNA hybridization probes show that *circGSK3β* isoforms (green) are more frequently distal to the nucleus than the linear *GSK3β* transcript (red) in human control frontal lobe brain slices. Tissue and nuclei were stained with hematoxylin. **C.** Pie charts representing quantification of soma versus neurite localization of linear *GSK3β* and circular isoforms in BaseScope images (not significant). D**.** Quantification of *GSK3β* circular isoforms in AD vs control in BaseScope images (no significant). **E.** Bright field microscopy of neuron-differentiated SH-Sy5y cells confirms development of neuron morphology including polarized cells, axons, and dendrites. **F.** SH-Sy5y neuron differentiation confirmed by western blot showing an enrichment of two neuronal markers, Synaptophysin and NeuN. **G.** Quantification of blots in (**S2.15F Fig**). N = 6 samples per group. **: $p < 0.01$, ***: $p < 0.001$. **H.** Quantification of blots in (**Fig 2.6E**). N = 8 samples per group Significance calculated by T-test. *: $p < 0.05$, **: $p < 0.01$, ***: $p < 0.001$, ****: $p < 0.0001$.

A

Summary

General

fastp version:	0.20.1 (https://github.com/OpenGene/fastp)
sequencing:	paired end (150 cycles + 150 cycles)
mean length before filtering:	150bp, 150bp
mean length after filtering:	137bp, 137bp
duplication rate:	8.211013%
Insert size peak:	124
Detected read1 adapter:	GATCGGAAGAGCACACGTCTGAACTCCAGTCAC
Detected read2 adapter:	GATCGGAAGAGCGTCGTGTAGGGAAAGAGTGT

Before filtering

total reads:	344.870000 K
total bases:	51.730500 M
Q20 bases:	43.175978 M (83.463291%)
Q30 bases:	39.056047 M (75.499071%)
GC content:	56.516111%

Before filtering: read1: quality

Value of each position will be shown on mouse over.

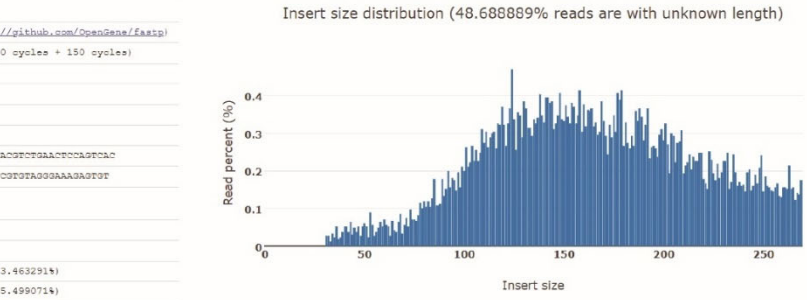

Before filtering: read2: quality

Value of each position will be shown on mouse over.

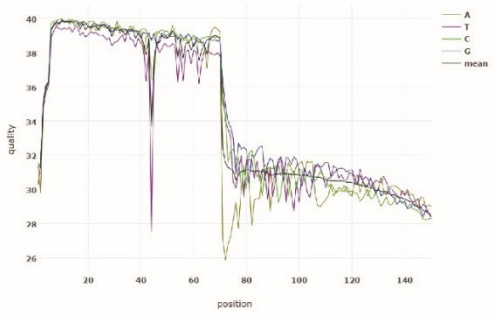

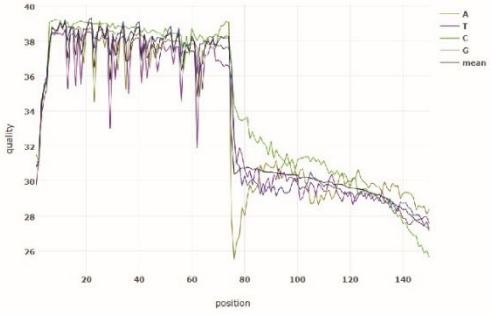

B

Summary

General

fastp version:	0.19.5 (https://github.com/OpenGene/fastp)
sequencing:	paired end (150 cycles + 150 cycles)
mean length before filtering:	150bp, 150bp
mean length after filtering:	143bp, 143bp
duplication rate:	12.173005%
Insert size peak:	170
Detected read2 adapter:	AGATCGGAAGAGCGTCGTGTAGGGAAAGAGTGT

Before filtering

total reads:	86.299126 M
total bases:	12.944869 G
Q20 bases:	11.805754 G (91.200256%)
Q30 bases:	11.091162 G (85.679987%)
GC content:	47.227005%

Before filtering: read1: quality

Value of each position will be shown on mouse over.

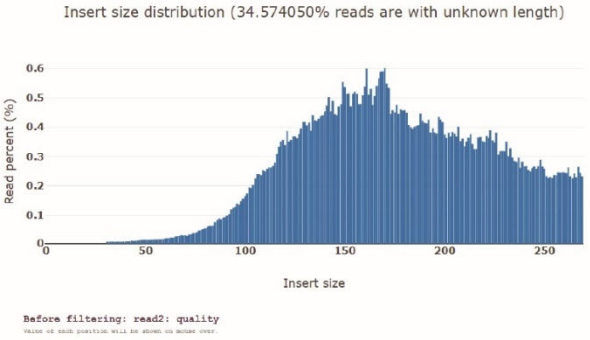

Before filtering: read2: quality

Value of each position will be shown on mouse over.

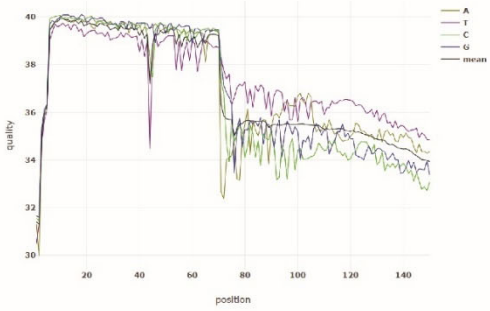

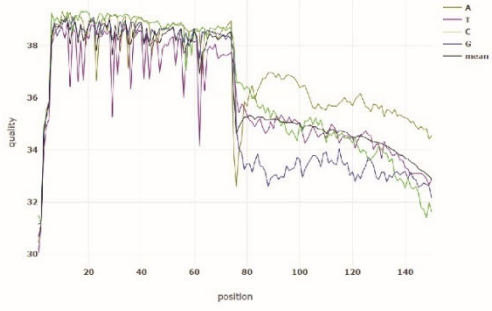

S2.16 Fig. Quality assessment of sequencing. Screenshots from the output of quality assessment tool, Fastp, found on the Galaxy online resource. **A.** Representative quality assessment of a homogenate sample. **B.** Representative quality assessment of a synaptosome sample [148].

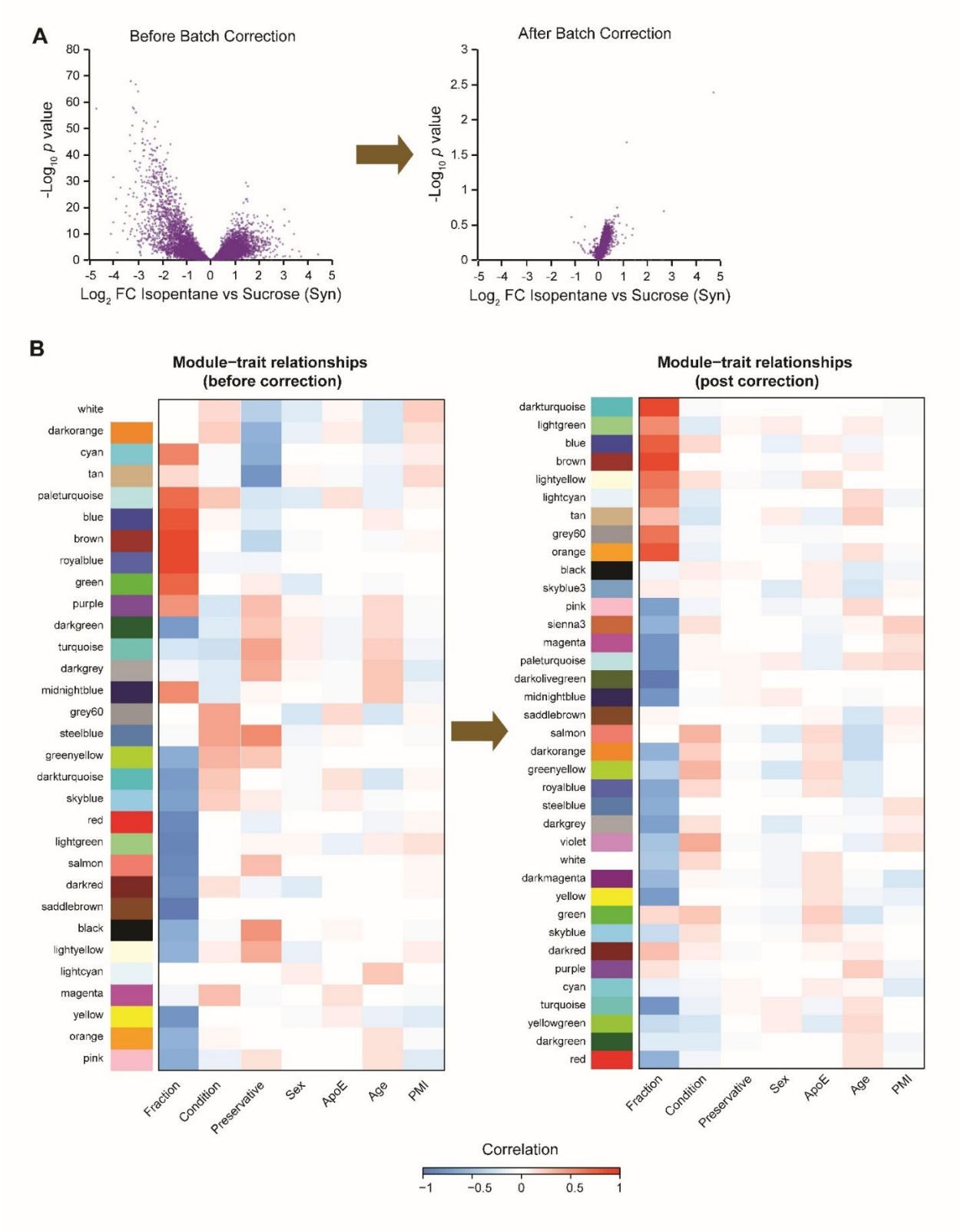
A
Before Batch Correction
After Batch Correction
-Log10 p value
Log2 FC Isopentane vs Sucrose (Syn)
B
Module−trait relationships
(before correction)
Module−trait relationships
(post correction)
white
darkorange
cyan
tan
paleturquoise
blue
brown
royalblue
green
purple
darkgreen
turquoise
darkgrey
midnightblue
grey60
steelblue
greenyellow
darkturquoise
skyblue
red
lightgreen
salmon
darkred
saddlebrown
black
lightyellow
lightcyan
magenta
yellow
orange
pink
darkturquoise
lightgreen
blue
brown
lightyellow
lightcyan
tan
grey60
orange
black
skyblue3
pink
sienna3
magenta
paleturquoise
darkolivegreen
midnightblue
saddlebrown
salmon
darkorange
greenyellow
royalblue
steelblue
darkgrey
violet
white
darkmagenta
yellow
green
skyblue
darkred
purple
cyan
turquoise
yellowgreen
darkgreen
red
Fraction
Condition
Preservative
Sex
ApoE
Age
PMI
Correlation
−1
−0.5
0
0.5
1

S2.17 Fig. Brain tissue preservation method has a major impact on mRNA measurements and can be successfully corrected for. A. Volcano plots comparing isopentane vs sucrose tissue preservation among both AD and control frontal lobe synaptosome samples before and after batch correction. ComBat_seq appears to substantially reduce the variation among samples based on this variable [118]. **B.** Weighted gene correlation network analysis (WGCNA) among human AD and control frontal lobe homogenate and synaptosome samples identifies confounding variables before and after ComBat_seq batch correction which shows that batch correction almost completely removes gene expression modules that correlate with preservation method with little impact on the expression variation defined by modules correlated with other variables including fraction and condition.

Chapter 3: microRNAs are differentially expressed at AD synapses and may explain mRNA mislocalization

3.1 Abstract

MicroRNAs (miRNAs) are a class of small, non-coding RNAs that regulate the expression of other transcripts including coding mRNAs. They function by binding to complementary sequences in the 3′ UTR of target mRNAs and recruit factors that either facilitate the target's degradation or repress its translation. miRNAs have previously been found to be dysregulated in AD and have also been shown to localize near synapses. In Chapter 2, we found enrichment of common miRNA binding sites among mislocalized transcripts. This could mean that differences in miRNAs are contributing to alteration of expression dynamics of transcripts localized to synapses impacting the efficiency of localized translation in AD. In this chapter, we use small-RNA sequencing to determine differences in miRNA abundance in AD and control human tissue and synaptosomes. We discover differences in miRNAs that correlate with differences in their targets' localization to synapses in AD.

3.2 Introduction

MicroRNAs (miRNAs) are a non-coding class of RNAs that play an essential role in regulating the expression of mRNA transcripts. Transcribed miRNAs produce stem loop

structures that are recognized by the Drosha microprocessor complex which cleaves the primary transcript to a precursor (pre)-miRNA stem loop for export from the nucleus. In the cytoplasm the pre-miRNA undergoes further processing by Dicer to produce an approximately 21-22 nucleotide sequence which then binds to argonaute (AGO) proteins as part of the RNA induced silencing complex (RISC). miRNAs serve the general role of translational regulation of mRNAs by 6-8 nucleotide seed sequences that target regions in mRNA 3′ UTRs. This miRNA binding can regulate translation either by endoluclease degradation of the mRNA by AGO2, recruiting exonucleases to the 5′ or 3′ ends, blocking translation initiation by interacting with the 5′ cap and eIF proteins, or stalling ribosomes by recruiting RNA-binding proteins (RBPs) such as FMRP[149].

Initially, miRNA identification and pairing often had to be done on a one-by-one basis whereby single miRNAs were knocked-down or overexpressed and the downstream effects were measured. Then parallel approaches developed in which AGO proteins could be immunoprecipitated and bound RNAs sequenced[150]. Predictive software was developed that used collective evidence to identify putative mRNAs with miRNA target sequences in their 3′ UTRs, leveraging the sequence conservation that often exists at *bona fide* target sites[125]. In fact, almost all mRNAs include sites that can interact with miRNAs[151,152]. Over time, experimental evidence could be extensively catalogued into online resources such as miRbase[153]. qPCR and microarrays could also be employed to analyze differential miRNA expression. Finally, small RNA sequencing approaches were developed to identify widespread differences among miRNAs in disease which differ from traditional RNAseq approaches by adding a size selection step[154].

miRNAs have been found to have an integral role in synaptic plasticity and the progression of AD pathology[155-157]. miRNAs and RISC have been found localized at synapses[158]. Well known examples that are known to repress APP and Aβ production include

miR-20, miR-101, and miR-153[159-161]. miRNAs known to affect BACE1 include miR-29 and miR-107[162,163]. Also, miR-132 and miR-137 have been shown to reduce tau hyperphosphorylation[164-166]. These data have led to speculation that modulation of miRNAs could mitigate neurodegenerative diseases or be used as biomarkers in cerebrospinal fluid or blood[68,167].

Studies into the differential expression of miRNAs at synapses in AD has recently garnered attention. A micro-array experiment found that there was an enrichment in miR-9, let-7d, and miR-124 in synaptosomes from healthy controls[130]. miR-9 is a well-established neuronal miRNA and its targets include several genes involved in neurogenesis such as *FOXG1* and *ELAV2* as well as synaptic plasticity including *DMD* and *SAP97*[168,169]. let-7d is known to modulate *HMGA2* which affects neural cell proliferation[170,171]. miR-124 similarly has an established role in synaptic plasticity and is being explored as a therapeutic target for neurodegeneration[172-174]. In a comparison between AD patient synaptosomes and controls, significant upregulation of miR-103a-3p, miR-501-3p, and miR-502-3p were observed. miR-103a is known to inhibit neural stem cell proliferation, miR-501 targets glutamatergic receptor mRNAs, and miR-502 targets GABA receptor mRNAs[175-177].

In this chapter we employ a new strategy to explore the differences of miRNA present in AD synaptosomes by using small-RNA sequencing. In contrast to a microarray, this approach has the added benefit of capturing different isoforms of miRNAs that may be driving the fine-tuned regulation of mRNAs at synapses. Small RNA sequencing has a higher dynamic range of miRNA expression that can be measured and importantly can reveal small RNAs in the genome that are not pre-spotted on the microarray. This study is a follow-up to the previous chapter (Chapter 2.4.5) in which we discovered mislocalized mRNAs in AD and generated predictions of miRNAs that could be influencing these differences.

3.3 Methods

3.3.1 Human brain samples

As described in Chapter 2, human brain tissue samples used in this study were derived from brains donated for research by participants in the UW ADRC and the Kaiser Permanente Washington (KPW) ACT study including both healthy controls and neuropathologically-confirmed AD dementia. For miRNA analysis, seven controls and five AD patients were used. All samples were collected following approved protocols with informed consent as approved by the University of Washington Institutional Review Board (IRB). Tissues from the frontal lobe (middle frontal gyrus – dorsolateral prefrontal cortex) were collected during rapid brain autopsy and flash frozen in liquid nitrogen or supercooled isopentane.

3.3.2 Small RNA sequencing

RNA material from the same preparations in Chapter 2 underwent small RNA sequencing conducted using the NextFlex kit (Perkin Elmer cat#NOVA-5132-32). We started with 100-200ng of RNA and used 24 PCR cycles as part of the amplification step. Samples were barcoded and pooled and sequenced on an Illumina NovaSeq S4 instrument using 150bp paired-end reads. Adapters were clipped from the reads using the fastx-toolkit. We obtained roughly 10 million reads per sample, with over 60% of reads mapping to miRNAs.

3.3.3 miRNA data analysis

miRNA data analysis followed a similar paradigm as described in Chapter 2. First, clipped reads were mapped to an index of miRNAs using Bowtie2[121]. Then the number of reads mapping to each miRNA were counted and this count matrix was imported into DESeq2 to determine fold differences between AD and control as well as synaptosome and homogenate[115]. Localization analysis followed the same formulae described in Chapter 2.3.6. Significantly differentially expressed miRNAs were input into targetscan v. 7.0 to identify coding transcripts that may be targeted by the miRNAs[125].

3.4 Results

3.4.1 miRNA differential expression in both AD synaptosomes and homogenate suggests differences in transcript expression at synapses

Using the same human frontal lobe homogenate and synaptosome samples used for total mRNA and circRNA sequencing, we prepared small RNA libraries for sequencing to identify miRNAs differences between AD and control that may correlate with previously observed synaptic localization differences. We identified 558 different species of miRNA in our samples. Although not as robust as mRNAs or circRNAs, using multidimensional scaling analysis we observe a general difference in synaptosome versus homogenate and AD vs control (**Fig 3.1A**). The greater degree of variability is also observed based on clustering on a heatmap where we also see age as a potential covariable (**S3.1A Fig**). By comparing

synaptosome versus homogenate in control samples, we also see that the majority miRNAs are localized to the bulk homogenate as opposed to synapses (**Fig 3.1B** and **S3.1 Table**). Notably, miR-7, miR-17, miR-34a, miR-103, miR-107, and miR-127 are enriched at synapses which corroborates previous evidence[130]. When comparing synaptosome versus homogenate between AD and control, we see a weak correlation with an R^2 of 0.356 demonstrating that major differences in miRNAs are present at synapses in disease (**Fig 3.1C**). When comparing AD versus control in synaptosome versus homogenate, we observe an even weaker correlation with an R^2 of 0.123 indicating that miRNA localization differences between AD and control is largely independent from differences in the bulk homogenate (**Fig 3.1D**).

Comparing between AD and control in the homogenate fraction we observe 59 differentially expressed miRNAs ($p<0.1$; **Fig 3.1E** and **S3.2 Table**). Of the downregulated miRNAs, we saw members of the let-7 family, miR-24, miR-34c, and miR-134c. Upregulated miRNAs include miR-20b, miR-106a/b, and miR-515. In the synaptosome fraction we observed 81 differentially expressed miRNAs between AD and control ($p<0.1$; **Fig 3.1F** and **S3.3 Table**). Downregulated miRNAs include miR-17, miR-21, miR-34b/c, and miR-219. Members of the let-7 family are actually found to be upregulated in AD synaptosomes along with miR-1, miR-7, miR-9, and miR-101. Of the differentially expressed miRNAs, only 13 are differentially expressed in both fractions with concordant fold change (**Fig 3.1G** and **S3.4 Table**). These included downregulation of miR-34c and miR-132 as well as upregulation of miR-144. When running the mislocalization analysis, we identify 103 mislocalized miRNAs between AD and control. miR-1 and members of the let-7 family were found to be positively mislocalized in AD synaptosomes whilst miR-34b, miR-214, miR-506 were negatively mislocalized with miR-608 showing the greatest fold change of -2.8. miR-1238 showed the largest degree of positive mislocalization with a 3.1 fold-change.

Next, we sought to identify what potential mRNA targets these miRNAs may be affecting and if they matched with any of our previously identified mislocalized transcripts. Overall, there

were over 4000 implicated targets of the differentially expressed miRNAs. Upregulated miRNAs in the homogenate had matches to 58 mislocalized mRNAs in AD frontal lobes. Downregulated miRNAs matched to 76 mislocalized mRNAs. Upregulated miRNAs in synaptosomes matched to 57 targets and downregulated miRNAs matched to 80 targets. Of the miRNAs that were mislocalized between synaptosomes and homogenate in AD versus control, upregulated miRNAs had 57 matching targets, and downregulated miRNAs had 83 matching targets (**S3.5 Table**).

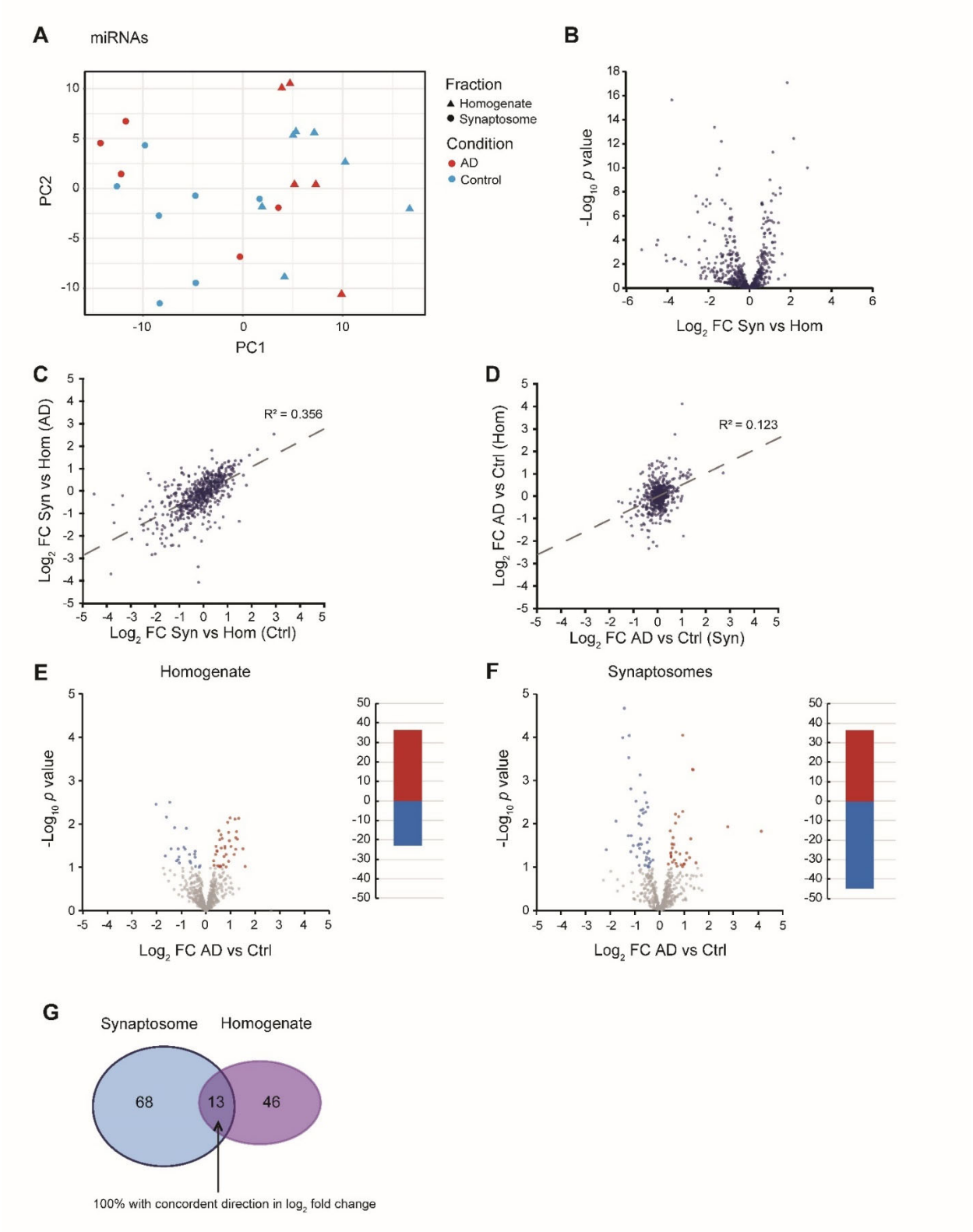
A
miRNAs
PC2
PC1
Fraction
Homogenate
Synaptosome
Condition
AD
Control
B
-Log10 p value
Log2 FC Syn vs Hom
C
R² = 0.356
Log2 FC Syn vs Hom (AD)
Log2 FC Syn vs Hom (Ctrl)
D
R² = 0.123
Log2 FC AD vs Ctrl (Hom)
Log2 FC AD vs Ctrl (Syn)
E
Homogenate
-Log10 p value
Log2 FC AD vs Ctrl
F
Synaptosomes
-Log10 p value
Log2 FC AD vs Ctrl
G
Synaptosome
Homogenate
68
13
46
100% with concordent direction in log2 fold change

Fig 3.1. miRNA differential expression in human AD and control frontal lobe synaptosomes and homogenates. A. Multidimensional scaling analysis showing moderate separation between synaptosome and homogenate miRNA expression profiles and substantial heterogeneity between AD and control. **B.** Volcano plot showing fold differences between synaptosome and homogenate fractions in control samples. **C.** Correlation between AD and control miRNA synaptic enrichment. **D.** Correlation between synaptosome and homogenate AD vs control miRNA fold changes. **E.** Volcano plot comparing expression differences between AD and control in the bulk, unfractionated homogenate. **F.** Volcano plot comparing expression differences between AD and control just within the synaptosome particles. **G.** Venn diagram comparing the significant expression differences in homogenate (**E**) and synaptosome (**F**).

3.4.2. Sequenced miRNAs show modest alignment with predictions from mislocalized mRNAs and target genes

In the previous chapter, we used the 3′ UTR sequences of mislocalized mRNAs to make predictions on what miRNAs have the potential to be regulating expression dynamics at the synapse. Therefore, we wanted to compare the data from small RNA sequencing to our predictions to test the efficiency of using sequence predictions to hypothesize regulatory mechanisms possibly driving differences in mRNA localization and expression dynamics at synapses.

For our data we compared both true-matches and false-matches between the predicted and observed data. A true-match would be the case where we predicted either an upregulated miRNA or a downregulated miRNA based on the sequence analysis of mislocalized mRNAs and the differences observed via small-RNA sequencing were congruent with these predictions. A false-match would be the case where the differences observed in small-RNA sequencing were

opposite of the trends we predicted based on sequence analysis of mislocalized genes. We found that approximately 30% of predicted miRNAs matched with the small-RNA sequencing results with the differences in the homogenate, on average, matching the most. However, our false-matching rate was substantially higher at a rate of approximately 50% (**Fig 3.2A**). The downregulation of miR-219 in synaptosomes and miR-132 in both synaptosomes and homogenate matched our prediction of enriched miRNA binding sites among positively mislocalized transcripts the best (see Chapter 2.4.5). And the upregulation of miR-515 in the homogenate also matched our prediction for negatively mislocalized transcript miRNA binding site enrichment.

Next, we ran the lists of differentially expressed miRNAs in the software Targetscan to see if their targets matched with any of the mislocalized mRNAs. Here we found a matching rate of approximately 40% among upregulated miRNAs that have the potential to affect mislocalized mRNAs (**Fig 3.2B**).

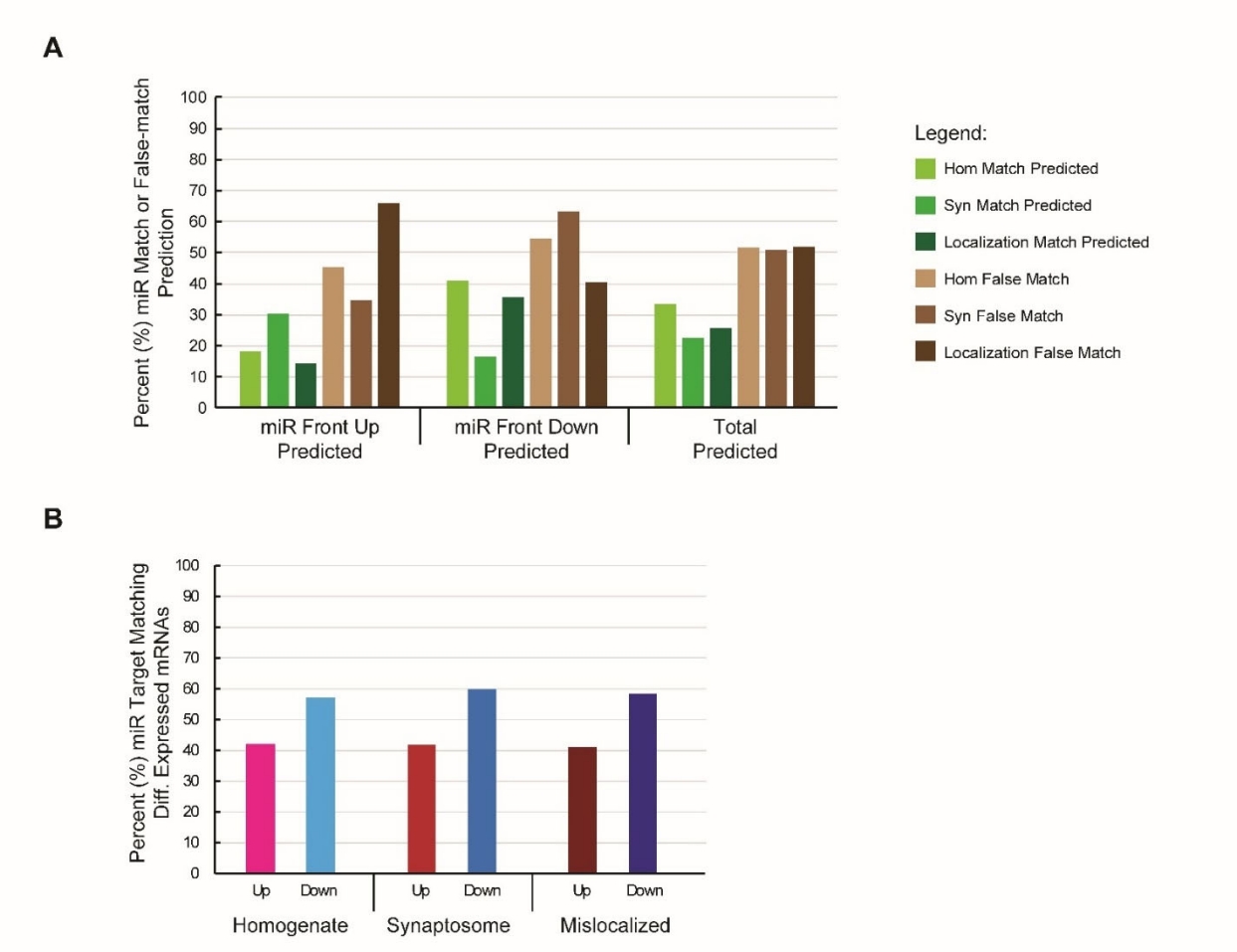

Fig 3.2. Differentially expressed miRNA correspondence to mislocalized mRNA targets (From Chapter 2). A. Plot showing the percentage of miRNA differences identified by sequencing matching, or falsely matching, predicted enrichment based on mislocalized mRNAs' 3′ UTR sequences. Graph is partitioned based on miRNAs that were predicted to be upregulated, predicted to be downregulated, and in total. Bars correspond to matches or false-matches among the miRNA differences observed in either only the homogenate fraction, only the synaptosome fraction, or among mislocalized miRNAs. A match indicates that the miRNA fold change from sequencing is alignment with its predicted fold change based on mRNA 3′ UTR analysis. A false match indicates that the miRNA fold change from sequencing is opposite of its predicted fold change direction. **B.** Plot showing the percentage of upregulated or

downregulated mislocalized mRNAs that are targets of differentially expressed miRNAs in either the homogenate fraction, the synaptosome fraction, or mislocalized miRNAs.

3.4.3 Sequence analysis of reads mapping to miRNAs show isoform differences between miRNAs localized to synapses versus the bulk homogenate

The technique of small RNA sequencing affords us the opportunity to capture isoform differences in miRNAs. Although arising from the same pre-miRNA transcript, there can be differences in cleavage leading to alternative nucleotide inclusion within the ~22nt sequence. Differences in miRNA isoforms could possibly be driving different localization patterns or disease outcomes.

After mapping the small RNA sequencing data to the small RNA transcriptome, we took an in-depth analysis of the reads themselves that matched. We discovered multiple isoforms mapping to the same miRNA with 1-2 nucleotide alterations to the beginning or end of sequences. Amazingly, distinct isoforms showed preferential enrichment in the synaptosome fraction versus the bulk homogenate. For example, the miRNA miR-9-3p had more than five different isoforms. In synaptosomes, the predominant sequence was “TAAAGCTAGATAACCGAAAGTA”, whereas in the homogenate the predominant sequence was “ATAAAGCTAGATAACCGAAAGT”. The difference is a 1nt offset in the starting position of the miRNA (**Fig 3.3A**). This was similar for both AD and control samples. We also saw different distributions of isoforms in miR-124-3p and miR-132 (**Fig 3.3B** and **Fig 3.3C**).

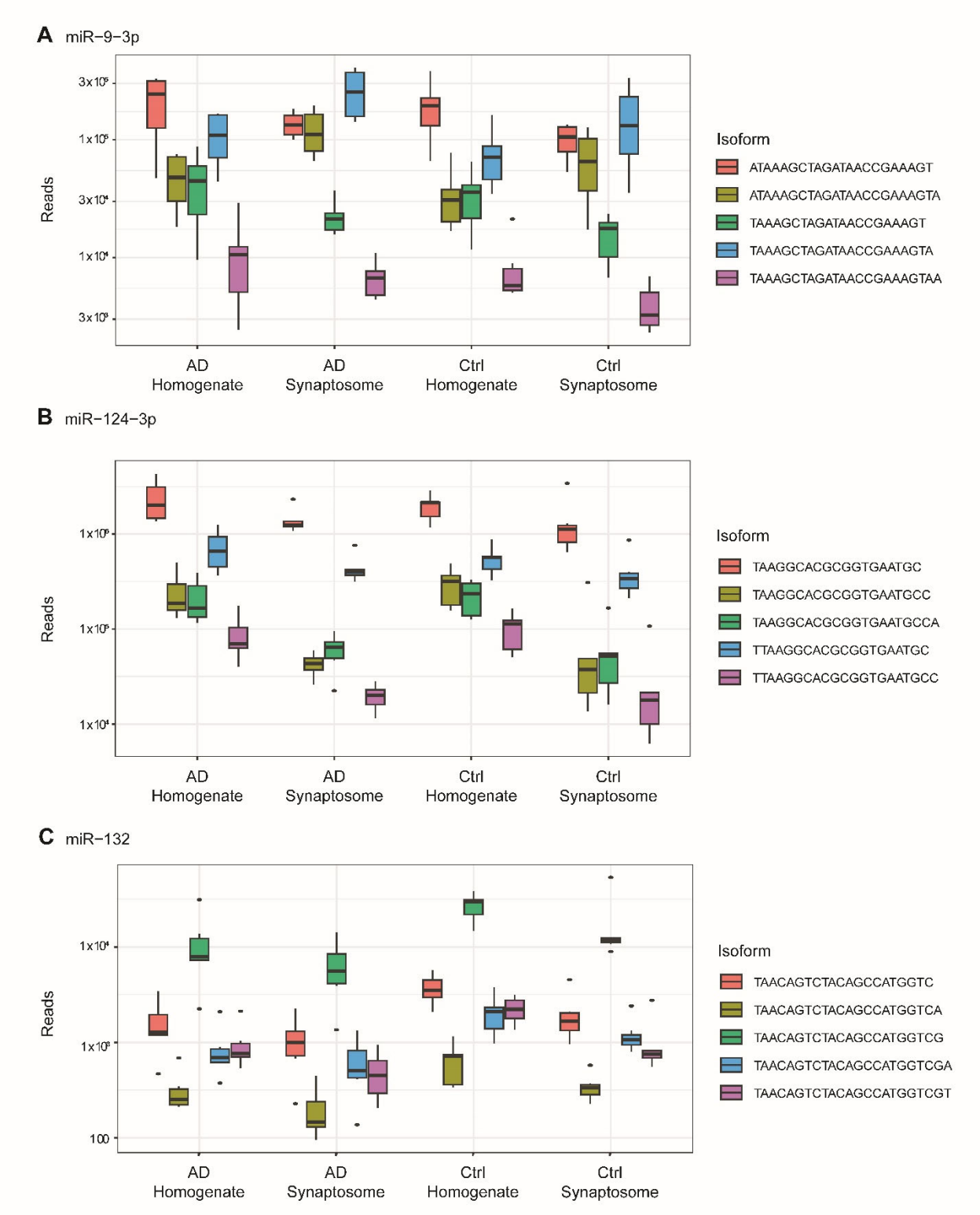

Fig 3.3. Different miRNA isoforms have preferential localization to synapses versus bulk homogenate. A. Normalized reads of different miR-9-3p isoforms showing differential synaptic

enrichment. **B.** Normalized reads corresponding to miR-124-3p isoforms in synapses and homogenate. **C.** Normalized reads corresponding to miR-132 isoforms in synapses and homogenate.

3.5 Discussion

The primary takeaways from this research analyzing miRNAs in AD synaptosomes include: 1) differential expression of miRNAs in both the bulk homogenate and synaptosomes are a possible explanation for differences in mRNA localization dynamics at AD synapses since there are many matching targets; 2) small RNA sequencing has the enhanced capability of discovering isoform differences that may be driving miRNA localization patterns and their regulatory effects.

We discovered that a fair degree of AD-related differentially expressed miRNAs in our homogenate and synaptosome data align with previous studies including that of miR-17, miR-24, miR-34c, miR-132, and miR-134c. We also confirmed enrichment of miR-7, miR-34a, and miR-103 at synapses as well as many new candidates including miR-30c, miR-107, and miR-139. We showed that a large percentage of differentially expressed miRNAs aligned with targets among mislocalized transcripts which suggest the miRNA regulation could be a mechanism driving differences in localized translation. One intriguing new discovery is the downregulation of miR-219 in synaptosomes. This is relevant because there is evidence that expression of miR-219 prevents tau hyperphosphorylation. Therefore, its downregulation at synapses may be a mechanism propagating tau pathology in AD.

It has been mentioned in the literature that frequent inconsistencies exist among the miRNA studies in AD tissue[68]. This dataset adds an additional resource to integrate into meta-analyses of the data that is available and come to a better consensus. An important note to

consider is that these meta-analyses often cover studies using a wide diversity of methods. We show here that small-RNA sequencing provides some of the most comprehensive data from which to analyze both differential expression and isoform differences among miRNAs in neurodegenerative disease. Another important consideration is sample quality. We source our postmortem tissue from brain banks with high quality standards with collection taking place less than eight hours after being declared deceased. Small RNAs may have different degradation kinetics than longer transcripts, so quality control is paramount to interpreting the accuracy of the data. As seen in Chapter 2, collection methods can also show substantial variation that needs to be corrected for. For this study, our sample size is low and multidimensional scaling analysis shows that there is more variability among the small-RNA sequencing versus mRNA sequencing in Chapter 2. Therefore, continued efforts to sequence more samples will need to be done to achieve a more accurate view of consistent changes taking place in AD.

Another possible explanation for sample variability is that miRNAs are intrinsically more variable than global transcriptomes or proteomes. Protein expression and localized translation are controlled by a very complex regulatory network orchestrated by a combination of underlying genetic variation, transcriptional processing, cytoskeletal dynamics, RNA-protein interactions, other RNA species including circRNAs, miRNAs, and lncRNAs, as well as synaptic signaling. A deficit among any of these regulatory factors in an individual may be compensated by differences in others yet arriving at the same phenotypes and final disease outcome. This has been studied in other neurodegenerative diseases such as FXS. Compensatory effects may also explain AD resilient subjects. This all underscores the need for studies including more comprehensive medical and sample data and multi-omic experiments to produce a more complete picture of pathological pathways in AD.

Experiments that can take this research further include modulating the expression of identified miRNAs in neuronal cultures to see if they drive localization differences of their target mRNAs. FISH experiments could determine whether a target mRNA is appropriately localized.

Pulse-chase experiments could determine target mRNA half-life. Fluorescent click-chemistry experiments could determine differences in translational efficiency and similarly, ribo-seq could determine differences in ribosome occupancy. In synaptosome preparations from the cultures RNA-seq could determine mRNA localization differences as well. Electrophysiology experiments could determine if there is ultimately an effect on synaptic signaling as a result of miRNA modulation. Finally, each of these experiments could be scaled up to mouse models to assess downstream phenotypes. In summary, analyzing the differences among miRNAs in AD synaptosomes sets the stage for homing in on pathological pathways leading to synaptic dysfunction in AD.

Finally, research into miRNAs correlated with differences in synaptic localized transcripts in AD provide a basis by which to assess targets for therapeutic intervention to restore synaptic function in AD and other neurodegenerative diseases. Many gene therapy studies taking place utilize delivery of small hairpin RNAs (which mimic the mechanism of miRNAs) to modulate gene expression. Other studies related to miRNAs in AD have suggested let-7, miR-9, and miR-124 as possible targets, and our data here corroborates this hypothesis[169,173,174,178]. Therefore, studying the impact of miR-9 or miR-124 modulation on localized translation and synaptic function could be the next step in assessing their therapeutic potential.

In conclusion, the combination of synaptosome small RNA sequencing along with total RNA sequencing (in chapter 2) provide a more complete picture of how synaptic function may be going awry in AD. The mislocalization of mRNAs could be dependent on miRNA expression differences in both the bulk homogenate as well as in synaptosomes. This is evidenced by strong correlations between the differentially expressed miRNAs identified here and their target mRNAs which are differentially localized in AD. Therefore, miRNA expression differences could be impacting synaptic plasticity and result in synaptic degeneration.

3.6 Supplemental Data

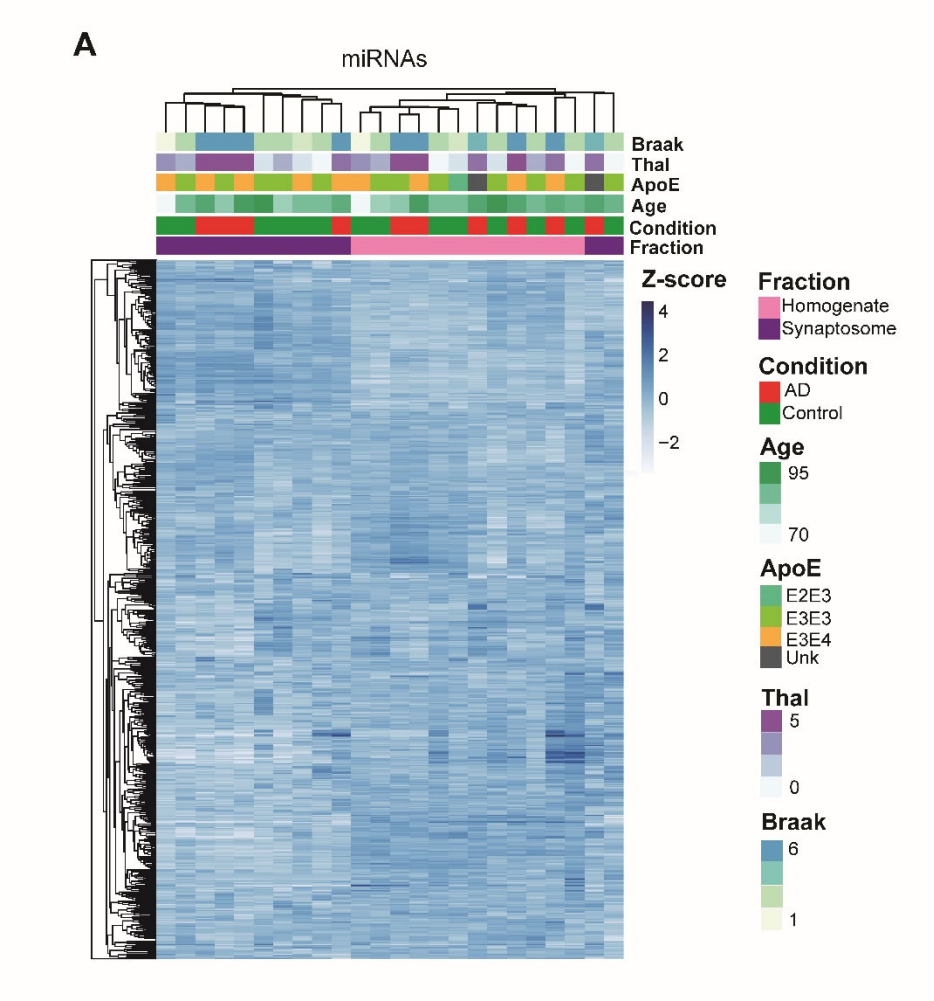

S3.1 Fig. Extended data for Fig 3.1; Heatmap of miRNA expression patterns. A. Heatmap showing strong clustering of synaptosome and homogenate fractions yet limited partitioning between disease condition. Age may have a moderate effect on sample variation.

Chapter 4: Differential RNA synaptic localization across lifespan in mice suggests differences observed in AD models represent accelerated aging

4.1 Abstract

Synaptic plasticity is an intrinsic feature of the brain essential for cognition and memory. Substantial differences in neuronal RNA and protein expression take place across development and during aging. Regardless of dementia diagnosis, cognitive abilities generally decline with human aging. Given how integral synaptic-localized translation is for cognitive function and the fine-tuned regulatory mechanisms required, it is likely that cognitive development and decline correlate with changes in the RNA localized to synapses. To differentiate between the neuronal changes associated with dementia and changes associated with healthy aging, it is important to understand how the localization changes seen in AD compare to ordinary changes taking place across healthy lifespan. In this chapter, we sequence synaptosomes from WT mice at various time points, and we discover common trajectories of mRNA and circRNA localization changes. Furthermore, differences observed in AD mice appear to continue these trends as an example of accelerated brain aging.

4.2 Introduction

In 1994, Dr. David Drachman asked the question “If we live long enough, will we all be demented?”[179] This question becomes ever more pertinent in the 21st century as US human life expectancy has been extended from 75.8 to 79.3 between 1994 and 2024 with a projection of it reaching 83.4 by 2050 according to United Nations data[180]. It has been established that age is the largest risk factor for developing Alzheimer’s[1]. We have also seen in Chapter 2 that age was the second strongest explanatory variable behind RNA localization differences. Therefore, it would be pragmatic to understand how RNA synaptic localization changes during healthy aging to determine if synaptic differences observed in AD are more broadly relevant; particularly because AD molecular pathologies can precede cognitive symptoms by decades. Aging in all tissues can be traced to several hallmarks including loss of proteostasis, stem-cell exhaustion, mitochondrial dysfunction, inflammation, and altered cellular communication[181,182]. Notably, all of these hallmarks also encompass many of the changes seen in AD[7].

One of the most well-studied hallmarks of brain aging is mitochondrial dysfunction and bioenergetic defects. Throughout brain aging it has been found that there is reduced efficiency of the electron transport chain, membrane potential, and NAD^+ production as well as an enlargement or fragmentation of the mitochondria. Phospho-tau buildup is also found in the synaptic mitochondria of aged mice[183]. The generation of reactive oxygen species (ROS) is a common source of cellular deterioration, and experiments in neuronal cultures and mouse models have shown improvement with the treatment of antioxidants. One signaling network central to aging and metabolism is mammalian target of rapamycin (mTOR) which functions as a regulator of protein translation and is also closely intertwined with insulin signaling[184]. Aging research has demonstrated that reducing the activity of mTOR in model organisms using caloric restriction or pharmaceuticals such as rapamycin or metformin leads to positive health

outcomes including improvements in cognitive function, retardation of aging phenotypes such as oxidative damage, and lifespan extension[185-189]. However, there is debate whether these paradigms work in humans. mTOR has also been studied in the context of AD where it is found to have increased activation and inhibition of mTOR reduces tau pathology. In AD, the generation of ROS has been found to lead to attenuation of AKT signaling in synapses which is downstream of mTOR signaling and found to interfere with localized-translation[190].

Inflammation also appears to unite the pathologies of several diseases in the brain including not only dementias, but also cancers, autoimmune diseases, and aging in general (often called “inflammaging”)[191]. A prime example is that of chronic or early-life stress where increased activated microglia proliferation is observed[192]. It has also been found that poor mental health, such as depression, is associated with decreases in brain grey matter which can be interpreted as accelerated aging[193]. Increases in inflammatory markers such as TNF-α and IL-6 are also positively correlated with cognitive decline.

Loss of proteostasis is observed as a consequence of many diseases including AD and ALS which exacerbates downstream effects[75,194]. It has been found that Aβ oligomers inhibit proteasomal function which can lead to a buildup of damaged proteins further contributing to synaptic dysfunction[195]. A reduction in lysosomal acidity is also observed in neuronal aging leading to synapse loss. Proteostasis is also closely intertwined with mTOR and insulin signaling.

Studies have shown that considerable proteomic and transcriptional changes happen in neurons and synapses throughout lifespan. One proteomic study found that the TGF-β signaling cascade was a unifying correlation of the aging brain[196]. Another proteomic study found that cognitive resilience was correlated with a decrease in inflammatory and apoptotic proteins and an increase in mitochondrial and synaptic proteins in human DLPFC homogenates. This could imply that maintaining stable localized translation is essential for healthy cognition in old age.

In this chapter, we aim to address the consistency of RNA synaptic localization through lifespan and compare healthy aging trends to the differences we observed in fAD mice. We selected mice from various age groups to fractionate synaptosomes and sequence localized mRNAs and circRNAs. We calculate trends in localization differences that are independent of global expression changes, thus they are a result of perturbations of upstream pathways including RNA-RBP interactions, alternative splicing, and cytoskeletal transport across lifespan.

4.3 Methods

4.3.1 Mouse brain samples

As in Chapter 2, The University of Washington Institutional Animal Care and Use Committee (IACUC) approved all mouse studies (protocols 4387-01 and 4419-01). Mice were maintained on an irradiated diet and provided free access to filtered water, with housing conditions maintained as previously described[112]. Following CO_2 asphyxiation according to AVMA guidelines, brains were dissected from three male and three female WT C57BL/6J mice (Jackson Laboratory) at a two-month time point, a six-month time point, and eight-month time point. Brains were sectioned based on brain regions, of which the frontal cortex was used for sequencing. The same WT and fAD mouse data used in Chapter 2 experiments were used as an eleven-month time point and the fAD group, respectively. The fAD mice APP Swedish mutation (K595N/M596L) and deletion of *PSEN1* exon 9 in the C57BL/6J background with WT littermates used as controls[113].

4.3.2 Synaptosome fractionation

As in Chapter 2, we adapted established protocols to isolate synaptosomes[56,57]. Approximately 300 mg of brain tissue was homogenized using a glass douncer in 1.5 mL of homogenization buffer. 120 µL of homogenate was set aside for RNA extraction and sequencing. The remaining homogenate was spun down at 750 × g for 10 min at 4ºC followed by centrifuging the supernatant at 13,800 × g to produce a pellet of crude synaptosomes. The crude synaptosome pellet was resuspended in 1 mL of homogenization buffer and a discontinuous sucrose gradient was prepared in a 4.2 mL ultracentrifuge tube with a 1 mL bottom layer of 1.2 M sucrose, 1 mL middle layer of 1.0 M sucrose, and a 1 mL top layer of 0.85 M sucrose buffers. The 1 mL of resuspended crude synaptosome was layered on top of the gradient and spun using a swinging bucket rotor in an ultracentrifuge at 28,000 rpm (~82,000 × g). The purified synaptosomes were collected from the interface between the 1.2 M and 1.0 M layers. RNA was subsequently extracted from 500 µl of the collected synaptosomes with Trizol/chloroform for sequencing.

4.3.3 Sequencing

100 ng of RNA from synaptosome and pre-fractionated homogenate fractions were aliquoted for library preparation using the Illumina stranded total RNA with rRNA removal (human). Since the experiments we completed in Chapter 2, Illumina released a new version of the RNA sequencing kit and discontinued the one we used previously. Therefore, to retain consistency, the eleven-month mouse controls were prepared again for sequencing using the new kit. Samples were barcoded and pooled into batches of twelve for sequencing submission to GeneWiz (Azenta) using 2 x 150 bp reads on an

Illumina NovaSeq S4 instrument. Data was demultiplexed and delivered as fastq files pertaining to each sample.

4.3.4 Data analysis

As in Chapter 2, transcriptome mapping and quantification was conducted with Salmon[114]. Transcriptome references were retrieved from Gencode (version M31 Mus musculus). Salmon quant files for each sample were imported into R for differential expression analysis using the DESeq2 package and workflow[115,116]. Expression analysis was normalized based on default DESeq2 parameters which takes into account the total number of reads as well as the length of each gene. We first ran DESeq2 on a dataset of all samples with (design = ~ Fraction + Age). We filtered our gene list by having 10 counts in at least 8 samples. From this, we used sample clustering and multidimensional scaling analysis to identify outliers and hierarchical clustering to identify confounding variables. Clustering by fraction and age was most robust, and sex did not appear to be a confounding variable.

Localization analysis was done by creating a ratio of ratios fold change acquired from DESeq2 as follows:

$$Fold\ Change = \log_2 \frac{\left(\frac{[Age_{older}]}{[Age_{younger}]}\right)_{Synaptosome}}{\left(\frac{[Age_{older}]}{[Age_{younger}]}\right)_{Homogenate}}$$

p values were calculated by generating a T-statistic as follows and matching to a two-tailed normal distribution with N-1 degrees of freedom:

$$T = \frac{R_w}{\frac{\sqrt{\frac{\sum_{i=1}^{number\ of\ genes} {R_w}^2}{number\ of\ genes}}}{\sqrt{Number\ of\ Samples}}}$$

Where:

$$R_w = \frac{1}{SE} \times \log_2 \left(\frac{[Age_{older}]}{[Age_{younger}]} \right)_{Synaptosome} - \frac{1}{SE} \times \log_2 \left(\frac{[Age_{older}]}{[Age_{younger}]} \right)_{Homogenate}$$

To determine a combined *p* value for genes that changed in their localization the most over lifespan, we used Fisher's Method as below which sums the natural log of each *p* value for each age comparison and matches the value to a χ^2 distribution with 2k degrees of freedom where k represents the number of *p* values being combined:

$$\chi^2_{2k} = -2 \sum_{i=1}^{k} \ln p_i$$

The three *p* values that were combined were from 6mo vs 2mo, 8mo vs 2mo, and 11mo vs 2mo. For comparisons with fAD mice, a fourth *p* value was added that represented AD vs 2mo. A significance cut-off was set at 0.01. Analysis of mRNAs and circRNAs followed the same principle, except circRNAs had a *p* value cut-off of 0.1.

Gene ontology analysis was conducted using GOpanther "biological process complete"[119]. Genome alignments for visualization were conducted using RNA-STAR in which mouse genomes were aligned to GRCm39 from Ensembl[120].

4.4 Results

4.4.1 mRNAs show distinct localization patterns over time

To determine how RNA localization changes with age as opposed to disease, we collected mouse frontal lobe tissue from wild-type (WT) two-month, six-month, and eight-month mice in addition to the eleven-month controls we had already sequenced. These age groups roughly correspond to 15 year, 30 year, 38 year, and 41 year humans respectively covering adolescence to middle-age[197]. We fractionated synaptosomes as described previously and isolated and sequenced the total RNA from both the synaptosomes and bulk homogenate. Using multidimensional scaling analysis, we saw a clear distinction between age groups for each fraction (**Fig 4.1A**). Heatmap visualization also showed robust clustering between age groups, and to a lesser degree, sex (**S4.1A Fig**). We compared synaptosome to homogenate enrichment of transcripts across all age groups and found consistent alignment with R^2 value ranging from 0.69-0.92 (**S4.2A Fig**). Six-months versus two-months synaptic enrichment showed the least concordance with two-month mice showing greater synaptic fold enrichment of transcripts. Eleven-months versus eight months showed the most concordance with a 1:1 ratio in synaptic enrichment. Both eight-month versus six-month and eleven-month versus six-month showed greater enrichment of synaptic transcripts as well as greater concordance with the two-month group. These correlations appear to explain some of the variation evidenced by the multidimensional scaling plot. This also seems to distinguish the six-month time point as a unique point in synaptic development.

We compared these results to our previous sequencing of AD mice to see correlations between the eleven-month AD mice and each of the other age groups. We found that AD mRNA synaptic enrichment was most concordant to the eleven-month WT mice with progressively less

concordance with younger age (with the exception of the six-month group) (**S4.3A Fig**). This indicates that AD mRNA synaptic enrichment correlates with aging.

Next, we looked at localization differences independent from global expression changes between each of the age groups using the statistical method described in Chapter 2. For example, we compared expression six-month mice to two-month mice in synaptosomes and then compared these values to expression in the homogenate of six-month versus two-month mice. We then repeated this analysis for each pair of age groups (**Fig 4.1B**). We found the greatest localization changes taking place between six-month and two-month followed by eight-month versus six-month (**Fig 4.1C**, and **S4.4A Fig**). We wanted to understand the patterns of these transcripts across lifespan, and we discovered that the most common trend was upregulation at six months, followed by a downregulation at eight months, and then an upregulation at ten months (**Fig 4.1D**). The next most common trend was an initial upregulation followed by successive downregulation over time.

We conducted a GO analysis to see if there were common functions that corresponded to these changes in localization. Of the mRNAs upregulated at six-months compared to two-months, top GO terms included cellular component and extracellular matrix organization, as well as cell adhesion and vasculature development (**Fig 4.2A**). Downregulated mRNAs included regulation of gene silencing by ncRNA and transmembrane transport. Curiously, several of these same or related terms showed opposite regulatory trends in eight-month versus six-months (**Fig 4.2B**). This matches the Up-Down-Up/Down patterns observed for many of the individual transcripts. At eleven-months versus eight-months, we see an upregulation of metabolic GO terms as well as immune terms and a downregulation of signal transduction, protein modification, and response to stress (**Fig 4.2C**). Curiously, many of these GO terms are semantically similar to those between AD and eleven-month WT mice in Chapter 2.

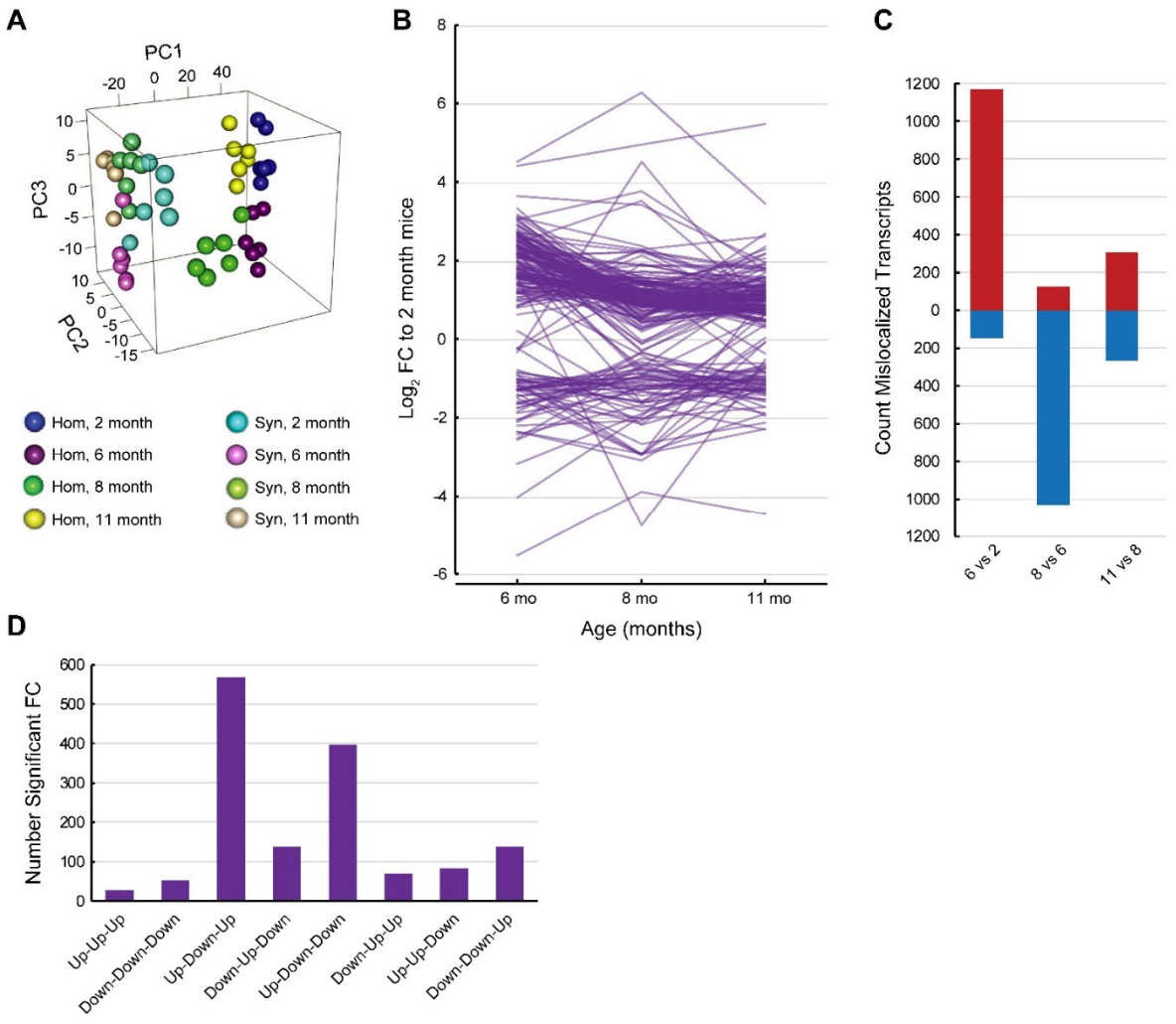

Fig 4.1. mRNA localization trends across WT mouse lifespan. A. Multidimensional scaling analysis of aging mice mRNA expression show robust partitioning between synaptosome and homogenate fractions as well as between each age group. **B.** Localization fold changes of mRNAs among 6mo, 8mo, and 11mo mice vs 2mo mice (Top 200 significant, $p < 0.05$). Fold changes represent the formula: $([Age_2] \text{ vs } [Age_1])_{Synaptosome} / ([Age_2] \text{ vs } [Age_1])_{Homogenate}$. **C.** Quantification of localization changes shown in (**B**). **D.** Quantification of localization patterns across lifespan in (**B**) where Up/Down indicates the direction of fold change at the next later timepoint compared to the previous fold change value. (i.e. [6 vs 2] – [8 vs 6] – [11 vs 8]).

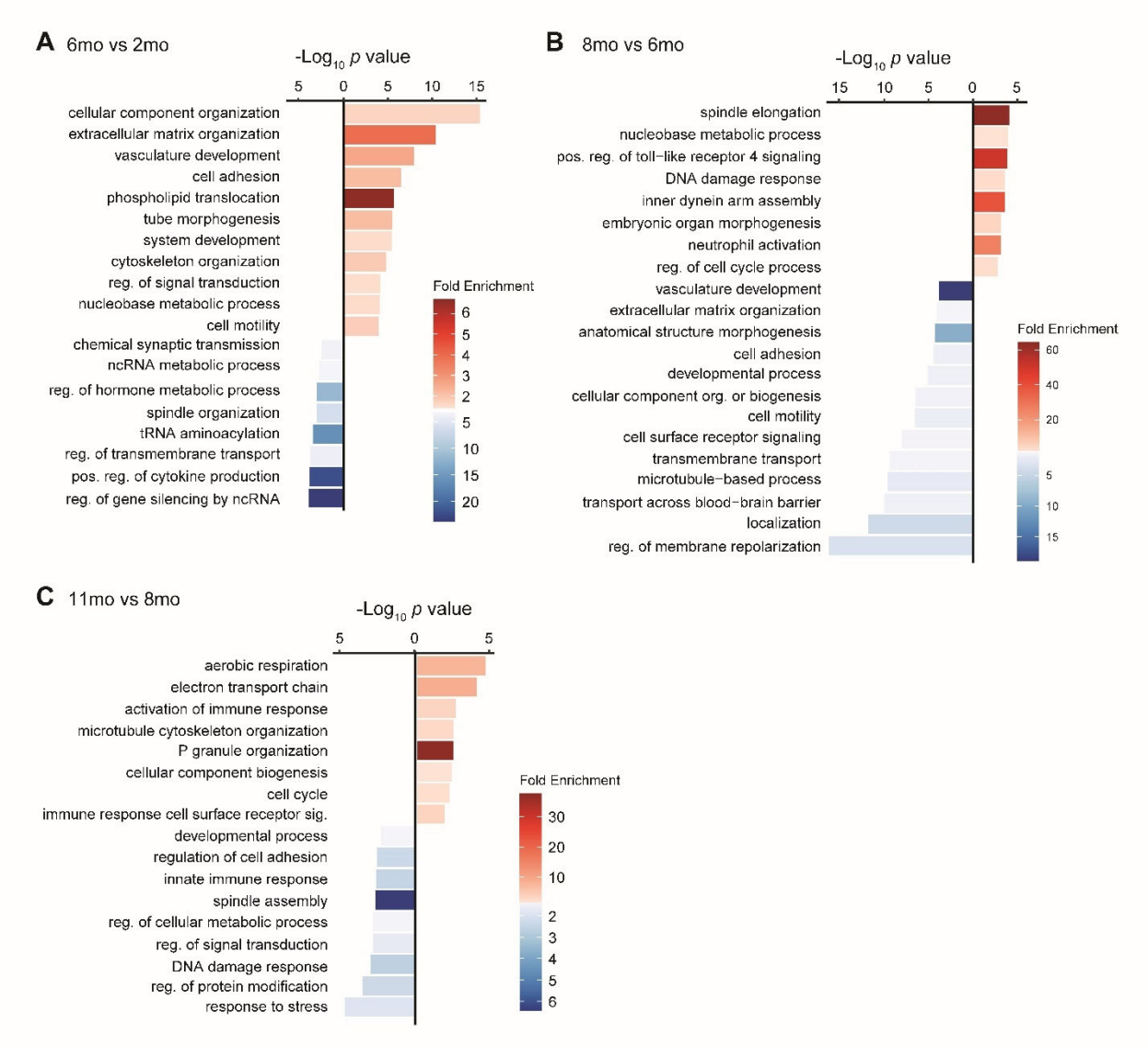

Fig 4.2. GO analysis of mRNAs changing in synaptic localization across lifespan. A. mRNAs that are either upregulated (red) or downregulated (blue) in their synaptic localization at 6mo vs 2mo. **B.** 8mo vs 6mo. And **C.** 11mo vs 8mo.

4.4.2 AD mice show exacerbated mislocalization trends across lifespan

We wanted to understand how the synaptic changes we observe previously in fAD mice fit into the general context of aging. In essence, we sought to understand if the transcriptional profile of diseased synapses was a unique state or showed general trends that aligned with changes across lifespan. There are lines of evidence we discovered that hint at both these possibilities.

We first conducted multidimensional scaling analysis to see how fAD mice synaptosomes and brain homogenates clustered compared to each of the mouse age groups, which had already showed distinctive clustering profiles. Indeed, we found robust separation of AD mice from all other mouse age groups with substantially more distance (**Fig. 4.3A**). AD homogenates appeared relatively equidistant from each of the other age groups, but AD synaptosomes appeared to cluster closer to the ten-month synaptosomes. Heatmap clustering also shows robust separation between the AD condition and all other age groups (**S4.5A Fig**).

In a similar manner to the localization trends plotted in Fig 4.2, we added the fAD mice as a fourth data point following the eleven-month group comparing fold change to the two-month mice (**Fig 4.4B** and **S4.6A Fig**). We observed a most prominent continuation of the age-related trend with an Up-Down-Up-Up pattern accounting for the majority of mislocalized transcripts (**Fig 4.3C**). We also saw a major subset of transcripts showing a trend reversal showing an Up-Down-Down-Up pattern. When comparing the total number of mislocalizations taking place in fAD mice compared to just the eleven-month mice, we see an overlap of 41% and almost twice as many mislocalizations in fAD versus the eleven-month mice (**Fig 4.3D**). Examples showing exacerbated aging trends include transcripts relating to GABAergic and cholinergic receptors, as well as numerous cell-adhesion genes (**Table 4.1** and **S4.1 Table**).

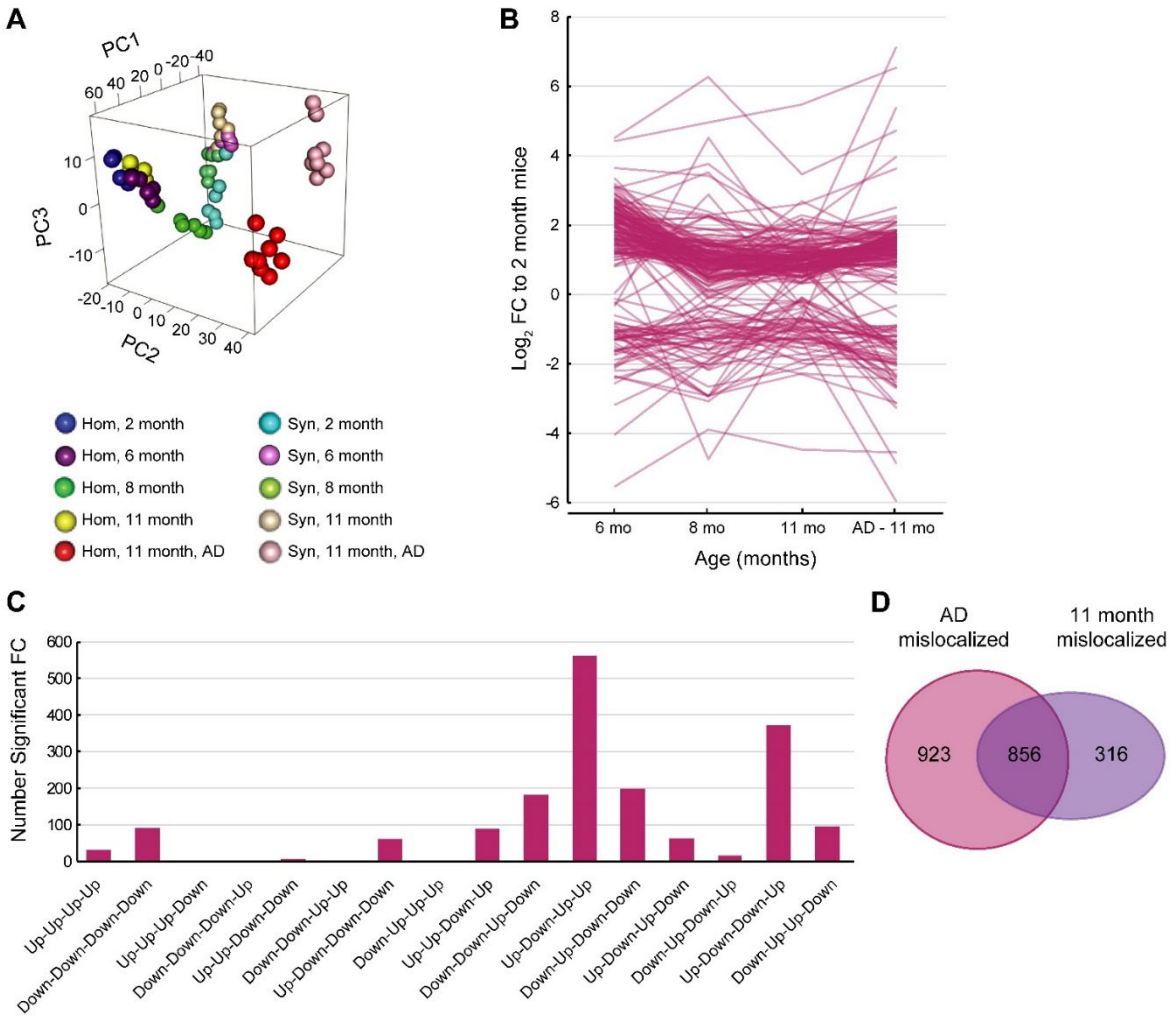

Fig 4.3: Comparing AD synaptic mRNA localization to other age groups. A. Multidimensional scaling analysis showing substantial separation of AD 11mo mice to all other WT age groups' expression profiles among both synaptosome and homogenate fractions. **B.** AD 11mo mice are added as a fourth datapoint succeeding 6mo, 8mo, and 11mo WT mice as in (**Fig 4.1B**). **C**. Quantification of localization patterns across lifespan in (**B**) where Up/Down indicates the direction of fold change at the next later timepoint/group compared to the previous fold change value. (i.e. [6 vs 2] – [8 vs 6] – [11 vs 8] – [AD-11mo vs WT-11mo]). **D.** Venn diagram comparing the synaptic mislocalized mRNAs found in either AD-11mo vs WT-11mo or WT-11mo vs WT-2mo.

Table 4.1: Major fold change localization differences in aging mice and fAD mice

Fold changes represent the formula: $([Age_2] \text{ vs } [Age_1])_{Synaptosome} / ([Age_2] \text{ vs } [Age_1])_{Homogenate}$. Raw *p* value is reported combined from the *p* values of each of the four fold-change values being compared using Fisher's Method.

Gene Symbol	Log_2 FC 6mo vs 2mo	Log_2 FC 8mo vs 2mo	Log_2 FC 11mo vs 2mo	Log_2 FC AD vs 2mo	*p* value
Cholinergic Receptors:					
Chrm5	-0.277	-0.696	-0.753	-0.957	0.0101
Chrna2	-0.810	-1.00	-0.468	-0.710	9.38E-4
Chrna3	-0.420	-1.02	-0.848	-0.958	2.40E-4
Chrna4	-0.549	-0.736	-0.647	-0.910	8.05E-3
Chrna7	-0.401	-0.556	-0.695	-0.940	0.0360
Chrnb3	-0.791	-0.510	-0.788	-1.24	3.91E-3
GABAergic Receptors:					
Gabra1	-0.920	-0.903	-0.756	-1.22	8.51E-5
Gabrb2	-0.518	-0.730	-0.540	-0.741	0.0222
Gabrg2	-0.656	-0.736	-0.741	-1.05	2.15E-3
Cell-Adhesion:					
Cdh1	-0.518	-0.954	-1.08	-1.20	4.21E-5
Cdhr3	1.83	0.838	0.618	0.514	2.42E-6

Cldn5	3.44	0.193	-0.122	-0.507	9.96E-6
Col4a5	-0.0480	-0.722	-0.831	-0.780	5.25E-3
Dcn	0.214	-0.946	-0.631	-1.05	4.20E-3
Edn3	2.07	0.866	0.554	0.294	1.12E-6
Epha7	-0.339	-0.614	-0.624	-0.813	0.0475
Fbln2	1.93	1.46	0.913	0.284	8.03E-10
Fn1	1.58	-0.193	-0.303	-0.788	4.71E-3
Lama5	2.05	0.425	0.275	0.380	2.58E-4
Matn2	-0.386	-0.614	-0.668	-0.781	0.0303
Nectin2	-0.248	-0.605	-0.755	-0.863	0.0211
Metabolic/Other:					
Ctsb	-0.688	-0.569	-0.739	-0.974	7.12E-3
Igf2r	-0.572	-0.613	-0.591	-1.07	0.0300
Igfbp7	1.68	-0.110	-0.463	-0.994	1.41E-3
Kif22	-1.40	-2.93	-2.29	-2.44	5.31E-15
Syp	-0.632	-0.535	-0.635	-0.926	0.0282

4.4.3 Progressive circRNA isoform changes at synapses increase over lifespan

Given previous studies, we wanted to confirm whether circRNAs accumulate at synapses as mice aged. We compared synaptosome to homogenate enrichment at each age group (**Fig 4.4A**). This validated that more circRNAs become increasingly enriched at synapses over lifespan ($p < 0.1$) (**Fig 4.4B**, **Fig 4.4C**, and **S4.2 Table**). Curiously, synaptosome

enrichment is not nearly as prominent as the human samples analyzed in Chapter 2 and there are still many circRNAs in the homogenate, although still less than half of all identified circRNAs.

To analyze differences in aging mouse synaptosomes we first conducted a multidimensional scaling analysis of the aging mice circRNA samples in the synaptosomes only. As with the linear mRNA analysis, we saw a clear distinction between all age groups (**Fig 4.4D**). As we tracked the significant circRNA changes over time in synaptosomes, we saw substantial divergence at the eleven-month age group with 846 differentially expressed circRNAs in contrast to only 261 and 337 in the six-month and eight-month groups respectively (**Fig 4.4E**). We also saw, similar to mRNAs, the prevailing expression trend over time for circRNAs is an initial upregulation at six-months, followed by a downregulation at eight-months, then subsequent upregulation at eleven-months (**Fig 4.4F**). We also saw the opposite trend taking place with an almost equal group of circRNAs with the degree of expression fold changes increasing over time.

Among the differentially expressed circRNAs, we also saw major differences in which splice isoforms, arising from the same gene, are present at the synapse (**Table 4.2** and **S4.3 Table**). Notably, isoforms of *Actb*, *Tuba1a*, and *Tspan7* show the most disparate fold changes over lifespan. We also observed several isoforms of synapse relevant genes including *Camkii*, *Aldoa*, and *Shank3*. We also identified a significant fold change of *circApoe* which has a previously established role in neurodegeneration.

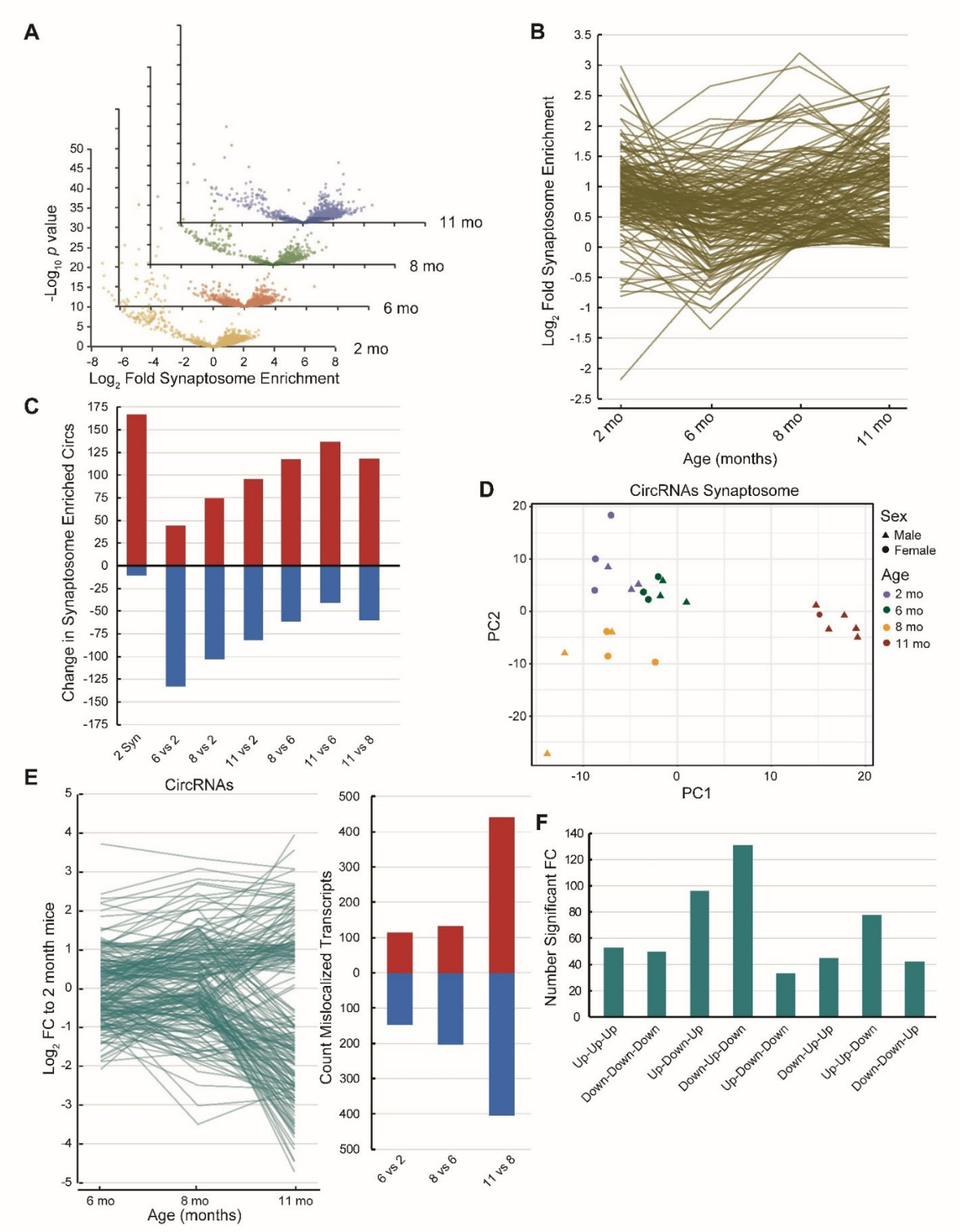
A
-Log10 p value
Log2 Fold Synaptosome Enrichment
11 mo
8 mo
6 mo
2 mo
B
Log2 Fold Synaptosome Enrichment
Age (months)
2 mo
6 mo
8 mo
11 mo
C
Change in Synaptosome Enriched Circs
2 Syn
6 vs 2
8 vs 2
11 vs 2
8 vs 6
11 vs 6
11 vs 8
D
CircRNAs Synaptosome
PC2
PC1
Sex
Male
Female
Age
2 mo
6 mo
8 mo
11 mo
E
CircRNAs
Log2 FC to 2 month mice
Age (months)
6 mo
8 mo
11 mo
Count Mislocalized Transcripts
6 vs 2
8 vs 6
11 vs 8
F
Number Significant FC
Up-Up-Up
Down-Down-Down
Up-Down-Up
Down-Up-Down
Up-Down-Down
Down-Up-Up
Up-Up-Down
Down-Down-Up

Fig 4.4. Synaptic circRNA expression differences across lifespan. A. Series of volcano plots comparing circRNA synaptic enrichment at various ages in WT mice. **B.** Plot showing the progression of circRNA synaptic enrichment across lifespan (Top 200, $p < 0.05$). **C.** Quantification of synaptic enrichment changes in (**B**). **D.** Multidimensional scaling analysis of aging mice circRNA expression in synaptosomes show robust partitioning between each age group. **E.** Expression fold changes of circRNAs among 6mo, 8mo, and 11mo mice vs 2mo mice (Top 200 significant, $p < 0.05$). Quantification of changes to the right. **F.** Quantification of circRNA expression patterns at synapses across lifespan in (**E**) where Up/Down indicates the direction of fold change at the next later timepoint compared to the previous fold change value. (i.e. [6 vs 2] – [8 vs 6] – [11 vs 8]).

Table 4.2 Examples of circRNA isoform switches across lifespan in frontal lobe mouse synaptosomes.

Comparing RNA sequencing data mapped to circRNA back-splice junctions among mice of various age groups including 2mo, 6mo, 8mo, and 11mo WT mice. “Donor” refers to the downstream exon by which its 3′ end is spliced back onto the upstream “Acceptor” exon’s 5′ end. We report the raw *p* value.

Gene	Donor	Acceptor	Log_2 FC 6mo vs 2mo	Log_2 FC 8mo vs 2mo	Log_2 FC 11mo vs 2mo	*p* value
Tuba1a	4	2	-0.253	0.506	-2.64	2.17E-5
Tuba1a	4	1	0.446	1.47	-0.605	1.35E-4
Tuba1a	4	4	-0.699	1.08	1.13	3.06E-3
Aldoa	9	6	0.0845	1.54	-1.26	9.61E-10
Aldoa	9	7	-0.476	0.975	-1.38	3.01E-8

Aldoa	9	8	-0.382	1.42	-2.34	1.98E-5
Tspan7	8	1	0.253	1.26	-0.698	1.17E-7
Tspan7	8	5	-0.0235	1.80	0.942	9.49E-6
Tspan7	1	1	-0.380	-0.805	-2.23	5.49E-5
Tspan7	7	2	-0.627	-1.17	-0.499	1.09E-3
Actb	4	4	0.877	-0.598	2.02	1.95E-9
Actb	6	2	-0.686	-0.0939	-3.61	9.12E-7
Actb	6	4	-0.578	-0.332	-2.78	1.37E-5
Actb	6	1	-0.604	-0.320	-0.974	5.07E-5
Actb	3	2	0.373	1.51	-0.520	4.53E-3
Actb	3	1	-0.803	-0.136	-0.935	6.51E-3
Eif1	2	1	-0.472	-1.57	-1.85	1.2E-12
Eif1	1	1	-1.28	-0.595	1.02	2.94E-4

4.5 Discussion

In this research, we have shown that changes in RNA localization to synapses is a pervasive feature of development. Whether these developmental changes are in any way pathological remains to be seen. It is likely that these changes are simply a means behind cognitive development and correlates with other synaptic processes such as synaptic pruning. Evidence that supports this notion is the most dramatic differences between six-month and two-month age groups which roughly correspond to human middle age and human adolescence, respectively[197]. Additional evidence comes from the GO terms associated with the changes in synaptic-localized mRNAs; particularly changes in vascular genes, cell-adhesion genes, and cellular component organization genes which are

strikingly similar to the GO terms associated between fAD mice and WT mice in Chapter 2 suggesting that localization changes in fAD appear to be on a trajectory of accelerated aging in this aspect of synaptic biology.

Notable groups of genes that stood out were cholinergic receptor units, GABAergic receptor units, and various cell-adhesion proteins (**Table 4.1**). There is a persistent decreasing trend in the synaptic-localization of these transcripts from six to eleven months, and even more so in fAD mice. A decrease in cholinergic neuron related genes has been observed before in AD and therapeutic avenues have been investigated to mitigate cognitive impairment by increasing cholinergic signaling[7,198]. The decrease in GABAergic neuron related genes also fits into a model of the AD hyperexcitability phase of disease in which case excess glutamate accumulates between synapses and increases Ca^{2+} influx. Increase in Ca^{2+} influx is also associated with an increase in ROS in old age[91]. Finally, the decrease in cell-adhesion protein genes could explain models in which synaptic plasticity decreases with age. Given the data here, it may be that these are common features of brain aging overall and similar therapeutic explorations directed towards dementia could have more broad applications towards maintaining cognitive resilience in both healthy and diseased subjects.

More could be done to pursue answering the question of whether mislocalization trends in fAD represent accelerated synaptic aging. What sets the fAD cohort apart from the aged WT mice is the greater quantity of differentially localized mRNAs by almost two-fold. The most straightforward next step would be to sequence synaptosomes and homogenates from WT mice at even later timepoints such as fourteen or sixteen months.

This research also confirmed previous observations that circRNAs accumulate at synapses across lifespan[110]. One other important consideration from the circRNAs observed here is that the localization of circRNAs to synapses is not as prominent as humans and there are much less circRNA differences overall. This could reflect that synaptic utilization of circRNAs is a more recent evolutionary development and may be associated with more complex

brains. This observation also suggests that circRNAs in mouse brains tend to serve different functions in the cytoplasm or other cell types in contrast to humans.

These data point to possible limitations to studying localization changes across lifespan. It is uncertain how these observations relate to humans. It is not easily feasible to acquire brain samples from heathy humans at different ages since premature death is usually a consequence of disease, although accidents of injury, such as vehicle collisions, are a possible resource. However, the take-away from this collection of research is that synaptic localization changes in RNA species over time is a feature of cognitive development and aging. Subsequent studies could aim to artificially modulate both mRNAs or circRNAs to identify the consequences of localization changes on other RNAs and protein composition at synapses as well as morphological features such as dendritic spine density. This would be a follow-up to previous discoveries regarding localization changes as a consequence of changes in 3′ UTR composition or RNA binding proteins. Another exciting prospect would be probing the effects of differentially expressed circRNAs on synaptic changes.

In summary, the research in this chapter demonstrates RNA synaptic localization is a flexible process and a possible driver of cognitive development and age-related cognitive decline. This research also distinguishes healthy aging from disease states given that changes in fAD mice are more pronounced. However, it remains to be seen how the differences in fAD mice compare to healthy mice at older ages. Another valuable observation arising from this research are the changes in circRNAs which suggest that they play regulatory roles in the RNA dynamics at synapses and likely different than the functions they may be serving in human brains. Taken together, this research underscores the importance of changes in synaptic localized translation in driving cognitive development and aging which can inform therapeutic interventions for cognitive resilience both in healthy aging and disease.

4.6 Supplemental Data

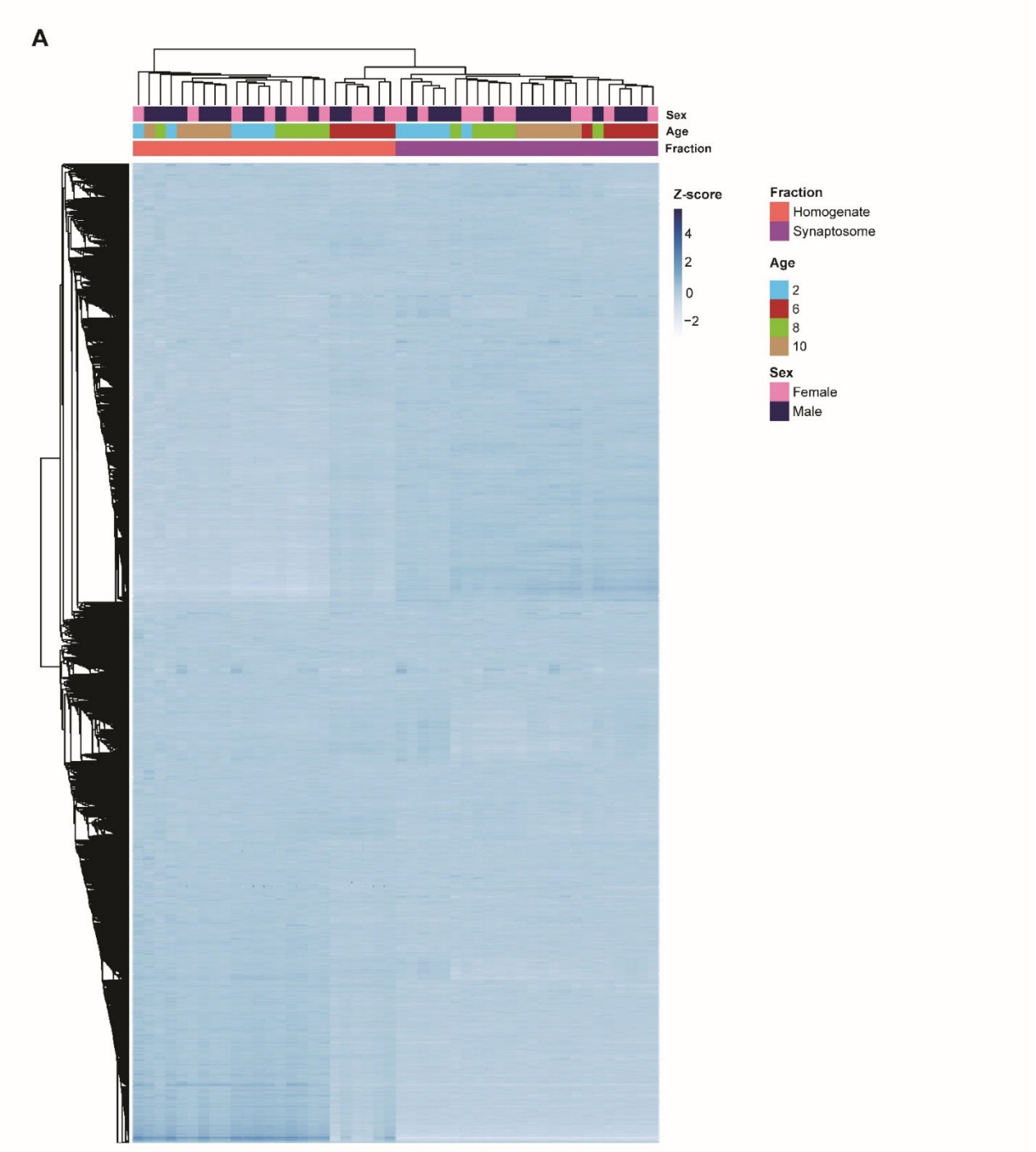

S4.1 Fig. Extended data for Fig 4.1; Heatmap of mRNA expression patterns across age groups. A. Heatmap showing robust clustering of synaptosome and homogenate fractions as well as strong partitioning between age groups.

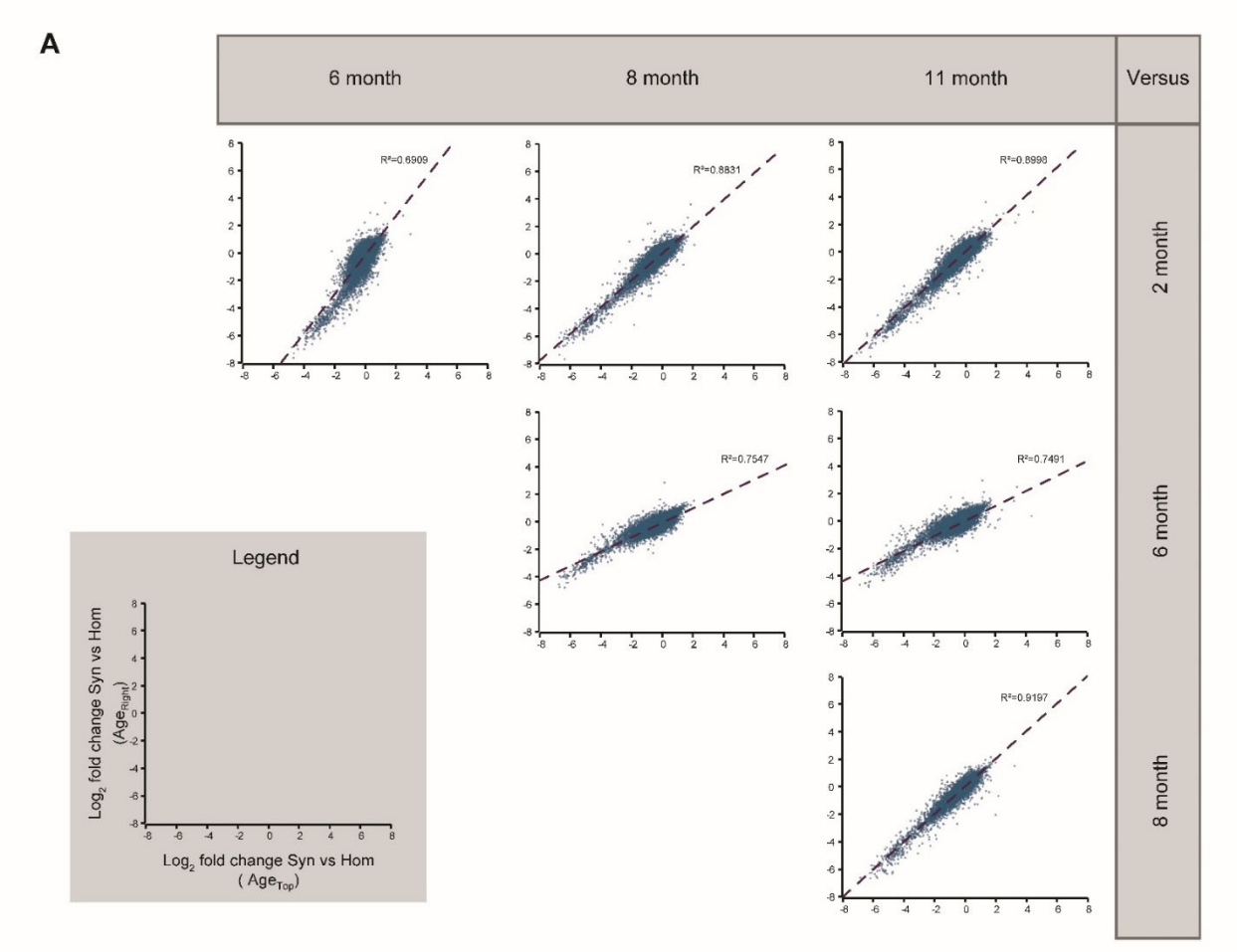

S4.2 Fig. mRNA synaptic enrichment between age groups. A. Correlation of synaptic enrichment of mRNAs between older mice and younger mice. Fold changes represent the formula: $(\text{Synaptosome vs Homogenate})_{[\text{Age-Top}]} / (\text{Synaptosome vs Homogenate})_{[\text{Age-Right}]}$.

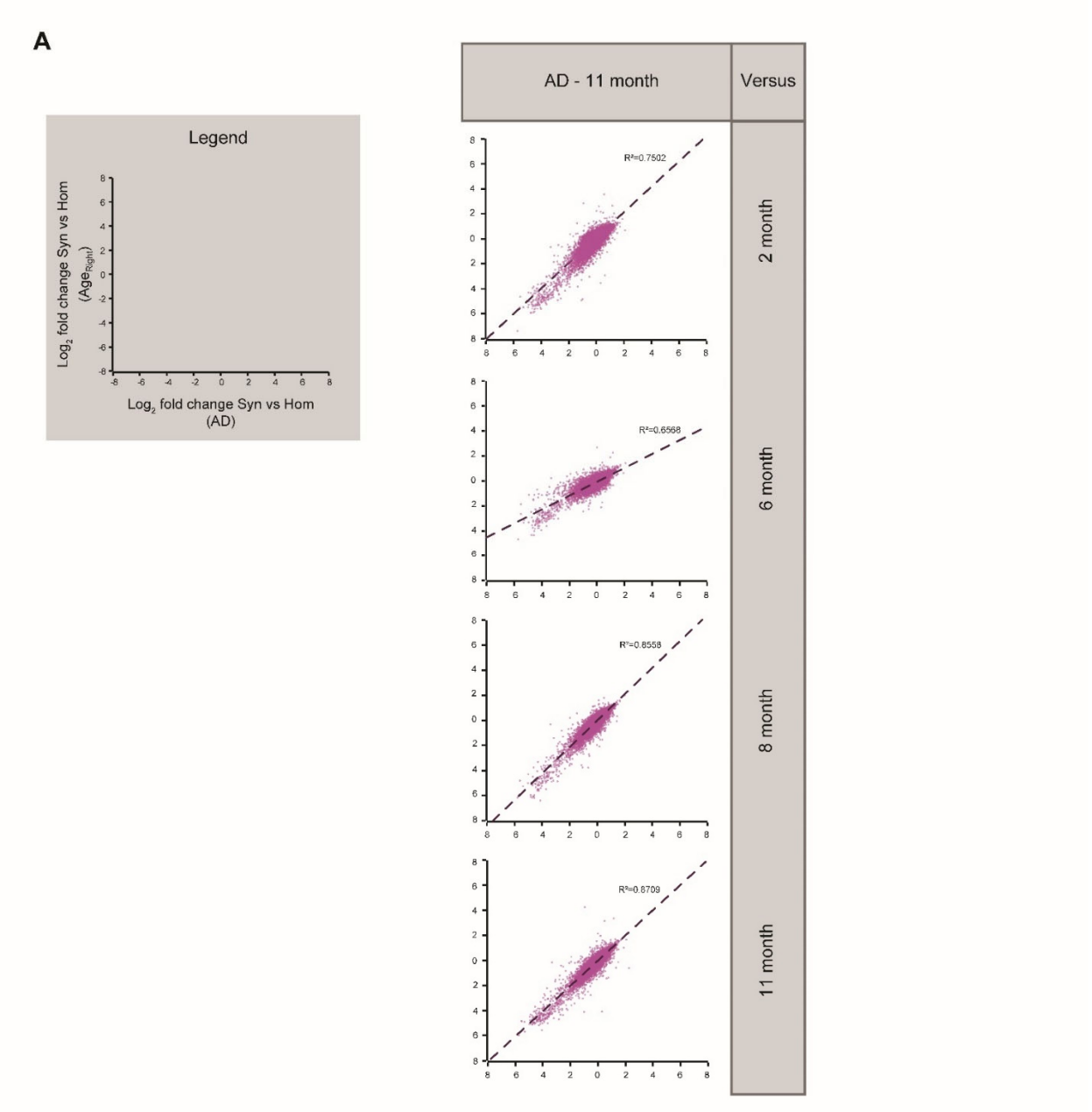

S4.3 Fig. mRNA synaptic enrichment between fAD mice and other age groups. A. Correlation of synaptic enrichment between fAD mice and other age groups. Fold changes represent the formula: $(\text{Synaptosome vs Homogenate})_{AD}$ / $(\text{Synaptosome vs Homogenate})_{[Age]}$.

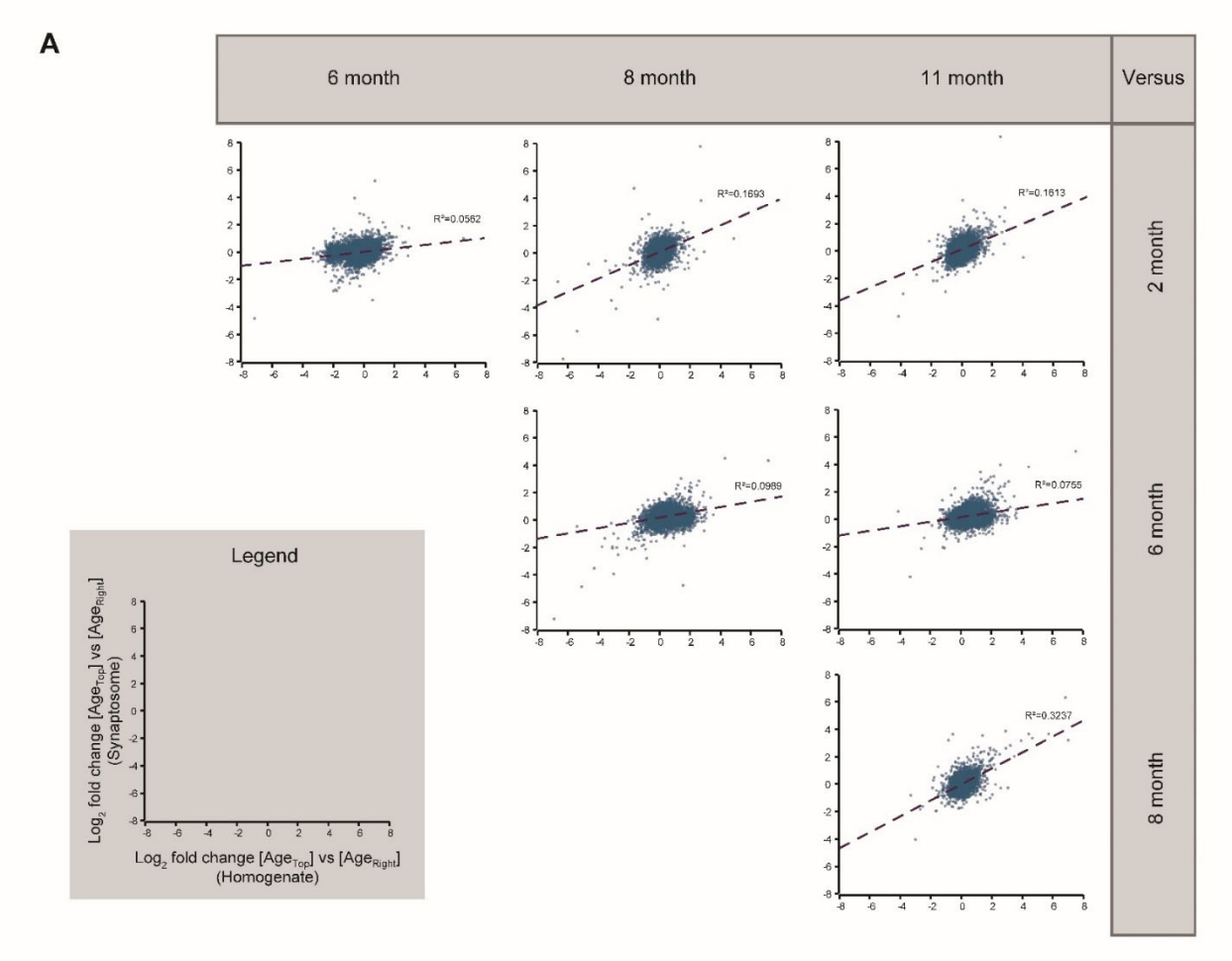

S4.4 Fig. Extended data for Fig 4.1; mRNA localization changes between age groups. A. Correlations between older mice vs younger mice in synaptosomes and older mice vs younger mice in homogenate. Fold changes represent the formula: $([Age_2] \text{ vs } [Age_1])_{Synaptosome} / ([Age_2] \text{ vs } [Age_1])_{Homogenate}$.

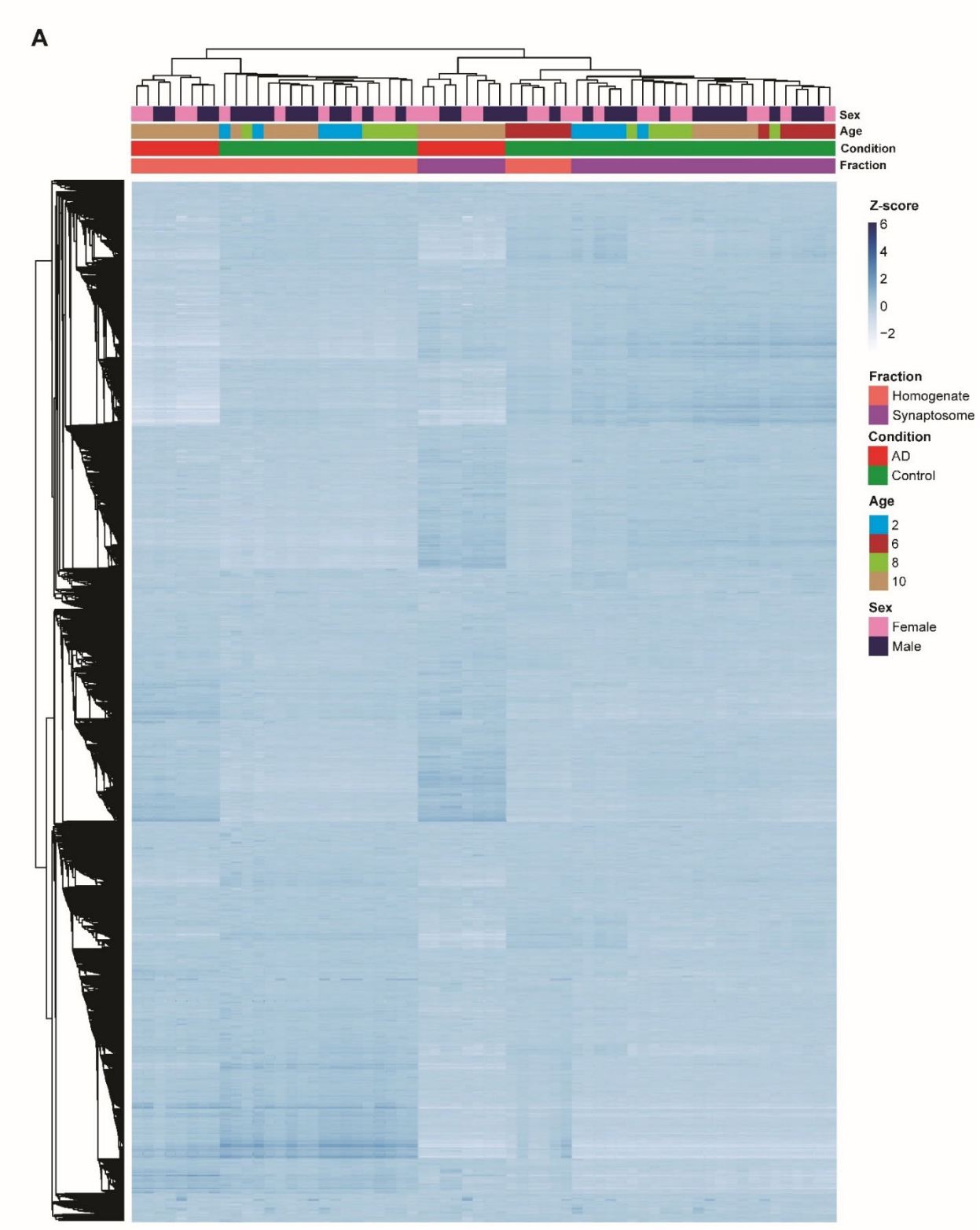

S4.5 Fig. Extended data for Fig 4.3; Heatmap of mRNA expression patterns across age groups including fAD mice. A. Heatmap showing robust clustering of both synaptosome and

homogenate fractions as well as efficient separation between AD and control, plus between age groups.

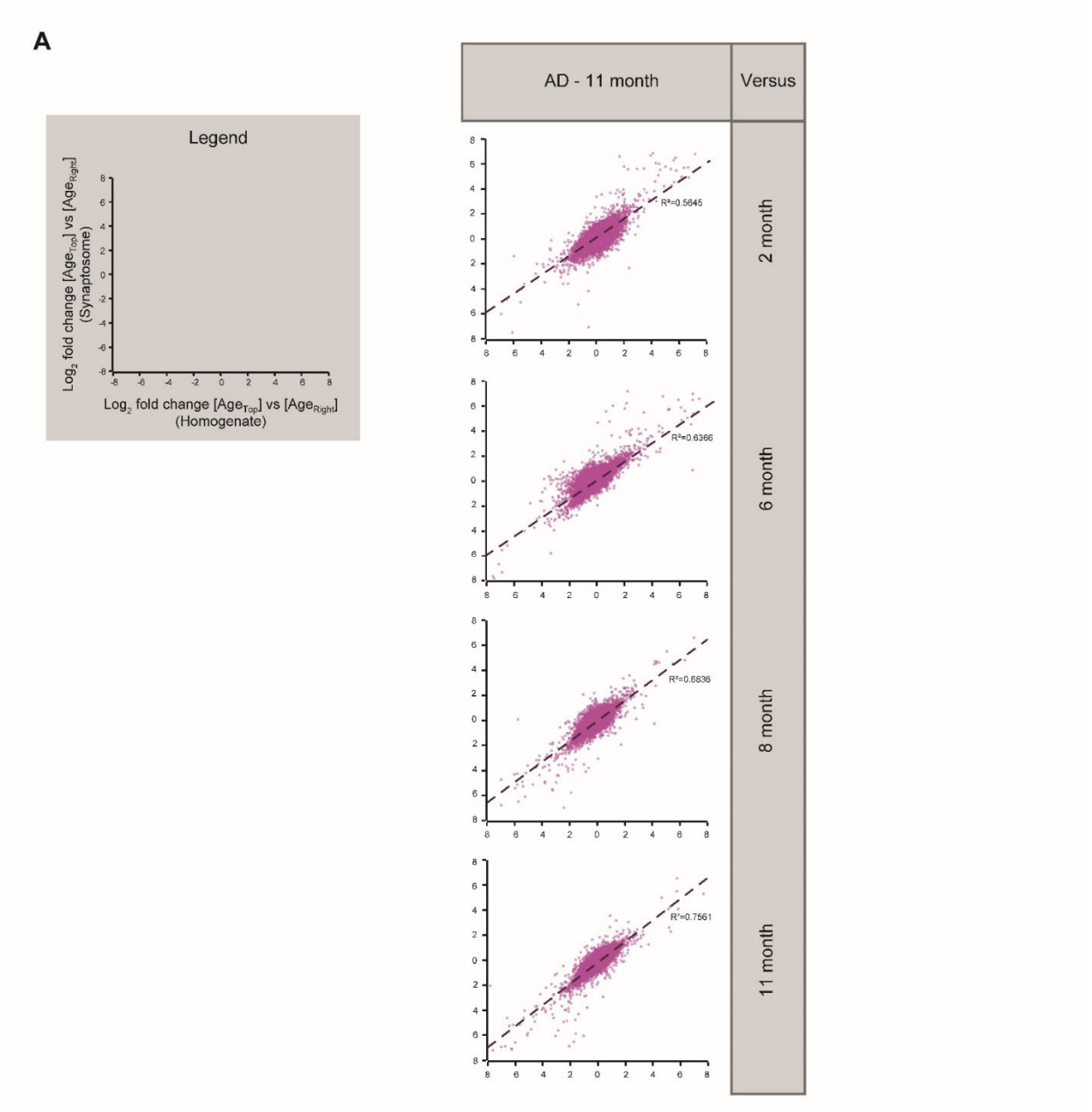

S4.6 Fig. Extended data for Fig 4.3; mRNA localization differences between fAD mice and other age groups. A. Correlations between fAD mice vs aged WT mice in synaptosomes and fAD mice vs aged WT mice in homogenate. Fold changes represent the formula: ([AD] vs [Age])$_{Synaptosome}$ / ([AD] vs [Age])$_{Homogenate}$.

Chapter 5: Concluding remarks

5.1 Impact of presented research

This collection of research highlights a new dimension to understanding synaptic defects in Alzheimer's disease and aging, and this methodology can also be applied to many other neurodegenerative diseases. The novelty of this presented approach lies in the method by which synaptic-localized RNAs are compared to bulk homogenate brain tissue to identify changes specifically occurring at synapses that are exclusively due to mislocalization independent of global expression changes. Although this has been done many times before in other models, this is the first application of the method to analyzing RNA mislocalization in human AD brains. In addition, this study encompasses a wide array of RNA isoform synaptic differences in AD including circRNAs and miRNAs. The study uses a combination of both total-RNA (with ribosome depletion) and small-RNA sequencing to understand the complete repertoire of RNA regulatory changes that may be occurring. These are all important features of synaptic function that cannot be addressed by simply studying protein composition at the synapse and global transcriptional changes because there are intricate regulatory steps taking place between the steps of transcription to translation.

Localized translation is a fine-tuned process that involves coordination between many mechanistic components including alternative splicing, cytoskeletal trafficking, biomolecular condensate dynamics, the interaction between multiple RNA species, and synaptic signaling. The research presented in this thesis demonstrates that differential localization of RNAs to synapses in AD and aging is occurring. These differences could be due to disruption of any of the aforementioned factors involved in accurately transporting RNAs to synapses, which sets

the stage for future experiments. Our research suggests that miRNAs may be playing a role in the abundance of mRNAs at synapses given that there are correlations between differentially expressed miRNAs and their targets among our datasets in AD.

We also highlight the importance of circRNAs at synapses. We validate previous evidence that circRNAs are enriched at synapses implying that they serve regulatory roles in the expression of other localized transcripts. This could be due to interactions with miRNAs or RBPs. We show that there are differences in the splice isoforms present at synapses in AD and throughout age. We highlighted an example of how a difference in *circGSK3β* isoforms may have a differential effect on tau phosphorylation suggesting that changes in circRNAs at synapses play causal roles.

We also show that changes in synaptic RNA localization is a pervasive feature of brain aging, and that localization patterns in an fAD model appear to follow aging trends to a greater degree suggesting that fAD pathologies may represent “accelerated” brain aging. This suggests that RNA mislocalization is not a feature exclusive to neurodegenerative disease, yet still a target for understanding processes of neurodegeneration and possible therapeutic strategies. This also could mean that therapeutic interventions that target RNA localization in AD may also be relevant towards retaining cognitive resilience in otherwise healthy aging individuals.

Limitations

There are notable limitations to this study of mRNA mislocalization. The most prominent concern is the diversity of cell types in the brain. The bulk homogenate we use as a reference to compare synaptosomes is derived from brain tissue that contains diverse cell types including astrocytes, oligodendrocytes, and glia. It would be ideal to use only neurons since we are comparing transcripts that are specifically localized to synapses. It is also of note that synaptic terminals also form connections between these other cell types and mixed

processes such as both synapse-to-glia processes and synapse-to-astrocyte processes can occur and co-fractionate with synaptosomes. Among neurons themselves, there are also a diversity of cell types including glutamatergic excitatory neurons or GABAergic inhibitory neurons. Therefore, all these considerations must be taken into account when interpreting these results. Alternative methods could address these issues such as fluorescence activated cell, or synaptosome, sorting which can isolate specific populations of interest. Barcoding methods such as single cell RNA sequencing could also tackle these questions. Both of these approaches would require substantially more tissue input, however the study presented here underscores the value these other endeavors could have since it clearly demonstrates RNA localization is a key component of neurodegeneration.

Another limitation that was revealed during this study was the impact of co-variables. Firstly, a weighted gene correlation network analysis (WGCNA) on our human frontal lobe samples revealed that tissue preservation has a substantial effect on RNA sequencing results and variation. We compared a selection of samples that were preserved using slow freezing in a sucrose buffer and a selection of samples that were preserved using flash freezing in isopentane. We demonstrated that combat_seq, which is a program that uses linear regression to correct for batch variation between samples, successfully eliminates the variation between the two tissue preservation methods whilst keeping the variables of interest intact. Nevertheless, this will be a critical consideration for future studies into synaptic RNA localization and additional examinations on the effects of different freezing methods will have to take place.

The second major co-variable was age. In this study we compare both the effects of localization based on age as well as disease condition. We found both by hierarchical clustering and WGCNA that age influenced sample variation, albeit secondary to disease status. Although in our sample selection for AD patient samples, we tried to control for age as much as possible, it cannot be dismissed that age contributes to differences in RNA synaptic localization. Thus, we conducted a second experiment observing the differences in localization across lifespan in

aging mice and compared that to the differences we observed in fAD mice. Remarkably we found that there was considerable overlap between the indicated mRNAs that become mislocalized in both age and disease, and that disease resulted in more significantly mislocalized mRNAs overall. Thus, when studying RNA localization, disease will likely be the primary variable, though age is something that also must be controlled or accounted for when interpreting results between cohorts.

Therapeutic potential

These discoveries of mRNA synaptic mislocalization suggest new targets for therapies that could mitigate synaptic dysfunction and degeneration in disease as well as the resultant cognitive impairments.

As seen with studies on FXS, targeting the RNA-binding protein FMRP or any of the downstream processes it affects can rescue cognitive deficits. In the context of AD or other neurodegenerative diseases, the research here suggests that targeting any of the mechanisms responsible for RNA localization and translational regulation at the synapse have the potential to restore synaptic function and thus mitigate resulting cognitive deficits[72]. These targets could include targeting FMRP or any other RBPs responsible for transporting mRNAs to synapses.

Other possibilities for intervention include expressing miRNAs or circRNAs that can drive regulatory differences in synaptic-localized translation. This could include the delivery of RNAs using viral or lipid nanoparticles. For example, there are current efforts to deliver miRNAs via adeno-associated virus (AAV) vectors to treat Huntington's disease by targeting a pathogenic repeat expansion in the *HTT* gene[199]. There are also a wide variety of clinical trials taking place testing the delivery of anti-sense oligonucleotides (which block pathogenic mRNAs) and miRNAs that target ALS-associated genetic mutations[200]. CircRNAs appear to have a most promising potential for such therapies giving their multifunctional regulatory

nature and molecular stability. Delivery of circRNAs has been proposed as a gene therapy approach for disease[201]. The research here suggests that differences in circRNAs at synapses is a major component of synaptic changes in aging and disease. Therefore, delivering circRNAs of regulatory significance to synapses may be a therapeutic avenue to explore.

Given the research here on differential miRNA expression in the same samples studied for mRNA mislocalization, we show that these differentially expressed miRNAs have targets that overlap with the mislocalized mRNAs. We also make predictions on other miRNAs that could affect localization patterns. This means that expression of any of the miRNAs by therapeutic delivery of shRNA constructs to neurons or their synapses could be tested as a means of modulating the localization to and translation of mRNAs in synapses.

5.2 Future directions

One critical piece of information that has been left out of this presented research is the role of RNA-binding proteins (RBPs). As seen with other neurological diseases including Fragile X syndrome and ALS, pathogenic variants among RNA-binding proteins show causal impacts on disease pathology and progression. Previous transcriptome and proteomic studies in AD indicate differential expression of RBPs[86]. Given the observations in the research described in this thesis regarding the mislocalization of RNAs at synapses, understanding its relationship to RBP differential expression may explain a mechanistic pathway by which RNA localization becomes disrupted. Specifically, the differences in RBP-RNA binding dynamics can be measured.

There are a few methods by which RBP-RNA interactions can be investigated. One method is UV-crosslinking and enrichment of protein-RNA complexes. These complexes can be separated from unbound RNA and protein by organic phase separation and the bound and

unbound proteins can be quantified by mass spectrometry[202]. If there is a correlation between differential RBP interactions and RBP motifs in the mislocalized transcripts, it would indicate that these interactions are a likely mechanism driving differential RNA synaptic-localization and localized translation in AD. Another method could employ crosslinking and poly-A pulldown of transcripts to quantify differences in RBP abundance.

Other experiments that can follow this work include a variety of functional studies that can directly measure differences in newly synthesized proteins between AD and control conditions. The research in this thesis largely demonstrates correlation, and leads to inferences about how protein composition at the synapses may be impaired in AD. However, demonstrating RNA mislocalization as a causal mechanism remains to be examined. This could be done by stimulating brain slices from AD and control mice at late age and measuring differences in nascent protein synthesis. There is also evidence this can work in freshly prepared synaptosomes that retain metabolic activity[138,203,204]. Another approach could utilize Ribo-seq which is a technique that crosslinks ribosomes to transcripts being actively translated, then the bound ribosomes can be isolated and their attached transcripts sequenced. This technique has been used to show differences in translation efficiency between soma and neuropil in micro dissected brain tissue[54].

Another area to be investigated is that of resilient AD patients. AD resilience is defined as patients having demonstrable AD pathological hallmarks such as amyloid plaques, but little to no cognitive impairment or other clinical symptoms. If we conclude that synaptic dysfunction may be a consequence of improper localized translation resulting from mislocalized RNAs, it could be that RNA localization is one of the explanatory variables defining AD resilience. It may be that despite classic molecular hallmarks such as amyloid being present, mRNA synaptic localization is not affected thus not impacting synaptic function and cognitive function is retained. Repeating synaptosome sequencing on tissue from AD resilient patients could test the merit of this hypothesis.

In summary, research into the relationship between localized translation and synaptic dysfunction in neurodegenerative disease and aging has a long way to go. The research in this thesis sets the stage for realizing the magnitude and importance of how RNA mislocalization at synapses may be contributing to disease pathologies and cognitive impairment. Subsequent experiments can address possible causes behind mislocalization and assess whether they could be therapeutically targeted to restore synaptic plasticity and cognitive function in neurodegenerative disease or aging.

Bibliography

1. Masters CL, Bateman R, Blennow K, Rowe CC, Sperling RA, Cummings JL. Alzheimer's disease. *Nature Reviews Disease Primers*. 2015-12-17 2015;1(1):15056. doi:10.1038/nrdp.2015.56

2. Patterson C. The state of the art of dementia research: New frontiers. *London: Alzheimer's Disease International*. 2018;

3. Bellenguez C, Grenier-Boley B, Lambert JC. Genetics of Alzheimer's disease: where we are, and where we are going. *Curr Opin Neurobiol*. Apr 2020;61:40-48. doi:10.1016/j.conb.2019.11.024

4. Bellenguez C, Kucukali F, Jansen IE, et al. New insights into the genetic etiology of Alzheimer's disease and related dementias. *Nat Genet*. Apr 2022;54(4):412-436. doi:10.1038/s41588-022-01024-z

5. Corder E, Saunders A, Strittmatter W, et al. Gene dose of apolipoprotein-E type-4 allele and the risk of Alzheimer's disease in late-onset families. *Science*. 1993;261(5123):921-923. doi:10.1126/science.8346443

6. Allen D. Roses MD. Apolipoprotein E alleles as risk factors in Alzheimer's disease. *Annual Review of Medicine*. 1996;47(1):387-400. doi:10.1146/annurev.med.47.1.387

7. Sharma P, Srivastava P, Seth A, Tripathi PN, Banerjee AG, Shrivastava SK. Comprehensive review of mechanisms of pathogenesis involved in Alzheimer's disease and potential therapeutic strategies. *Progress in Neurobiology*. 03/2019 2019;174:53-89. doi:10.1016/j.pneurobio.2018.12.006

8. Chen Y, Fu AKY, Ip NY. Synaptic dysfunction in Alzheimer's disease: Mechanisms and therapeutic strategies. *Pharmacology & Therapeutics*. 03/2019 2019;195:186-198. doi:10.1016/j.pharmthera.2018.11.006

9. Bourke AM, Schwarz A, Schuman EM. De-centralizing the Central Dogma: mRNA translation in space and time. *Mol Cell*. Feb 2 2023;83(3):452-468. doi:10.1016/j.molcel.2022.12.030

10. Rangaraju V, tom Dieck S, Schuman EM. Local translation in neuronal compartments: how local is local? *EMBO reports*. 05/2017 2017;18(5):693-711. doi:10.15252/embr.201744045

11. Das S, Vera M, Gandin V, Singer RH, Tutucci E. Intracellular mRNA transport and localized translation. *Nat Rev Mol Cell Biol*. Jul 2021;22(7):483-504. doi:10.1038/s41580-021-00356-8

12. Das S, Lituma PJ, Castillo PE, Singer RH. Maintenance of a short-lived protein required for long-term memory involves cycles of transcription and local translation. *Neuron*. Jul 5 2023;111(13):2051-2064 e6. doi:10.1016/j.neuron.2023.04.005

13. Baleriola J, Walker Chandler A, Jean Ying Y, et al. Axonally Synthesized ATF4 Transmits a Neurodegenerative Signal across Brain Regions. *Cell*. 08/2014 2014;158(5):1159-1172. doi:10.1016/j.cell.2014.07.001

14. Ma H, Khaled HG, Wang X, et al. Excitation-transcription coupling, neuronal gene expression and synaptic plasticity. *Nat Rev Neurosci*. Nov 2023;24(11):672-692. doi:10.1038/s41583-023-00742-5

15. Donlin-Asp PG, Polisseni C, Klimek R, Heckel A, Schuman EM. Differential regulation of local mRNA dynamics and translation following long-term potentiation and depression. *Proc Natl Acad Sci U S A*. Mar 30 2021;118(13)doi:10.1073/pnas.2017578118

16. Mason AJ, Deppmann C, Winckler B. Emerging Roles of Neuronal Extracellular Vesicles at the Synapse. *Neuroscientist*. Apr 2024;30(2):199-213. doi:10.1177/10738584231160521

17. Wagle S, Kraynyukova N, Hafner AS, Tchumatchenko T. Computational insights into mRNA and protein dynamics underlying synaptic plasticity rules. *Mol Cell Neurosci*. Jun 2023;125:103846. doi:10.1016/j.mcn.2023.103846

18. Steward O, Wallace CS, Lyford GL, Worley PF. Synaptic Activation Causes the mRNA for the IEG Arc to Localize Selectively near Activated Postsynaptic Sites on Dendrites. *Neuron*. 10/1998 1998;21(4):741-751. doi:10.1016/S0896-6273(00)80591-7

19. Pastuzyn ED, Day CE, Kearns RB, et al. The Neuronal Gene Arc Encodes a Repurposed Retrotransposon Gag Protein that Mediates Intercellular RNA Transfer. *Cell*. 01/2018 2018;172(1-2):275-288.e18. doi:10.1016/j.cell.2017.12.024

20. Zhang W, Chuang Y-A, Na Y, et al. Arc Oligomerization Is Regulated by CaMKII Phosphorylation of the GAG Domain: An Essential Mechanism for Plasticity and Memory Formation. *Molecular Cell*. 07/2019 2019;75(1):13-25.e5. doi:10.1016/j.molcel.2019.05.004

21. Kedrov AV, Durymanov M, Anokhin KV. The Arc gene: Retroviral heritage in cognitive functions. *Neuroscience & Biobehavioral Reviews*. 04/2019 2019;99:275-281. doi:10.1016/j.neubiorev.2019.02.006

22. Ashley J, Cordy B, Lucia D, Fradkin LG, Budnik V, Thomson T. Retrovirus-like Gag Protein Arc1 Binds RNA and Traffics across Synaptic Boutons. *Cell*. 01/2018 2018;172(1-2):262-274.e11. doi:10.1016/j.cell.2017.12.022

23. Ciolli Mattioli C, Rom A, Franke V, et al. Alternative 3′ UTRs direct localization of functionally diverse protein isoforms in neuronal compartments. *Nucleic Acids Research*. 2019-03-18 2019;47(5):2560-2573. doi:10.1093/nar/gky1270

24. Sharangdhar T, Sugimoto Y, Heraud-Farlow J, et al. A retained intron in the 3'-UTR of Calm3 mRNA mediates its Staufen2- and activity-dependent localization to neuronal dendrites. *EMBO Rep*. Oct 2017;18(10):1762-1774. doi:10.15252/embr.201744334

25. Taliaferro JM, Vidaki M, Oliveira R, et al. Distal Alternative Last Exons Localize mRNAs to Neural Projections. *Molecular Cell*. 03/2016 2016;61(6):821-833. doi:10.1016/j.molcel.2016.01.020

26. Mayford M, Baranes D, Podsypanina K, Kandel ER. The 3'-untranslated region of CaMKIIa is a cis-acting signal for

the localization and translation of mRNA in dendrites. *Proc Natl Acad Sci U S A*. 1996;93:13250-13255. doi:10.1073/pnas.93.23.13250

27. Tushev G, Glock C, Heumüller M, Biever A, Jovanovic M, Schuman EM. Alternative 3′ UTRs Modify the Localization, Regulatory Potential, Stability, and Plasticity of mRNAs in Neuronal Compartments. *Neuron*. 05/2018 2018;98(3):495-511.e6. doi:10.1016/j.neuron.2018.03.030

28. Lekk I, Cabrera-Cabrera F, Turconi G, et al. Untranslated regions of brain-derived neurotrophic factor mRNA control its translatability and subcellular localization. *J Biol Chem*. Feb 2023;299(2):102897. doi:10.1016/j.jbc.2023.102897

29. Farberov L, Ionescu A, Zoabi Y, et al. Multiple Copies of microRNA Binding Sites in Long 3'UTR Variants Regulate Axonal Translation. *Cells*. Jan 6 2023;12(2)doi:10.3390/cells12020233

30. Andreassi C, Crerar H, Riccio A. Post-transcriptional Processing of mRNA in Neurons: The Vestiges of the RNA World Drive Transcriptome Diversity. *Frontiers in Molecular Neuroscience*. 2018-8-28 2018;11:304. doi:10.3389/fnmol.2018.00304

31. Castro-Hernandez R, Berulava T, Metelova M, et al. Conserved reduction of m(6)A RNA modifications during aging and neurodegeneration is linked to changes in synaptic transcripts. *Proc Natl Acad Sci U S A*. Feb 28 2023;120(9):e2204933120. doi:10.1073/pnas.2204933120

32. Loedige I, Baranovskii A, Mendonsa S, et al. mRNA stability and m(6)A are major determinants of subcellular mRNA localization in neurons. *Mol Cell*. Aug 3 2023;83(15):2709-2725 e10. doi:10.1016/j.molcel.2023.06.021

33. Banani SF, Lee HO, Hyman AA, Rosen MK. Biomolecular condensates: organizers of cellular biochemistry. *Nature Reviews Molecular Cell Biology*. 5/2017 2017;18(5):285-298. doi:10.1038/nrm.2017.7

34. Chen X, Wu X, Wu H, Zhang M. Phase separation at the synapse. *Nature Neuroscience*. 3/2020 2020;23(3):301-310. doi:10.1038/s41593-019-0579-9

35. Lee J, Cho H, Kwon I. Phase separation of low-complexity domains in cellular function and disease. *Exp Mol Med*. Sep 2022;54(9):1412-1422. doi:10.1038/s12276-022-00857-2

36. Nam J, Gwon Y. Neuronal biomolecular condensates and their implications in neurodegenerative diseases. *Front Aging Neurosci*. 2023;15:1145420. doi:10.3389/fnagi.2023.1145420

37. Wilkerson JR, Ifrim MF, Valdez-Sinon AN, et al. FMRP phosphorylation and interactions with Cdh1 regulate association with dendritic RNA granules and MEF2-triggered synapse elimination. *Neurobiol Dis*. Jun 15 2023;182:106136. doi:10.1016/j.nbd.2023.106136

38. Jung J, Ohk J, Kim H, Holt CE, Park HJ, Jung H. mRNA transport, translation, and decay in adult mammalian central nervous system axons. *Neuron*. Mar 1 2023;111(5):650-668 e4. doi:10.1016/j.neuron.2022.12.015

39. Antar LN, Dictenberg JB, Plociniak M, Afroz R, Bassell GJ. Localization of FMRP-associated mRNA granules and requirement of microtubules for activity-dependent trafficking in hippocampal neurons. *Genes, Brain and Behavior*. 08/2005 2005;4(6):350-359. doi:10.1111/j.1601-183X.2005.00128.x

40. Hirokawa N, Niwa S, Tanaka Y. Molecular motors in neurons: transport mechanisms and roles in brain function, development, and disease. *Neuron*. Nov 18 2010;68(4):610-38. doi:10.1016/j.neuron.2010.09.039

41. Franker MA, Hoogenraad CC. Microtubule-based transport - basic mechanisms, traffic rules and role in neurological pathogenesis. *J Cell Sci*. Jun 1 2013;126(Pt 11):2319-29. doi:10.1242/jcs.115030

42. Zhao J, Fok AHK, Fan R, et al. Specific depletion of the motor protein KIF5B leads to deficits in dendritic transport, synaptic plasticity and memory. *Elife*. Jan 21 2020;9doi:10.7554/eLife.53456

43. Muhia M, Thies E, Labonte D, et al. The Kinesin KIF21B Regulates Microtubule Dynamics and Is Essential for Neuronal Morphology, Synapse Function, and Learning and Memory. *Cell Rep*. May 3 2016;15(5):968-977. doi:10.1016/j.celrep.2016.03.086

44. Yin X, Takei Y, Kido MA, Hirokawa N. Molecular motor KIF17 is fundamental for memory and learning via differential support of synaptic NR2A/2B levels. *Neuron*. Apr 28 2011;70(2):310-25. doi:10.1016/j.neuron.2011.02.049

45. Makrythanasis P, Maroofian R, Stray-Pedersen A, et al. Biallelic variants in KIF14 cause intellectual disability with microcephaly. *Eur J Hum Genet*. Mar 2018;26(3):330-339. doi:10.1038/s41431-017-0088-9

46. Swarnkar S, Avchalumov Y, Espadas I, et al. Molecular motor protein KIF5C mediates structural plasticity and long-term memory by constraining local translation. *Cell Rep*. Jul 13 2021;36(2):109369. doi:10.1016/j.celrep.2021.109369

47. Shang R, Lee S, Senavirathne G, Lai EC. microRNAs in action: biogenesis, function and regulation. *Nat Rev Genet*. Dec 2023;24(12):816-833. doi:10.1038/s41576-023-00611-y

48. Kristensen LS, Andersen MS, Stagsted LVW, Ebbesen KK, Hansen TB, Kjems J. The biogenesis, biology and characterization of circular RNAs. *Nature Reviews Genetics*. 11/2019 2019;20(11):675-691. doi:10.1038/s41576-019-0158-7

49. Curry-Hyde A, Ueberham U, Chen BJ, et al. Analysis of the Circular Transcriptome in the Synaptosomes of Aged Mice. *Neuroscience*. 11/2020 2020;449:202-213. doi:10.1016/j.neuroscience.2020.09.009

50. Liau WS, Zhao Q, Bademosi A, et al. Fear extinction is regulated by the activity of long noncoding RNAs at the synapse. *Nat Commun*. Nov 22 2023;14(1):7616. doi:10.1038/s41467-023-43535-1

51. Chen BJ, Ueberham U, Mills JD, et al. RNA sequencing reveals pronounced changes in the noncoding transcriptome of aging synaptosomes. *Neurobiol Aging*. Aug 2017;56:67-77. doi:10.1016/j.neurobiolaging.2017.04.005

52. Zappulo A, van den Bruck D, Ciolli Mattioli C, et al. RNA localization is a key determinant of neurite-enriched proteome. *Nat Commun*. Sep 19 2017;8(1):583. doi:10.1038/s41467-017-00690-6

53. Biever A, Glock C, Tushev G, et al. Monosomes actively translate synaptic mRNAs in neuronal processes. *Science*. 2020-01-31 2020;367(6477):eaay4991. doi:10.1126/science.aay4991

54. Glock C, Biever A, Tushev G, et al. The translatome of neuronal cell bodies, dendrites, and axons. *Proc Natl Acad Sci U S A*. Oct 26 2021;118(43)doi:10.1073/pnas.2113929118

55. Cajigas Iván J, Tushev G, Will Tristan J, tom Dieck S, Fuerst N, Schuman Erin M. The Local Transcriptome in the Synaptic Neuropil Revealed by Deep Sequencing and High-Resolution Imaging. *Neuron*. 05/2012 2012;74(3):453-466. doi:10.1016/j.neuron.2012.02.036

56. Whittaker V, Michaelson I, Kirkland R. The separation of synaptic vesicles from nerve-ending particles ('synaptosomes'). *Biochemical Journal*. 1964-02-01 1964;90(2):293-303. doi:10.1042/bj0900293

57. Tenreiro P, Rebelo S, Martins F, et al. Comparison of simple sucrose and percoll based methodologies for synaptosome enrichment. *Analytical Biochemistry*. 01/2017 2017;517:1-8. doi:10.1016/j.ab.2016.10.015

58. Jhou J-F, Tai H-C. The Study of Postmortem Human Synaptosomes for Understanding Alzheimer's Disease and Other Neurological Disorders: A Review. *Neurology and Therapy*. 7/2017 2017;6(S1):57-68. doi:10.1007/s40120-017-0070-z

59. Ahmad F, Liu P. Synaptosome as a tool in Alzheimer's disease research. *Brain Research*. 11/2020 2020;1746:147009. doi:10.1016/j.brainres.2020.147009

60. Hesse R, Hurtado ML, Jackson RJ, et al. Comparative profiling of the synaptic proteome from Alzheimer's disease patients with focus on the APOE genotype. *Acta Neuropathologica Communications*. 12/2019 2019;7(1):214. doi:10.1186/s40478-019-0847-7

61. Richter KN, Wildhagen H, Helm MS, Ussling JE, Schikorski T, Rizzoli SO. Comparative synaptosome imaging: a semi-quantitative method to obtain copy numbers for synaptic and neuronal proteins. *Sci Rep*. Oct 4 2018;8(1):14838. doi:10.1038/s41598-018-33130-6

62. van Oostrum M, Blok TM, Giandomenico SL, et al. The proteomic landscape of synaptic diversity across brain regions and cell types. *Cell*. Nov 22 2023;186(24):5411-5427 e23. doi:10.1016/j.cell.2023.09.028

63. Biesemann C, Grønborg M, Luquet E, et al. Proteomic screening of glutamatergic mouse brain synaptosomes isolated by fluorescence activated sorting. *The EMBO Journal*. 01/2014 2014;33(2):157-170. doi:10.1002/embj.201386120

64. Apostolo N, Smukowski SN, Vanderlinden J, et al. Synapse type-specific proteomic dissection identifies IgSF8 as a hippocampal CA3 microcircuit organizer. *Nat Commun*. Oct 14 2020;11(1):5171. doi:10.1038/s41467-020-18956-x

65. Fazal FM, Han S, Parker KR, et al. Atlas of Subcellular RNA Localization Revealed by APEX-Seq. *Cell*. Jul 11 2019;178(2):473-490 e26. doi:10.1016/j.cell.2019.05.027

66. Middleton SA, Eberwine J, Kim J. Comprehensive catalog of dendritically localized mRNA isoforms from sub-cellular sequencing of single mouse neurons. *BMC Biology*. 12/2019 2019;17(1):5. doi:10.1186/s12915-019-0630-z

67. Niu M, Cao W, Wang Y, et al. Droplet-based transcriptome profiling of individual synapses. *Nat Biotechnol*. Jan 16 2023;doi:10.1038/s41587-022-01635-1

68. Yoon S, Kim SE, Ko Y, et al. Differential expression of MicroRNAs in Alzheimer's disease: a systematic review and meta-analysis. *Mol Psychiatry*. May 2022;27(5):2405-2413. doi:10.1038/s41380-022-01476-z

69. Batish M, van den Bogaard P, Kramer FR, Tyagi S. Neuronal mRNAs travel singly into dendrites. *Proceedings of the National Academy of Sciences*. 2012-03-20 2012;109(12):4645-4650. doi:10.1073/pnas.1111226109

70. Dieterich DC, Lee JJ, Link AJ, Graumann J, Tirrell DA, Schuman EM. Labeling, detection and identification of newly synthesized proteomes with bioorthogonal non-canonical amino-acid tagging. *Nat Protoc*. 2007;2(3):532-40. doi:10.1038/nprot.2007.52

71. Akbalik G, Langebeck-Jensen K, Tushev G, et al. Visualization of newly synthesized neuronal RNA in vitro and in vivo using click-chemistry. *RNA Biol*. Jan 2 2017;14(1):20-28. doi:10.1080/15476286.2016.1251541

72. Hagerman RJ, Berry-Kravis E, Hazlett HC, et al. Fragile X syndrome. *Nat Rev Dis Primers*. Sep 29 2017;3:17065. doi:10.1038/nrdp.2017.65

73. Goering R, Hudish LI, Guzman BB, et al. FMRP promotes RNA localization to neuronal projections through interactions between its RGG domain and G-quadruplex RNA sequences. *Elife*. Jun 8 2020;9doi:10.7554/eLife.52621

74. Hale CR, Sawicka K, Mora K, et al. FMRP regulates mRNAs encoding distinct functions in the cell body and dendrites of CA1 pyramidal neurons. *Elife*. Dec 23 2021;10doi:10.7554/eLife.71892

75. Smukowski SN, Maioli H, Latimer CS, Bird TD, Jayadev S, Valdmanis PN. Progress in Amyotrophic Lateral Sclerosis Gene Discovery: Reflecting on Classic Approaches and Leveraging Emerging Technologies. *Neurol Genet*. Jun 2022;8(3):e669. doi:10.1212/NXG.0000000000000669

76. Josephs KA, Whitwell JL, Weigand SD, et al. TDP-43 is a key player in the clinical features associated with Alzheimer's disease. *Acta Neuropathol*. 2014;127(6):811-24. doi:10.1007/s00401-014-1269-z

77. Latimer CS, Stair JG, Hincks JC, et al. TDP-43 promotes tau accumulation and selective neurotoxicity in bigenic Caenorhabditis elegans. *Dis Model Mech*. Apr 1 2022;15(4)doi:10.1242/dmm.049323

78. Williams C, Mehrian Shai R, Wu Y, et al. Transcriptome Analysis of Synaptoneurosomes Identifies Neuroplasticity Genes Overexpressed in Incipient Alzheimer's Disease. *PLoS ONE*. 2009-3-19 2009;4(3):e4936. doi:10.1371/journal.pone.0004936

79. Raghavan NS, Brickman AM, Andrews H, et al. Whole-exome sequencing in 20,197 persons for rare variants in Alzheimer's disease. *Ann Clin Transl Neurol*. Jul 2018;5(7):832-842. doi:10.1002/acn3.582

80. Patel H, Dobson RJB, Newhouse SJ. A Meta-Analysis of Alzheimer's Disease Brain Transcriptomic Data. *Journal of Alzheimer's Disease*. 2019-04-23 2019;68(4):1635-1656. doi:10.3233/JAD-181085

81. Mathys H, Davila-Velderrain J, Peng Z, et al. Single-cell transcriptomic analysis of Alzheimer's disease. *Nature*. 6/2019 2019;570(7761):332-337. doi:10.1038/s41586-019-1195-2

82. Young JE, Boulanger-Weill J, Williams DA, et al. Elucidating molecular phenotypes caused by the SORL1 Alzheimer's disease genetic risk factor using human induced pluripotent stem cells. *Cell Stem Cell*. Apr 2 2015;16(4):373-85. doi:10.1016/j.stem.2015.02.004

83. Knupp A, Mishra S, Martinez R, et al. Depletion of the AD Risk Gene SORL1 Selectively Impairs Neuronal Endosomal Traffic Independent of Amyloidogenic APP Processing. *Cell Rep*. Jun 2 2020;31(9):107719. doi:10.1016/j.celrep.2020.107719

84. Kimura N, Yanagisawa K. Traffic jam hypothesis: Relationship between endocytic dysfunction and Alzheimer's disease. *Neurochem Int*. Oct 2018;119:35-41. doi:10.1016/j.neuint.2017.07.002

85. Latimer CS, Liachko NF. Tau and TDP-43 synergy: a novel therapeutic target for sporadic late-onset Alzheimer's disease. *Geroscience*. Aug 2021;43(4):1627-1634. doi:10.1007/s11357-021-00407-0

86. Johnson ECB, Dammer EB, Duong DM, et al. Deep proteomic network analysis of Alzheimer's disease brain reveals alterations in RNA binding proteins and RNA splicing

associated with disease. *Mol Neurodegener*. Oct 4 2018;13(1):52. doi:10.1186/s13024-018-0282-4

87. Zhang Q, Ma C, Gearing M, Wang PG, Chin L-S, Li L. Integrated proteomics and network analysis identifies protein hubs and network alterations in Alzheimer's disease. *Acta Neuropathologica Communications*. 2018;6(1)doi:10.1186/s40478-018-0524-2

88. Johnson ECB, Carter EK, Dammer EB, et al. Large-scale deep multi-layer analysis of Alzheimer's disease brain reveals strong proteomic disease-related changes not observed at the RNA level. *Nat Neurosci*. Feb 2022;25(2):213-225. doi:10.1038/s41593-021-00999-y

89. Ghatak S, Dolatabadi N, Trudler D, et al. Mechanisms of hyperexcitability in Alzheimer's disease hiPSC-derived neurons and cerebral organoids vs isogenic controls. *Elife*. Nov 29 2019;8doi:10.7554/eLife.50333

90. Minkeviciene R, Rheims S, Dobszay MB, et al. Amyloid beta-induced neuronal hyperexcitability triggers progressive epilepsy. *J Neurosci*. Mar 18 2009;29(11):3453-62. doi:10.1523/JNEUROSCI.5215-08.2009

91. Targa Dias Anastacio H, Matosin N, Ooi L. Neuronal hyperexcitability in Alzheimer's disease: what are the drivers behind this aberrant phenotype? *Transl Psychiatry*. Jun 22 2022;12(1):257. doi:10.1038/s41398-022-02024-7

92. Lehmann L, Lo A, Knox KM, Barker-Haliski M. Alzheimer's Disease and Epilepsy: A Perspective on the Opportunities for Overlapping Therapeutic Innovation. *Neurochem Res*. Aug 2021;46(8):1895-1912. doi:10.1007/s11064-021-03332-y

93. Miller JA, Guillozet-Bongaarts A, Gibbons LE, et al. Neuropathological and transcriptomic characteristics of the aged brain. *eLife*. 2017-11-09 2017;6:e31126. doi:10.7554/eLife.31126

94. Hafner A-S, Donlin-Asp PG, Leitch B, Herzog E, Schuman EM. Local protein synthesis is a ubiquitous feature of neuronal pre- and postsynaptic compartments. *Science*. 2019 2019;364(6441):13. doi:10.1126/science.aau3644

95. Roy R, Shiina N, Wang DO. More dynamic, more quantitative, unexpectedly intricate: Advanced understanding on synaptic RNA localization in learning and memory. *Neurobiology of Learning and Memory*. 02/2020 2020;168:107149. doi:10.1016/j.nlm.2019.107149

96. Formicola N, Vijayakumar J, Besse F. Neuronal ribonucleoprotein granules: Dynamic sensors of localized signals. *Traffic*. 2019-07-29 2019:tra.12672. doi:10.1111/tra.12672

97. Bauer KE, Segura I, Gaspar I, et al. Live cell imaging reveals 3'-UTR dependent mRNA sorting to synapses. *Nat Commun*. Jul 18 2019;10(1):3178. doi:10.1038/s41467-019-11123-x

98. Paolantoni C, Ricciardi S, De Paolis V, et al. Arc 3' UTR Splicing Leads to Dual and Antagonistic Effects in Fine-Tuning Arc Expression Upon BDNF Signaling. *Frontiers in Molecular Neuroscience*. 2018 2018;11(145):18. doi:10.3389/fnmol.2018.00145

99. Chen S, Zhu J, Li P, et al. 3′UTRs Regulate Mouse Ntrk2 mRNA Distribution in Cortical Neurons. *Journal of Molecular Neuroscience*. 2020-5-19 2020;doi:10.1007/s12031-020-01579-8

100. Savas JN, Wang Y-Z, DeNardo LA, et al. Amyloid Accumulation Drives Proteome-wide Alterations in Mouse Models of Alzheimer's Disease-like Pathology. *Cell Reports*. 11/2017 2017;21(9):2614-2627. doi:10.1016/j.celrep.2017.11.009

101. Postupna NO, Keene CD, Latimer C, et al. Flow cytometry analysis of synaptosomes from post-mortem human brain reveals changes specific to Lewy body and Alzheimer's disease. *Laboratory Investigation*. 10/2014 2014;94(10):1161-1172. doi:10.1038/labinvest.2014.103

102. Gajera CR, Fernandez R, Postupna N, et al. Mass synaptometry: High-dimensional multi parametric assay for single synapses. *Journal of Neuroscience Methods*. 01/2019 2019;312:73-83. doi:10.1016/j.jneumeth.2018.11.008

103. Memczak S, Jens M, Elefsinioti A, et al. Circular RNAs are a large class of animal RNAs with regulatory potency. *Nature*. 3/2013 2013;495(7441):333-338. doi:10.1038/nature11928

104. Rybak-Wolf A, Stottmeister C, Glazar P, et al. Circular RNAs in the Mammalian Brain Are Highly Abundant, Conserved, and Dynamically Expressed. *Mol Cell*. Jun 4 2015;58(5):870-85. doi:10.1016/j.molcel.2015.03.027

105. Salzman J, Gawad C, Wang PL, Lacayo N, Brown PO. Circular RNAs Are the Predominant Transcript Isoform from Hundreds of Human Genes in Diverse Cell Types. *PLoS ONE*. 2012-2-1 2012;7(2):e30733. doi:10.1371/journal.pone.0030733

106. Pamudurti NR, Bartok O, Jens M, et al. Translation of CircRNAs. *Molecular Cell*. 04/2017 2017;66(1):9-21.e7. doi:10.1016/j.molcel.2017.02.021

107. Legnini I, Di Timoteo G, Rossi F, et al. Circ-ZNF609 Is a Circular RNA that Can Be Translated and Functions in Myogenesis. *Mol Cell*. Apr 6 2017;66(1):22-37 e9. doi:10.1016/j.molcel.2017.02.017

108. Hansen TB, Jensen TI, Clausen BH, et al. Natural RNA circles function as efficient microRNA sponges. *Nature*. 3/2013 2013;495(7441):384-388. doi:10.1038/nature11993

109. You X, Vlatkovic I, Babic A, et al. Neural circular RNAs are derived from synaptic genes and regulated by development and plasticity. *Nature Neuroscience*. 4/2015 2015;18(4):603-610. doi:10.1038/nn.3975

110. Gruner H, Cortes-Lopez M, Cooper DA, Bauer M, Miura P. CircRNA accumulation in the aging mouse brain. *Sci Rep*. Dec 13 2016;6:38907. doi:10.1038/srep38907

111. Latimer CS, Burke BT, Liachko NF, et al. Resistance and resilience to Alzheimer's disease pathology are associated with reduced cortical pTau and absence of limbic-predominant age-related TDP-43 encephalopathy in a community-based cohort. *Acta Neuropathol Commun*. 2019;7(1):91. doi:10.1186/s40478-019-0743-1

112. Meeker S, Beckman M, Knox KM, Treuting PM, Barker-Haliski M. Repeated Intraperitoneal Administration of Low-Concentration Methylcellulose Leads to Systemic Histologic Lesions Without Loss of Preclinical Phenotype. *J Pharmacol Exp Ther*. Oct 2019;371(1):25-35. doi:10.1124/jpet.119.257261

113. Jankowsky JL, Fadale DJ, Anderson J, et al. Mutant presenilins specifically elevate the levels of the 42 residue beta-amyloid peptide in vivo: evidence for augmentation of a 42-specific gamma secretase. *Hum Mol Genet*. Jan 15 2004;13(2):159-70. doi:10.1093/hmg/ddh019

114. Patro R, Duggal G, Love MI, Irizarry RA, Kingsford C. Salmon provides fast and bias-aware quantification of transcript expression. *Nat Methods*. Apr 2017;14(4):417-419. doi:10.1038/nmeth.4197

115. Love MI, Huber W, Anders S. Moderated estimation of fold change and dispersion for RNA-seq data with DESeq2. *Genome Biology*. 12/2014 2014;15(12):550. doi:10.1186/s13059-014-0550-8

116. Love MI, Soneson C, Patro R. Swimming downstream: statistical analysis of differential transcript usage following Salmon quantification. *F1000Research*. 2018-6-27 2018;7:952. doi:10.12688/f1000research.15398.1

117. Langfelder P, Horvath S. WGCNA: an R package for weighted correlation network analysis. *BMC Bioinformatics*. 12/2008 2008;9(1):559. doi:10.1186/1471-2105-9-559

118. Zhang Y, Parmigiani G, Johnson WE. *ComBat-Seq : batch effect adjustment for RNA-Seq count data*. preprint. 2020. 2020-01-14. Accessed 2020-07-30 20:26:49.

119. Mi H, Muruganujan A, Thomas PD. PANTHER in 2013: modeling the evolution of gene function, and other gene attributes, in the context of phylogenetic trees. *Nucleic Acids Res*. 2013;41(Database issue):D377-86. doi:10.1093/nar/gks1118

120. Dobin A, Gingeras TR. Mapping RNA-seq Reads with STAR. *Current Protocols in Bioinformatics*. 09/2015 2015;51(1)doi:10.1002/0471250953.bi1114s51

121. Langmead B, Salzberg SL. Fast gapped-read alignment with Bowtie 2. *Nat Methods*. Mar 4 2012;9(4):357-9. doi:10.1038/nmeth.1923

122. Danecek P, Bonfield JK, Liddle J, et al. Twelve years of SAMtools and BCFtools. *Gigascience*. Feb 16 2021;10(2)doi:10.1093/gigascience/giab008

123. Quinlan AR, Hall IM. BEDTools: a flexible suite of utilities for comparing genomic features. *Bioinformatics*. Mar 15 2010;26(6):841-2. doi:10.1093/bioinformatics/btq033

124. Cheng J, Metge F, Dieterich C. Specific identification and quantification of circular RNAs from sequencing data. *Bioinformatics*. 2016-04-01 2016;32(7):1094-1096. doi:10.1093/bioinformatics/btv656

125. Agarwal V, Bell GW, Nam JW, Bartel DP. Predicting effective microRNA target sites in mammalian mRNAs. *Elife*. Aug 12 2015;4doi:10.7554/eLife.05005

126. Durinck S, Spellman PT, Birney E, Huber W. Mapping identifiers for the integration of genomic datasets with the R/Bioconductor package biomaRt. *Nat Protoc*. 2009;4(8):1184-91. doi:10.1038/nprot.2009.97

127. Liang D, Wilusz JE. Short intronic repeat sequences facilitate circular RNA production. *Genes Dev*. Oct 15 2014;28(20):2233-47. doi:10.1101/gad.251926.114

128. Shipley MM, Mangold CA, Szpara ML. Differentiation of the SH-SY5Y Human Neuroblastoma Cell Line. *Journal of Visualized Experiments*. 2016-2-17 2016;(108):53193. doi:10.3791/53193

129. Hobson BD, Herzog E. Methodological concerns and lack of evidence for single-synapse RNA-seq. *Nat Biotechnol*. Sep 2023;41(9):1221-1224. doi:10.1038/s41587-023-01877-7

130. Kumar S, Orlov E, Gowda P, et al. Synaptosome microRNAs regulate synapse functions in Alzheimer's disease. *NPJ Genom Med*. Aug 8 2022;7(1):47. doi:10.1038/s41525-022-00319-8

131. (DIAN) tDIAN, Dube U, Del-Aguila JL, et al. An atlas of cortical circular RNA expression in Alzheimer disease brains demonstrates clinical and pathological associations. *Nature Neuroscience*. 11/2019 2019;22(11):1903-1912. doi:10.1038/s41593-019-0501-5

132. Toral-Rios D, Pichardo-Rojas PS, Alonso-Vanegas M, Campos-Pena V. GSK3beta and Tau Protein in Alzheimer's Disease and Epilepsy. *Front Cell Neurosci*. 2020;14:19. doi:10.3389/fncel.2020.00019

133. Hong M, Chen DC, Klein PS, Lee VM. Lithium reduces tau phosphorylation by inhibition of glycogen synthase kinase-3. *J Biol Chem*. Oct 3 1997;272(40):25326-32. doi:10.1074/jbc.272.40.25326

134. Tsang B, Arsenault J, Vernon RM, et al. Phosphoregulated FMRP phase separation models activity-dependent translation through bidirectional control of mRNA granule formation. *Proc Natl Acad Sci U S A*. Mar 5 2019;116(10):4218-4227. doi:10.1073/pnas.1814385116

135. Popper B. Staufen2 deficiency leads to impaired response to novelty in mice. *Neurobiology of Learning and Memory*. 2018 2018:9.

136. Ramaswami M, Taylor JP, Parker R. Altered ribostasis: RNA-protein granules in degenerative disorders. *Cell*. Aug 15 2013;154(4):727-36. doi:10.1016/j.cell.2013.07.038

137. Traunmüller L, Gomez AM, Nguyen T-M, Scheiffele P. Control of neuronal synapse specification by a highly dedicated alternative splicing program. *Science*. 2016;352(6288):982-986. doi:doi:10.1126/science.aaf2397

138. Cefaliello C, Penna E, Barbato C, et al. Deregulated Local Protein Synthesis in the Brain Synaptosomes of a Mouse Model for Alzheimer's Disease. *Molecular Neurobiology*. 3/2020 2020;57(3):1529-1541. doi:10.1007/s12035-019-01835-y

139. Kim B-Y, Lim H-S, Kim Y, Kim YJ, Koo I, Jeong S-J. Evaluation of Animal Models by Comparison with Human Late-Onset Alzheimer's Disease. *Molecular Neurobiology*. 12/2018 2018;55(12):9234-9250. doi:10.1007/s12035-018-1036-6

140. Cervera-Carles L, Dols-Icardo O, Molina-Porcel L, et al. Assessing circular RNAs in Alzheimer's disease and frontotemporal lobar degeneration. *Neurobiol Aging*. Aug 2020;92:7-11. doi:10.1016/j.neurobiolaging.2020.03.017

141. Colom-Cadena M, Davies C, Sirisi S, et al. Synaptic oligomeric tau in Alzheimer's disease — A potential culprit in the spread of tau pathology through the brain. *Neuron*. 2023;doi:10.1016/j.neuron.2023.04.020

142. Bhat RV, Andersson U, Andersson S, Knerr L, Bauer U, Sundgren-Andersson AK. The Conundrum of GSK3 Inhibitors: Is it the Dawn of a New Beginning? *Journal of Alzheimer's Disease*. 2018;64:S547-S554. doi:10.3233/JAD-179934

143. Cohen P, Goedert M. GSK3 inhibitors: development and therapeutic potential. *Nat Rev Drug Discov*. Jun 2004;3(6):479-87. doi:10.1038/nrd1415

144. Fleisher AS, Truran D, Mai JT, et al. Chronic divalproex sodium use and brain atrophy in Alzheimer disease. *Neurology*. 2011;77(13):1263-1271. doi:10.1212/WNL.0b013e318230a16c

145. Tariot PN, Schneider LS, Cummings J, et al. Chronic Divalproex Sodium to Attenuate Agitation and Clinical Progression of Alzheimer Disease. *Archives of General Psychiatry*. 2011;68(8):853-861. doi:10.1001/archgenpsychiatry.2011.72

146. Ingolia NT, Ghaemmaghami S, Newman JRS, Weissman JS. Genome-Wide Analysis in Vivo of Translation with Nucleotide Resolution Using Ribosome Profiling. *Science*. 2009-04-10 2009;324(5924):218-223. doi:10.1126/science.1168978

147. Simbriger K, Amorim IS, Chalkiadaki K, et al. Monitoring translation in synaptic fractions using a ribosome profiling strategy. *Journal of Neuroscience Methods*. 01/2020 2020;329:108456. doi:10.1016/j.jneumeth.2019.108456

148. Chen S, Zhou Y, Chen Y, Gu J. fastp: an ultra-fast all-in-one FASTQ preprocessor. *Bioinformatics*. Sep 1 2018;34(17):i884-i890. doi:10.1093/bioinformatics/bty560

149. McGeary SE, Lin KS, Shi CY, et al. The biochemical basis of microRNA targeting efficacy. *Science*. Dec 20 2019;366(6472)doi:10.1126/science.aav1741

150. Hafner M, Landthaler M, Burger L, et al. Transcriptome-wide identification of RNA-binding protein and microRNA target sites by PAR-CLIP. *Cell*. Apr 2 2010;141(1):129-41. doi:10.1016/j.cell.2010.03.009

151. Lewis BP, Burge CB, Bartel DP. Conserved seed pairing, often flanked by adenosines, indicates that thousands of human genes are microRNA targets. *Cell*. Jan 14 2005;120(1):15-20. doi:10.1016/j.cell.2004.12.035

152. Friedman RC, Farh KK, Burge CB, Bartel DP. Most mammalian mRNAs are conserved targets of microRNAs. *Genome Res*. Jan 2009;19(1):92-105. doi:10.1101/gr.082701.108

153. Griffiths-Jones S, Grocock RJ, van Dongen S, Bateman A, Enright AJ. miRBase: microRNA sequences, targets and gene nomenclature. *Nucleic Acids Res*. Jan 1 2006;34(Database issue):D140-4. doi:10.1093/nar/gkj112

154. Dobricic V, Schilling M, Schulz J, et al. Differential microRNA expression analyses across two brain regions in Alzheimer's disease. *Transl Psychiatry*. Aug 29 2022;12(1):352. doi:10.1038/s41398-022-02108-4

155. Wang M, Qin L, Tang B. MicroRNAs in Alzheimer's Disease. *Front Genet*. 2019;10:153. doi:10.3389/fgene.2019.00153

156. Kou X, Chen D, Chen N. The Regulation of microRNAs in Alzheimer's Disease. *Front Neurol*. 2020;11:288. doi:10.3389/fneur.2020.00288

157. Reza-Zaldivar EE, Hernandez-Sapiens MA, Minjarez B, et al. Dendritic Spine and Synaptic Plasticity in Alzheimer's Disease: A Focus on MicroRNA. *Front Cell Dev Biol*. 2020;8:255. doi:10.3389/fcell.2020.00255

158. Lugli G, Torvik VI, Larson J, Smalheiser NR. Expression of microRNAs and their precursors in synaptic fractions of adult mouse forebrain. *J Neurochem*. Jul 2008;106(2):650-61. doi:10.1111/j.1471-4159.2008.05413.x

159. Hébert SS, Horré K, Nicolaï L, et al. MicroRNA regulation of Alzheimer's Amyloid precursor protein expression. *Neurobiology of Disease*. 2009/03/01/ 2009;33(3):422-428. doi:https://doi.org/10.1016/j.nbd.2008.11.009

160. Vilardo E, Barbato C, Ciotti M, Cogoni C, Ruberti F. MicroRNA-101 regulates amyloid precursor protein expression in hippocampal neurons. *J Biol Chem*. Jun 11 2010;285(24):18344-51. doi:10.1074/jbc.M110.112664

161. Long JM, Ray B, Lahiri DK. MicroRNA-153 physiologically inhibits expression of amyloid-beta precursor protein in cultured human fetal brain cells and is dysregulated in a

subset of Alzheimer disease patients. *J Biol Chem*. Sep 7 2012;287(37):31298-310. doi:10.1074/jbc.M112.366336

162. Hébert SS, Horré K, Nicolaï L, et al. Loss of microRNA cluster miR-29a/b-1 in sporadic Alzheimer's disease correlates with increased BACE1/β-secretase expression. *Proceedings of the National Academy of Sciences*. 2008/04/29 2008;105(17):6415-6420. doi:10.1073/pnas.0710263105

163. Wang WX, Rajeev BW, Stromberg AJ, et al. The expression of microRNA miR-107 decreases early in Alzheimer's disease and may accelerate disease progression through regulation of beta-site amyloid precursor protein-cleaving enzyme 1. *J Neurosci*. Jan 30 2008;28(5):1213-23. doi:10.1523/JNEUROSCI.5065-07.2008

164. Weinberg RB, Mufson EJ, Counts SE. Evidence for a neuroprotective microRNA pathway in amnestic mild cognitive impairment. *Front Neurosci*. 2015;9:430. doi:10.3389/fnins.2015.00430

165. Jiang Y, Xu B, Chen J, et al. Micro-RNA-137 Inhibits Tau Hyperphosphorylation in Alzheimer's Disease and Targets the CACNA1C Gene in Transgenic Mice and Human Neuroblastoma SH-SY5Y Cells. *Med Sci Monit*. Aug 13 2018;24:5635-5644. doi:10.12659/MSM.908765

166. Palumbo MC, Gautam M, Sonneborn A, et al. MicroRNA137-loaded lipid nanoparticles regulate synaptic proteins in the prefrontal cortex. *Mol Ther*. Oct 4 2023;31(10):2975-2990. doi:10.1016/j.ymthe.2023.08.016

167. Miya Shaik M, Tamargo IA, Abubakar MB, Kamal MA, Greig NH, Gan SH. The Role of microRNAs in Alzheimer's Disease and Their Therapeutic Potentials. *Genes (Basel)*. Mar 21 2018;9(4)doi:10.3390/genes9040174

168. Shibata M, Nakao H, Kiyonari H, Abe T, Aizawa S. MicroRNA-9 regulates neurogenesis in mouse telencephalon by targeting multiple transcription factors. *J Neurosci*. Mar 2 2011;31(9):3407-22. doi:10.1523/JNEUROSCI.5085-10.2011

169. Sim SE, Lim CS, Kim JI, et al. The Brain-Enriched MicroRNA miR-9-3p Regulates Synaptic Plasticity and Memory. *J Neurosci*. Aug 17 2016;36(33):8641-52. doi:10.1523/JNEUROSCI.0630-16.2016

170. Shamsuzzama, Kumar L, Haque R, Nazir A. Role of MicroRNA Let-7 in Modulating Multifactorial Aspect of Neurodegenerative Diseases: an Overview. *Mol Neurobiol*. Jul 2016;53(5):2787-2793. doi:10.1007/s12035-015-9145-y

171. Lee YS, Dutta A. The tumor suppressor microRNA let-7 represses the HMGA2 oncogene. *Genes Dev*. May 1 2007;21(9):1025-30. doi:10.1101/gad.1540407

172. Wang X, Liu D, Huang HZ, et al. A Novel MicroRNA-124/PTPN1 Signal Pathway Mediates Synaptic and Memory Deficits in Alzheimer's Disease. *Biol Psychiatry*. Mar 1 2018;83(5):395-405. doi:10.1016/j.biopsych.2017.07.023

173. Han D, Dong X, Zheng D, Nao J. MiR-124 and the Underlying Therapeutic Promise of Neurodegenerative Disorders. *Front Pharmacol*. 2019;10:1555. doi:10.3389/fphar.2019.01555

174. Xu J, Zheng Y, Wang L, et al. miR-124: A Promising Therapeutic Target for Central Nervous System Injuries and Diseases. *Cell Mol Neurobiol*. Oct 2022;42(7):2031-2053. doi:10.1007/s10571-021-01091-6

175. Li W, Wang SS, Shan BQ, et al. miR-103-3p targets Ndel1 to regulate neural stem cell proliferation and differentiation. *Neural Regen Res*. Feb 2022;17(2):401-408. doi:10.4103/1673-5374.317987

176. Hu Z, Zhao J, Hu T, Luo Y, Zhu J, Li Z. miR-501-3p mediates the activity-dependent regulation of the expression of AMPA receptor subunit GluA1. *J Cell Biol*. Mar 30 2015;208(7):949-59. doi:10.1083/jcb.201404092

177. Sharma B, Torres MM, Rodriguez S, Gangwani L, Kumar S. MicroRNA-502-3p regulates GABAergic synapse function in hippocampal neurons. *Neural Regen Res*. Dec 1 2024;19(12):2698-2707. doi:10.4103/NRR.NRR-D-23-01064

178. Lehmann SM, Kruger C, Park B, et al. An unconventional role for miRNA: let-7 activates Toll-like receptor 7 and causes neurodegeneration. *Nat Neurosci*. Jun 2012;15(6):827-35. doi:10.1038/nn.3113

179. Drachman DA. If we live long enough, will we all be demented? : AAN Enterprises; 1994. p. 1563-1563.

180. United Nations DoEaSAPD. World Population Prospects 2022. Web Page. 2023. https://population.un.org/wpp/

181. López-Otín C, Blasco MA, Partridge L, Serrano M, Kroemer G. The Hallmarks of Aging. *Cell*. 06/2013 2013;153(6):1194-1217. doi:10.1016/j.cell.2013.05.039

182. Lopez-Otin C, Blasco MA, Partridge L, Serrano M, Kroemer G. Hallmarks of aging: An expanding universe. *Cell*. Jan 19 2023;186(2):243-278. doi:10.1016/j.cell.2022.11.001

183. Torres AK, Jara C, Olesen MA, Tapia-Rojas C. Pathologically phosphorylated tau at S396/404 (PHF-1) is accumulated inside of hippocampal synaptic mitochondria of aged Wild-type mice. *Scientific Reports*. 2021;11(1)doi:10.1038/s41598-021-83910-w

184. Johnson SC, Rabinovitch PS, Kaeberlein M. mTOR is a key modulator of ageing and age-related disease. *Nature*. 2013;493(7432):338-345. doi:10.1038/nature11861

185. Harrison DE, Strong R, Sharp ZD, et al. Rapamycin fed late in life extends lifespan in genetically heterogeneous mice. *Nature*. Jul 16 2009;460(7253):392-5. doi:10.1038/nature08221

186. Wilkinson JE, Burmeister L, Brooks SV, et al. Rapamycin slows aging in mice. *Aging Cell*. Aug 2012;11(4):675-82. doi:10.1111/j.1474-9726.2012.00832.x

187. Bitto A, Ito TK, Pineda VV, et al. Transient rapamycin treatment can increase lifespan and healthspan in middle-aged mice. *Elife*. Aug 23 2016;5doi:10.7554/eLife.16351

188. Dai DF, Karunadharma PP, Chiao YA, et al. Altered proteome turnover and remodeling by short-term caloric restriction or rapamycin rejuvenate the aging heart. *Aging Cell*. Jun 2014;13(3):529-39. doi:10.1111/acel.12203

189. Martin-Montalvo A, Mercken EM, Mitchell SJ, et al. Metformin improves healthspan and lifespan in mice. *Nat Commun*. 2013;4:2192. doi:10.1038/ncomms3192

190. Ahmad F, Singh K, Das D, et al. Reactive Oxygen Species-Mediated Loss of Synaptic Akt1 Signaling Leads to Deficient Activity-Dependent Protein Translation Early in Alzheimer's Disease. *Antioxidants & Redox Signaling*. 12/2017 2017;27(16):1269-1280. doi:10.1089/ars.2016.6860

191. Franceschi C, Campisi J. Chronic Inflammation (Inflammaging) and Its Potential Contribution to Age-Associated Diseases. *The Journals of Gerontology Series A: Biological Sciences and Medical Sciences*. 2014-06-01 2014;69(Suppl 1):S4-S9. doi:10.1093/gerona/glu057

192. Reemst K, Kracht L, Kotah JM, et al. Early-life stress lastingly impacts microglial transcriptome and function under basal and immune-challenged conditions. *Translational Psychiatry*. 2022;12(1)doi:10.1038/s41398-022-02265-6

193. Han LKM, Dinga R, Hahn T, et al. Brain aging in major depressive disorder: results from the ENIGMA major depressive disorder working group. *Molecular Psychiatry*. 2020;26(9):5124-5139. doi:10.1038/s41380-020-0754-0

194. Hipp MS, Kasturi P, Hartl FU. The proteostasis network and its decline in ageing. *Nature Reviews Molecular Cell Biology*. 7/2019 2019;20(7):421-435. doi:10.1038/s41580-019-0101-y

195. Ribeiro FC, Cozachenco D, Heimfarth L, et al. Synaptic proteasome is inhibited in Alzheimer’s disease models and associates with memory impairment in mice. *Communications Biology*. 2023;6(1)doi:10.1038/s42003-023-05511-9

196. Graham LC, Naldrett MJ, Kohama SG, et al. Regional Molecular Mapping of Primate Synapses during Normal Healthy Aging. *Cell Reports*. 04/2019 2019;27(4):1018-1026.e4. doi:10.1016/j.celrep.2019.03.096

197. Flurkey K, M. Currer J, Harrison DE. Chapter 20 - Mouse Models in Aging Research. In: Fox JG, Davisson MT, Quimby FW, Barthold SW, Newcomer CE, Smith AL, eds. *The Mouse in Biomedical Research (Second Edition)*. Academic Press; 2007:637-672.

198. Terry AV, Jr., Buccafusco JJ. The cholinergic hypothesis of age and Alzheimer's disease-related cognitive deficits: recent challenges and their implications for novel drug development. *J Pharmacol Exp Ther*. Sep 2003;306(3):821-7. doi:10.1124/jpet.102.041616

199. Evers MM, Miniarikova J, Juhas S, et al. AAV5-miHTT Gene Therapy Demonstrates Broad Distribution and Strong Human Mutant Huntingtin Lowering in a Huntington's Disease Minipig Model. *Mol Ther*. Sep 5 2018;26(9):2163-2177. doi:10.1016/j.ymthe.2018.06.021

200. ALS_Association. Therapies Targeting ALS-Linked Genetic Mutations. 2024. https://www.als.org/research/als-research-topics/genetics/therapies-targeting-als-linked-genetic

201. Holdt LM, Kohlmaier A, Teupser D. Circular RNAs as Therapeutic Agents and Targets. *Front Physiol*. 2018;9:1262. doi:10.3389/fphys.2018.01262

202. Villanueva E, Smith T, Queiroz RML, et al. Efficient recovery of the RNA-bound proteome and protein-bound transcriptome using phase separation (OOPS). *Nature Protocols*. 2020-7-10 2020;doi:10.1038/s41596-020-0344-2

203. Gharami K, Biswas SC. Glutamate treatment mimics LTP- and LTD-like biochemical activity in viable synaptosome preparation. *Neurochemistry International*. 03/2020 2020;134:104655. doi:10.1016/j.neuint.2019.104655

204. Ahmad F, Jing Y, Lladó A, Liu P. Chemical Stimulation of Rodent and Human Cortical Synaptosomes: Implications in Neurodegeneration. *Cells*. 2021;10(5)doi:10.3390/cells10051174

Appendix

Supplementary Tables

See attached spreadsheet.

Funding

Samuel Smukowski was supported by a fellowship from the National Science Foundation Graduate Research Fellowship Program (NSF, GRFP). Research for this thesis was supported by grants from the Alzheimer's Association (AARG-22-919611), the University of Washington Royalty Research Foundation, and National Institutes of Health National Institute of Aging (NIA) R21AG082032 awarded to Dr. Paul Valdmanis. Other resources include the UW ADRC Neuropathology Core, which is funded by the NIA (P30 AG066509) as well as the ACT study (U19 AG066567).